FINE-TUNING ENHANCER ACTIVITY IN DEVELOPMENT

Matthew J. Niederhuber

A dissertation submitted to the faculty at the University of North Carolina at Chapel Hill in partial fulfillment of the requirements for the degree of Doctor of Philosophy in the Curriculum in Genetics and Molecular Biology in the School of Medicine.

Chapel Hill
2023

Approved by:

Daniel J. McKay

Frank L. Conlon

Robert J. Duronio

Jill M. Dowen

Bob Goldstein

ABSTRACT

Matthew J. Niederhuber: Fine-tuning enhancer activity in development
(Under the direction of Daniel J. McKay)

The development of a multicellular organism, from the origin of a single cell, depends on the manipulation of a shared genome to generate increasingly differentiated and specialized gene expression programs. As cells progress through development, multiple layers of information come together to determine what identity a cell should adopt, how it should relate to other cells around it, and how identity should change over time. At the heart of these networks of information are enhancers. These *cis*-regulatory genomic elements integrate information in the form of bound transcription factors and relay this information to target promoters. In this way, enhancers are critical for controlling the where, when, and how much of gene expression during development.

A major goal of the field of developmental gene regulation is to understand how enhancer activity is controlled in space and time. Here we use the developmental model system of *Drosophila* wing development to interogate the regulation of enhancer activity from two complimentary perspectives. First, we explore the ability of a temporal transcription factor (tTF) to initiate and define phases of development by controlling enhancer chromatin accessibility. We find that the tTF Eip93F (E93) is sufficient to initiate stage-specific enhancer accessibility and activity. Secondly, we perform an *in vivo* screen for nucleosome remodeling complex components involved in regulating an E93-deactivated dynamic enhancer. We find that the *Drosophila* SWI/SNF BAP complex is required to directly constrain enhancer activity in the larval wing disc, demonstrating a possible mechanism for fine-tuning enhancer activity by adjusting chromatin accessibility. Together, our data provide new insights into the different and complimentary roles that tTFs and remodelers perform in regulating enhancer activity to coordinate development.

ACKNOWLEDGMENTS

No achievement is ever made in isolation. Many people have helped me complete this work, whether through direct guidance, mentorship, and assistance in the lab; or through the countless ways big and small that those close to me have supported my time at UNC.

To my mentor Dan, thank you for taking me on as a student and providing so many opportunities to develop as a scientist over the years. From my first days in the lab, you have always been willing to take the time to teach one-on-one. Whether it was writing out crosses on the backs of fly food boxes, demonstrating dissections, or having long meetings to troubleshoot experiments, I have always been grateful for the attention you have given me as a mentee and the effort you have made to be available to help. I also want to thank you for how supportive you have been of my family. As you know, starting a family while in a graduate program is a particular kind of challenge. You have been enormously understanding of that and the obligations that have come with it. Thank you.

To my dissertation committee, thank you all for the guidance you have provided over the years. Your collective scientific expertise has been indispensable in shaping this dissertation. Thank you for challenging me with tough questions, reassuring me when I was in doubt, and taking my work seriously.

To Jill, thank you for all of your guidance in our shared lab meetings, it has always been a great help to have your perspective on my work. Also, thank you for calling me some seven years ago in Boston to let me know I'd been accepted to UNC.

To my fellow McKay lab colleagues, thank you all for making the lab a genuinely good place to come every day. Thank you for all the conversations thinking through weird scientific ideas, or just talking about music, movies, and books. I feel very fortunate to have worked among a group of people who are so talented and intelligent. This work would not have come to pass without your intellectual contributions, not to mention all of the little ways we have all tried to help each other by flipping crosses, looking over data, and helping troubleshoot our impossible PCRs.

Mary, you have been a light along this long path and I am so grateful to have had you friendship and support over the years. You have been an amazing scientific collaborator, helping me troubleshoot so many different problems, teaching me your molecular witchcraft, and picking up the slack when I couldn't get everything done on my own. I could not have done this without your help, or all the coffee.

To all of my scientific advisors and colleagues that have taught me over the years, thank you. I would like to specifically acknowledge Dr. Jerard Hurwitz, who passed in 2019. Thank you Jerry for taking me on when I had no experience. That was my first exposure to working in a lab and it was a formative experience that instilled a deep love for working at the bench. I will always remember sitting in your corner office at MSKCC while you smoked a pipe and we looked over x-ray films of western blots together. Thank you for taking me seriously and giving me a start.

Of course, completing this degree would not have been remotely possible without the support of my family. They have sacrificed a great deal to give me the time, space, and resources to accomplish this degree. To Liz and Jerry, thank you for being the most wonderful grandparents. You helped us weather the storm of the pandemic, and I would not have been able to continue pursuing this degree without everything you have done to help us with the kids. I feel a great debt to both of you.

To my Dad, you have always been my role model in so many ways, not just in your professional and scientific accomplishments. You know better than most the effort needed to be successful in science, and that ability to work hard and push forward is something you have taught me from a young age. Thank you for being my friend and mentor, thank you for all our conversions about my work, and thank you for always cheering me on. I think Mom would be proud of both of us.

Last, but certainly not least, Sally. You have been a constant support for me during this time and I very much would not have reached this point without the many sacrifices you have made to keep the goal of completing my PhD alive. You have helped me through the difficult times and celebrated my accomplishments. In many ways you have had to put your own goals on hold while I complete this degree and I do not feel like I will every be able to fully repay you for that. Though presents may help some. You're my best friend, I love you.

TABLE OF CONTENTS

LIST OF FIGURES

LIST OF TABLES

LIST OF ABBREVIATIONS

3LW	Third Larval Wandering
APF	After Puparium Formation
ATAC	Assay for Transposase Accessible Chromatin
BAP	Brahma Associated Proteins
br	broad
ci	cubitus interruptus
CUT&RUN	Cleavage Under Tags & Release Using Nuclease
DNA	Deoxyribonucleic Acid
E93	Eip93F
EcR	Ecdysone Receptor
en	engrailed
eve	even-skipped
FAIRE	Formaldehyde Assisted Isolation of Regulatory Elements
FlOS	Flip-Out System
FLP	Flippase
GFP	Green Fluorescent Protein
GOF	Gain of Function
hs	heat shock
nub	nubbin
PBAP	Polybromo Associated Proteins
PF	Pioneer transcription Factor
PTM	Post Translational Modification
PWM	Position Weight Matrix
sc	single cell
seq	high-throughput sequencing
SWI/SNF	SWItch/Sucrose Non-Fermentable

tdTomato	tandem Tomato
TF	Transcription Factor
tTF	temporal Transcription Factor
tnc	tenectin
UAS	Upstream Activating Sequence
WT	Wild Type

CHAPTER 1: INTRODUCTION

1.1 Differential gene expression drives animal development

Animal development is a remarkable biological accomplishment. A single fertilized cell gives rise to a host of functionally distinct cell types, each having been progressively specified through multiple divisions and developmental stages. Ever since the foundational work of John Gurdon in the 1960's, who discovered through a series of nuclear transplantation experiments in *Xenopus* that differentiated cells could still function as pluripotent progenitors, it has been understood that the regulation of cell differentiation is not due to the gain or loss of genetic material but rather a differential utilization of that material (Gurdon and Uehlinger 1966). We now know that gene expression is both highly cell-type specific and highly dynamic during developmental programs. For example, transcriptome profiling of whole *Drosophila* from early embryos to adults has revealed stage-specific patterns of gene expression with many genes increasing and decreasing in expression across developmental time (Graveley *et al*. 2011). Gene expression patterns also diverge and refine over time between cell types, such that different combinations of genes end up defining specific cell identities. This idea is well demonstrated by the application of single-cell RNA-seq methods to categorize and identify separable cell types within larger heterogenous populations by clustering of shared gene expression profiles (Calderon *et al.,* 2022). In order for these patterns of transcription to be temporally dynamic and progressively refined, there must exist robust mechanisms to tightly regulate differential gene expression.

1.2 *Cis*-regulatory elements direct differential gene expression

Cis-regulatory elements such as enhancers are the key genomic features that make differential gene expression possible. First identified from SV40 viral DNA by Julian Banerji and Walter Schaffner in the early 1980's, enhancers are relatively short (~0.5-2kb) genetic elements that direct spatial and temporal patterns of gene expression. Enhancers, which contain clusters of transcription factor (TF) DNA

binding sites (motifs), function as integration points for multiple layers of information available to the cell (Banerji *et al.,* 1981; Shlyueva *et al.,* 2014). Several important characteristics define enhancer biology: they are located distally from target promoters, sometimes hundreds to thousands of kilobases away from the promoters they regulate; and their function is modular, often conferring the same spatiotemporal patterns of expression to any gene they are placed nearby. In some cases, the enhancer-promoter relationship can be a simple one-to-one, but generally the regulatory logic is more complex and involves multiple enhancers regulating a single gene with each enhancer conferring a discrete piece of the total expression pattern (Long *et al.,* 2016; Rickels and Shilatifard, 2018). This is well demonstrated by the *Drosophila* pair-rule gene *even-skipped*, which depends on the combination of multiple enhancers for expression in seven stripes of the embryo (Goto *et al.,* 1989; Vincent *et al.,* 2016). It is now understood that enhancers are not only necessary for proper control of gene expression, but are a dominant feature of the genomic landscape, with 100's of thousands of putative enhancers having been identified in the human genome (ENCODE Project Consortium, 2012). Notably, enhancers have historically be defined as *cis*-elements that promote transcription, while a separate class of *cis*-elements called "silencers" promoted gene repression. Today it is understood that a strict delineation between enhancer and silencer is largely meaningless, as these *cis*-elements can promote both activation and repression depending on context (Gisselbrecht *et al.,* 2021). For simplicity, I will use the terms "enhancer" and *cis*-regulatory element interchangeably to refer generally to distal regulatory elements throughout this dissertation.

The importance of enhancers for proper control of gene expression programs is exemplified by the consequences of mutations within these elements. Even small changes to enhancer DNA sequence can significantly impact the expression of the genes they regulate. A striking example of this is the highly conserved vertebrate ZRS limb bud enhancer of the *sonic hedgehog* (*Shh*) gene. Point mutations in the ZRS enhancer, which lies ~1Mb away from the Shh promoter, have been shown to promote ectopic expression beyond the normal *Shh* domain and are associated with polydactyly in mice and humans (Lettice *et al.,* 2017). Variations in this element have also been identified as important drivers of evolutionary divergence between species, such as the loss of limbs in snakes (Kvon *et al.,* 2016). Changes in enhancer sequence that lead to malfunction and/or target gene misexpression have also

been linked to oncogenesis (Sur and Taipale, 2016). For example, hyperactivation of the oncogene *MYC*, which is a prevalent feature of many human cancers, is associated with mutations within and the misuse of tissue-specific *MYC* enhancers (Lancho and Herranz, 2018). These examples serve to highlight the critical importance of enhancers in tuning gene expression programs, but also how remarkably sensitive these elements are to small perturbations.

1.3 Transcription factors encode developmental information

An individual enhancer's activity is a direct consequence of the TFs that bind it. Each TF may encode information about developmental time, spatial position relative to a larger tissue field, cell and tissue identity, or environmental status (Spitz and Furlong, 2012). Some of these TF inputs function exclusively as activators or repressors of transcription, while others are bifunctional and can function as activator or repressor in a context-specific manner (Parker *et al.,* 2011; DelRosso *et al.,* 2023). The integration of these different layers of information at an enhancer contributes to coordinating a particular amount and spatiotemporal pattern of expression from a target gene. Enhancer activity is not only determined by specific combinations of TFs, it is also a product of the relative abundance and strength of interaction of TFs at the enhancer.

TFs generally recognize specific but relatively short sequences of DNA (Spitz and Furlong, 2012). Large-scale screens applying a variety of methodologies have identified consensus DNA motifs, typically represented as position weight matrices (PWM) of base frequency, for many TFs of different organisms (Zhu *et al.,* 2011; Boer and Hughes 2012; Weirauch *et al.,* 2014; Kulakovskiy *et al.,* 2018). Surprisingly, *in vivo* experiments have repeatedly shown that TFs only bind a fraction of all possible motifs, and that binding often occurs at sites that are "sub-optimal" or "degenerate" relative to the consensus (Wang *et al.,* 2012; Kribelbauer *et al.,* 2019). Modification of binding sites to optimally match the TF consensus and maximize affinity often leads to ectopic enhancer activity, sometimes due to the inappropriate recognition of binding sites by paralogous factors, and increased expression levels (Farley *et al.,* 2015; Crocker *et al.,* 2015; Crocker *et al.,* 2016). For example, in *Drosophila* embryos the enhancers that respond to the Dorsal (Dl) TF gradient have either low or high-affinity Dl binding sites depending on whether they respond to

high or low Dl gradient. Conversion of low-affinity Dl sites to high-affinity ones was found to expand and prematurely activate the pattern of a Dl responsive enhancer reporter (Keller *et al.,* 2020). The relative number, orientation, and arrangement of TF binding sites, commonly referred to as enhancer "grammar," is also important for fine-tuning enhancer output. Some enhancers require particular arrangements of TFs motifs to properly coordinate cell-type specific patterns of expression (Swanson *et al.,* 2011; Jindal and Farley 2021). These observations illustrate how fine-tuning an enhancer's sensitivity to its target inputs, via changes in TF affinity, motif organization, or TF combinations, are involved in determining the total activity of a particular regulatory site.

1.4 Enhancers in the context of chromatin

While an enhancer's sensitivity to inputs is significantly influenced by both the abundance, position, and quality of TF binding sites, an additional layer of regulatory control lies at the level of the local chromatin environment. In all eukaryotes, the genome exists as a complex of DNA and protein called chromatin that is comprised of individual nucleosome units. Each nucleosome consists of ~146bp of DNA super-helically wrapped 1.7 times around an octamer of histone proteins. Nucleosomes aid in the structural organization of the genome by allowing higher order structures to form, but they also play a critical role in the regulation of gene expression. This is because as the DNA wraps around the octamer the major and minor grooves alternate between being solvent facing and histone facing, and only short stretches of DNA are solvent facing at a time (Michael and Thomä, 2021). *In vitro* studies have shown that many human TFs can only bind their sites when they are solvent facing, or when those sites are present at the more accessible DNA entry/exit points of the nucleosome (Zhu *et al.,* 2018). Thus, nucleosomes inhibit many TFs from effectively interacting with their target sites, and *cis*-regulatory elements must be depleted of nucleosomes or "opened" before they can be sensitive to input TFs. Increased chromatin accessibility is consequently a hallmark feature of sites with regulatory potential, and methods to map regions of open chromatin have become effective strategies for identifying putative enhancers genome-wide (Niederhuber and McKay, 2020).

In the context of developmental programs, patterns of chromatin accessibility are highly dynamic.

As an example, chromatin accessibility profiling in developing *Drosophila* embryos has found tens of thousands of sites with temporally dynamic accessibility, many of which have been verified as tissue-specific enhancers (Thomas *et al.,* 2011; McKay and Lieb, 2013; Cusanovich *et al.,* 2018; Calderon *et al.,* 2022). Furthermore, dynamic enhancer accessibility has been shown to strongly correlate with dynamic enhancer activity, as well as changes in gene expression (Uyehara et a., 2017; Ma *et al.,* 2019). Aberrant changes in enhancer chromatin accessibility are also correlated with disease states like cancer. For example, chromatin accessibility profiling of dozens of human cancer types identified cancer specific patterns of accessible regulatory elements that correlated with specific patterns of gene expression (Stergachis *et al.,* 2013; Corces *et al.,* 2018). These examples demonstrate the importance of the nucleosome barrier as a layer of regulation at enhancer elements, both in the context of normal temporal enhancer regulation and during disease progression. This layer of regulation ensures that enhancers are only sensitive to TF inputs in the right cell types at the right times.

1.5 The special role of pioneer transcription factors

While most TFs display an inability to sufficiently access binding sites when DNA is complexed with histones, a subclass of factors have a unique capacity to both bind nucleosomal DNA and subsequently facilitate local increases in chromatin accessibility. These so called “pioneer” TFs (PFs) perform critical rolls in priming enhancers and initiating transcriptional programs (Zaret and Mango 2016; Zaret 2020). Since their initial discovery in the 1990’s, a host of PFs have been identified from lower eukaryotes to vertebrates, including essential pluripotency factors, mediators of zygotic genome activation, cell identity factors, and tumor suppressors (Soufi *et al.,* 2015; Schulz *et al.,* 2015; Yu and Buck, 2019; Dodonova *et al.,* 2020). One example is the *Drosophila* epithelia-specifying PF Grainyhead (Grh), which has been shown to be both necessary and sufficient for increases in chromatin accessibility at most of the sites it normally binds during eye development (Jacobs *et al.,* 2018). In support of a direct role of PFs in opening chromatin, these factors are often found to effect local changes to nucleosome stability at sites they directly bind (Zaret, 2020). Structural studies of the mammalian Sox pluripotency PFs SOX2 and SOX11, in complex with nucleosomes, indicate that Sox factors physically disrupt histone-DNA

contacts (Dodonova *et al.,* 2020) However, several lines of evidence indicate that PFs are not always sufficient, and require additional steps and machinery to effect larger chromatin accessibility changes. Recent work on the hematopoietic lineage-specifying PF PU.1 has demonstrated that this factor requires interaction and collaboration with ATP-dependent nucleosome remodeling complexes to fully open the surrounding DNA (Frederick *et al.,* 2023). Thus, while PFs have the capacity to engage nucleosomal DNA and often alter the accessibility at their local target sites, active remodeling by additional factors of the surrounding chromatin environment appears to be necessary to fully establish accessible domains on the scale of enhancers and promoters.

1.6 Nucleosome remodeling complexes as regulators of enhancer activity

Changes in nucleosome occupancy is achieved by ATP-dependent nucleosome remodeling complexes. Nucleosome remodelers describe a general class of highly conserved multi-subunit protein complexes that use the energy of ATP-hydrolysis to physically translocate DNA on the nucleosome and effect either nucleosome sliding or ejection (Nodelman and Bowman, 2021). Remodeling complexes all have an ATPase motor subunit with a similar DNA translocase domain, but can be sub-divided into four families based on the different domains that flank the translocase domain: imitation switch (ISWI), chromodomain helicase DNA-binding (CHD), switch/sucrose non-fermentable (SWI/SNF), and INO80 (Tyagi *et al.,* 2016; Clapier *et al.,* 2017). Current models argue for a shared mechanism of DNA translocation among remodeling complexes, where ATP-hydrolysis powers an inch-worming of DNA around the nucleosome in short increments (Clapier *et al.,* 2017; Nodelman and Bowman, 2021). The consequence of DNA translocation is subsequently determined by the different domains of the ATPase and its accompanying subunits to achieve complex-specific remodeling effects.

Nucleosome remodeling complexes have been extensively studied in all major model organisms and are critical for maintenance of chromatin accessibility, as well as to properly coordinate differential accessibility and gene expression programs. For example, depletion of components of the mammalian SWI/SNF BAF complex leads to reduced accessibility at enhancers, changes in histone methylation, and gene expression (Kelso *et al.,* 2017; Blumli *et al.,* 2021). The SWI/SNF complex, and other nucleosome

remodelers, have also been deeply implicated in human cancers. For instance, mutations in SWI/SNF subunits are found in more than 20% of human cancers (Bracken *et al.,* 2019; Centore *et al.,* 2020). Importantly, while nucleosome remodeling complexes often demonstrate some capacity for binding DNA, they normally do so agnostic of DNA sequence-specificity and depend on the binding action of sequence-specific TFs for recruitment to specific sites.

1.7 Gaps in our understanding of developmental enhancer regulation

A great deal has been learned about the collaborative roles of TFs and nucleosome remodeling complexes in the control of differential gene expression during development. Yet there are still many open questions that would benefit from further study. For one, both standard TFs and PFs are observed to bind only a small fraction of their potential sites in the genome, as determined by motif occurrence, and exhibit cell-type specific patterns of binding, but it is not fully understood how this specificity is achieved (Donaghey *et al.,* 2018; Larson *et al.,* 2021). While TFs are typically classified as either activators or repressors of transcription, a significant fraction are bifunctional, including canonical PFs, and exhibit site-specific functionality (DelRosso *et al.,* 2023). In zebra fish, the PF FoxA has been reported to transition from functioning primarily as a pioneer in embryonic stem cells to a repressor later in neural crest cells, possibly due to interaction with distinct coregulators (Lukoseviciute *et al.,* 2018). Similarly, the TF Hunchback bifunctionally regulates different enhancers of the *even-skipped* gene in *Drosophila* embryos (Vincent *et al.,* 2018). One explanation for context-specific functionality is the unique combination of coregulators at an enhancer, but exactly how TF site-specific functions are determined remains an active area of research, particularly in terms of how coregulators mechanistically affect bifunctional factors.

At the level of chromatin accessibility and nucleosome remodeling, the process of enhancer activation via TF binding and remodeler recruitment is well established. However, the reverse process of enhancer closing and deactivation (sometimes termed decommissioning) is less well studied but also clearly an important mechanism for effectively silencing the previous gene expression program during developmental transitions (Wu *et al.,* 2023). This is well demonstrated by the observed loss of enhancer accessibility and active epigenetic signatures during the move from naïve to primed pluripotency in

mouse embryonic stem cells (Respuela *et al.,* 2016). While some factors and remodeling complexes have been identified in these deactivation processes, such as Foxd3 in the previous example, more studies are needed, particularly with *in vivo* developmental models, to better understand the role of enhancer deactivation as a general regulatory mechanism. Similarly, the nuances of how nucleosome remodeling fine-tunes enhancer activity are poorly understood. Genome-wide measurements of chromatin accessibility in the context of nucleosome remodeling complex loss-of-function have documented both wide-spread losses in accessibility but also many sites that increase in accessibility, suggesting that these complexes may also limit-accessibility or constrain activity.

1.8 *Drosophila* wing development as a model system to study enhancer biology

Ever since early work by Conrad Waddington, *Drosophila* wing development has been a foundational system for the study of developmental genetics and differential gene regulation (Waddington 1940). It has served as a model of homeotic specification, hormone signaling, spatial patterning, nervous regeneration, dynamic enhancer regulation, and much more. Over the years the genes and pathways that control wing development have been well characterized, establishing a deep foundational knowledge on which to build new research.

Development of the *Drosophila* wing begins in the second thoracic segment of the embryo in a small number of cells that divide and migrate dorsally from the Distal-less expressing leg primordium, concurrent with the expression of the TFs Snail and Vestigial (Requeña *et al.,* 2017). By the end of embryogenesis these wing primordial cells invaginate to form the imaginal wing disc, a simple epithelial sac. This sac is a monolayer of cells with one side comprised of cuboidal epithelium that will form the adult tissues, and the other comprised of squamous epithelium called the peripodial membrane (Tripathi and Irvine, 2022). During larval stages the wing disc proliferates and a series of overlapping morphogen gradients and region specifying TFs progressively define the domains that will give rise to the adult back, wing hinge, and wing blade (Cifuentes and Garcia-Bellido, 1997; Zirin and Mann, 2007). By the end of larval development the wing disc consists of approximately 50,000 cells and the specialized cells that will give rise to the sensory bristles and veins have been initially patterned. In the following prepupal stages

of metamorphosis wing cells enter a temporary cell cycle arrest during which time the tissue evaginates outward to form an epithelial bilayer, concordant with head, leg disc, and haltere disc eversion (Taylor and Adler 2008). A final synchronized round of cell division then occurs around 12-24h after puparium formation (APF) followed by a final cell cycle exit at 24h (Gou *et al.,* 2016). Despite no additional cell divisions, the wing blade continues to grow larger as cells flatten and expand around 40h APF, concurrent with the extension of the innervated and non-innervated bristle shafts that decorate the wing margins (Guild *et al.,* 2005; Cho *et al.,* 2020).

Progression through these developmental transitions is regulated by the steroid hormone ecdysone. Major systemic pulses of ecdysone at the onset of metamorphosis, during the prepupal-pupal transition, and then during mid-pupal stages activate stage-specific TFs to repress the gene expression program of the previous stage while defining the subsequent program (Thummel 1996; Yamanaka *et al.,* 2013). Throughout these processes, chromatin accessibility, enhancer activity, and gene expression are all highly dynamic (Uyehara *et al.,* 2017). Chromatin accessibility profiling of *Drosophila* appendages between larval and late pupal stages revealed that accessibility patterns were highly similar between tissues of the same stage, but differed significantly between stages, suggesting that chromatin accessibility regions were controlled systemically to define stage-specific patterns of enhancer activity and gene expression (McKay and Lieb, 2013). This work implicated an organism-wide developmental cue like ecdysone signaling as the coordinator of dynamic chromatin accessibility and developmental enhancer activity. In support of this, experiments on the specification of the pigmented bract cells that develop at the base of bristles in the *Drosophila* legs revealed that the ecdysone early-response TF Eip93F (E93) is required to make bract cells competent to respond to epidermal growth factor receptor (EGFR) signaling (Mou *et al.,* 2012). In the *Drosophila* appendages, E93 is expressed following the prepupal-pupal transition ~18-24h APF, and it is well conserved among both holo- and hemimetabolous insects as the primary specifier of adult identity (Ureña *et al.,* 2014). This type of TF function, where expression is both stage-specific and also required to determine identify at a particular phase within a developmental sequence, defines so called temporal TFs (tTFs). TTF function is exemplified in *Drosophila* neurodevelopment, where a temporal cascade of tTFs within each neuroblast lineage define a sequence

of progeny identities (Doe, 2017; Sen *et al.,* 2019). In combination with the observation that chromatin accessibility is systemically changed at subsequent stages of *Drosophila* development, the work of Mou *et al.,* suggested that one potential mechanism for how a tTF like E93 defines a particular stage of development is to instruct cells to become sensitive to inputs at specific times, and that it may do so by regulating changes in chromatin accessibility.

Genomics studies in the *Drosophila* wing subsequently found that E93 directly binds thousands of sites genome-wide that exhibit dynamic accessibility between larval and pupal stages. Furthermore, it was found that nearly half of all chromatin accessibility changes that normally occur between these stages, both opening and closing, fail to occur in E93 mutants (Uyehara *et al.,* 2017). These data support a model of E93 tTF function that involves genome-wide regulation of chromatin accessibility changes. In addition, several E93-bound and dependent dynamically accessible sites were confirmed to be functional enhancers that drive spatiotemporal-specific patterns of reporter activity. A number of these enhancers were found to be dependent on E93 to both dynamically activate and deactivate over time. These included the br^{disc} enhancer, which is highly-accessible and active in the larval wing disc, but then closes and deactivates in pupal wings in a direct E93-dependent manner (Uyehara *et al.,* 2017). Together, these experiments raise several questions about E93 function, dynamic enhancer regulation, and tTF function generally. Namely: is a tTF like E93 sufficient to cue chromatin accessibility changes outside of its normal window of expression; how does E93 bind and simultaneously coordinate differential regulation of both activated and deactivated enhancers; and does E93 coordinate with different coregulators such as nucleosome remodeling complexes to control enhancer accessibility?

In this work I endeavor to address some of the broad questions of differential enhancer and gene regulation. Through a combination of classic genetics, microscopy, and genomics I interrogate the function of E93 as a stage-specifying tTF and test the role of nucleosome remodeling complexes for their requirement to coregulate the repression of an E93-dependent dynamic enhancer. I first present a literature review of the current state of genomics applications in the study of chromatin accessibility and enhancer regulation in insect developmental model systems (**Chapter 2**). Next, I present findings from a series of collaborative experiments in which E93 was precociously expressed in the wing disc. We find

that E93 is sufficient at many, but not all, of its binding sites to initiate changes in enhancer accessibility and activity. We also find that the direction of these changes correlates with the normal changes occurring during the larval to pupal transition, supporting a model of chromatin accessibility regulation as the mechanism of tTF stage-specification (**Chapter 3**). In order to expand on our understanding of developmental dynamic enhancer regulation, with a particular focus on the question of how enhancers are deactivated over time, I next interrogated the role of ATP-dependent nucleosome remodeling complexes in regulating the E93-dependent and deactivated br^{disc} enhancer. From these experiments I find a surprising requirement for the *Drosophila* SWI/SNF BAP complex to constrain br^{disc} activity in the wing disc, but not to mediate closing or deactivation in the pupal wing. These observations introduce a theoretical model of tuning enhancer sensitivity by regulating chromatin dynamics (**Chapter 4**). Finally, I report preliminary results that attempt to bridge the gap between E93 and BAP complex function in developmental enhancer regulation (**Chapter 5**). In support of this research I have developed several transgenic enhancer reporters that better capture the temporal dynamics of deactivating enhancers, a series of inducible E93 mutants, and a reporter designed to identify E93 coregulators. All of which will be generally useful for the field. In whole, this work provides new insights into the functions of stage-specifying tTFs, their relationship to controlling enhancer accessibility, and raises new questions of how active nucleosome remodeling contributes to balancing enhancer sensitivity during development.

REFERENCES

Banerji J, Rusconi S, Schaffner W. 1981. Expression of a β-globin gene is enhanced by remote SV40 DNA sequences. Cell. 27(2 PART 1):299–308. doi:10.1016/0092-8674(81)90413-X.

Blümli S, Wiechens N, Wu M-Y, Singh V, Gierlinski M, Schweikert G, Gilbert N, Naughton C, Sundaramoorthy R, Varghese J, *et al*. 2021. Acute depletion of the ARID1A subunit of SWI/SNF complexes reveals distinct pathways for activation and repression of transcription. Cell Reports. 37(5):109943. doi:10.1016/j.celrep.2021.109943.

de Boer CG, Hughes TR. 2012. YeTFaSCo: a database of evaluated yeast transcription factor sequence specificities. Nucleic Acids Research. 40(D1):D169–D179. doi:10.1093/nar/gkr993.

Bracken AP, Brien GL, Verrijzer CP. 2019. Dangerous liaisons: interplay between SWI/SNF, NuRD, and Polycomb in chromatin regulation and cancer. Genes Dev. 33(15–16):936–959. doi:10.1101/gad.326066.119.

Calderon D, Blecher-Gonen R, Huang X, Secchia S, Kentro J, Daza RM, Martin B, Dulja A, Schaub C, Trapnell C, *et al*. 2022. The continuum of *Drosophila* embryonic development at single-cell resolution. Science. 377(6606):eabn5800. doi:10.1126/science.abn5800.

Centore RC, Sandoval GJ, Soares LMM, Kadoch C, Chan HM. 2020. Mammalian SWI/SNF Chromatin Remodeling Complexes: Emerging Mechanisms and Therapeutic Strategies. Trends in Genetics. 36(12):936–950. doi:10.1016/j.tig.2020.07.011.

Cho B, Song S, Axelrod JD. 2020. Prickle isoforms determine handedness of helical morphogenesis. Elife. 9:e51456. doi:10.7554/eLife.51456.

Cifuentes FJ, García-Bellido A. 1997. Proximo-distal specification in the wing disc of *Drosophila* by the nubbin gene. Proceedings of the National Academy of Sciences of the United States of America. 94(21):11405–11410. doi:10.1073/pnas.94.21.11405.

Clapier CR, Iwasa J, Cairns BR, Peterson CL. 2017. Mechanisms of action and regulation of ATP-dependent chromatin-remodelling complexes. Nature Reviews Molecular Cell Biology. 18(7):407–422. doi:10.1038/nrm.2017.26.

Corces MR, Granja JM, Shams S, Louie BH, Seoane JA, Zhou W, Silva TC, Groeneveld C, Wong CK, Cho SW, *et al*. 2018. The chromatin accessibility landscape of primary human cancers. Science. 362(6413). doi:10.1126/science.aav1898.

Crocker J, Abe N, Rinaldi L, McGregor AP, Frankel N, Wang S, Alsawadi A, Valenti P, Plaza S, Payre F, et al. 2015. Low affinity binding site clusters confer HOX specificity and regulatory robustness. Cell. 160(1–2):191–203. doi:10.1016/j.cell.2014.11.041.

Crocker J, Ilsley GR, Stern DL. 2016. Quantitatively predictable control of *Drosophila* transcriptional enhancers *in vivo* with engineered transcription factors. Nature Genetics. 48(3):292–298. doi:10.1038/ng.3509.

Cusanovich DA, Reddington JP, Garfield DA, Daza R, Aghamirzaie D, Marco-Ferreres R, Pliner HA, Christiansen L, Qiu X, Steemers FJ, *et al*. 2018. The *cis*-regulatory dynamics of embryonic development at single-cell resolution. Nature Publishing Group. 555. doi:10.1038/nature25981.

DelRosso N, Tycko J, Suzuki P, Andrews C, Aradhana null, Mukund A, Liongson I, Ludwig C, Spees K, Fordyce P, *et al*. 2023. Large-scale mapping and mutagenesis of human transcriptional effector

domains. Nature. 616(7956):365–372. doi:10.1038/s41586-023-05906-y.

Dodonova SO, Zhu F, Dienemann C, Taipale J, Cramer P. 2020. Nucleosome-bound SOX2 and SOX11 structures elucidate pioneer factor function. Nature. 580(7805):669–672. doi:10.1038/s41586-020-2195-y.

Donaghey J, Thakurela S, Charlton J, Chen JS, Smith ZD, Gu H, Pop R, Clement K, Stamenova EK, Karnik R, *et al*. 2018. Genetic determinants and epigenetic effects of pioneer-factor occupancy. Nature Genetics. 50(2):250–258. doi:10.1038/s41588-017-0034-3.

ENCODE Project Consortium. 2012. An integrated encyclopedia of DNA elements in the human genome. Nature. 489(7414):57–74. doi:10.1038/nature11247.

Farley EK, Olson KM, Zhang W, Brandt AJ, Rokhsar DS, Levine MS. 2015. Suboptimization of developmental enhancers. Science. 350(6258):325–328. doi:10.1126/science.aac6948.

Frederick MA, Williamson KE, Garcia MF, Ferretti MB, McCarthy RL, Donahue G, Monteiro EL, Takenaka N, Reynaga J, Kadoch C, *et al*. 2023. A pioneer factor locally opens compacted chromatin to enable targeted ATP-dependent nucleosome remodeling. Nat Struct Mol Biol. 30(1):31–37. doi:10.1038/s41594-022-00886-5.

Goto T, Macdonald P, Maniatis T. 1989. Early and late periodic patterns of even skipped expression are controlled by distinct regulatory elements that respond to different spatial cues. Cell. 57(3):413–422. doi:10.1016/0092-8674(89)90916-1.

Graveley BR, Brooks AN, Carlson JW, Duff MO, Landolin JM, Yang L, Artieri CG, Van Baren MJ, Boley N, Booth BW, *et al*. 2011. The developmental transcriptome of *Drosophila melanogaster*. doi:10.1038/nature09715.

Guild GM, Connelly PS, Ruggiero L, Vranich KA, Tilney LG. 2005. Actin Filament Bundles in *Drosophila* Wing Hairs: Hairs and Bristles Use Different Strategies for Assembly. Mol Biol Cell. 16(8):3620–3631. doi:10.1091/mbc.E05-03-0185.

Guo Y, Flegel K, Kumar J, McKay DJ, Buttitta LA. 2016. Ecdysone signaling induces two phases of cell cycle exit in *Drosophila* cells. Biology Open. 5(11):1648–1661. doi:10.1242/bio.017525.

Gurdon JB, Uehlinger V. 1966. “Fertile” Intestine Nuclei. Nature. 210(5042):1240–1241 doi:10.1038/2101240a0.

Jacobs J, Atkins M, Davie K, Imrichova H, Romanelli L, Christiaens V, Hulselmans G, Potier D, Wouters J, Taskiran II, *et al*. 2018. The transcription factor Grainy head primes epithelial enhancers for spatiotemporal activation by displacing nucleosomes. Nature Genetics. 50(7):1011–1020. doi:10.1038/s41588-018-0140-x.

Jindal GA, Farley EK. 2021. Enhancer grammar in development, evolution, and disease: dependencies and interplay. Developmental Cell. 56(5):575–587. doi:10.1016/j.devcel.2021.02.016.

Keller SH, Jena SG, Yamazaki Y, Lim B. 2020. Regulation of spatiotemporal limits of developmental gene expression via enhancer grammar. Proc Natl Acad Sci U S A. 117(26):15096–15103. doi:10.1073/pnas.1917040117.

Kelso TWR, Porter DK, Amaral ML, Shokhirev MN, Benner C, Hargreaves DC. 2017. Chromatin accessibility underlies synthetic lethality of SWI/SNF subunits in ARID1A-mutant cancers. eLife. 6:1–29. doi:10.7554/eLife.30506.001.

Kribelbauer JF, Rastogi C, Bussemaker HJ, Mann RS. 2019. Low-Affinity Binding Sites and the Transcription Factor Specificity Paradox in Eukaryotes. Annual Review of Cell and Developmental Biology. 35(1):357–379. doi:10.1146/annurev-cellbio-100617-062719.

Kulakovskiy IV, Vorontsov IE, Yevshin IS, Sharipov RN, Fedorova AD, Rumynskiy EI, Medvedeva YA, Magana-Mora A, Bajic VB, Papatsenko DA, *et al*. 2018. HOCOMOCO: towards a complete collection of transcription factor binding models for human and mouse via large-scale ChIP-Seq analysis. Nucleic Acids Research. 46(D1):D252–D259. doi:10.1093/nar/gkx1106.

Kvon EZ, Kamneva OK, Melo US, Barozzi I, Osterwalder M, Mannion BJ, Tissières V, Pickle CS, Plajzer-Frick I, Lee EA, *et al*. 2016. Progressive Loss of Function in a Limb Enhancer during Snake Evolution. Cell. 167(3):633-642.e11. doi:10.1016/j.cell.2016.09.028.

Lancho O, Herranz D. 2018. The MYC Enhancer-ome: Long-Range Transcriptional Regulation of MYC in Cancer. Trends Cancer. 4(12):810–822. doi:10.1016/j.trecan.2018.10.003.

Larson ED, Komori H, Gibson TJ, Ostgaard CM, Hamm DC, Schnell JM, Lee C-Y, Harrison MM. 2021. Cell-type-specific chromatin occupancy by the pioneer factor Zelda drives key developmental transitions in *Drosophila*. Nat Commun. 12(1):7153. doi:10.1038/s41467-021-27506-y.

Larson ED, Marsh AJ, Harrison MM. 2021. Pioneering the developmental frontier. Molecular Cell. 81(8):1640–1650. doi:10.1016/j.molcel.2021.02.020.

Lettice LA, Devenney P, De Angelis C, Hill RE. 2017. The Conserved Sonic Hedgehog Limb Enhancer Consists of Discrete Functional Elements that Regulate Precise Spatial Expression. Cell Reports. 20(6):1396–1408. doi:10.1016/j.celrep.2017.07.037.

Long HK, Prescott SL, Wysocka J. 2016. Ever-Changing Landscapes: Transcriptional Enhancers in Development and Evolution. Cell. 167(5):1170–1187. doi:10.1016/j.cell.2016.09.018.

Lukoseviciute M, Gavriouchkina D, Williams RM, Hochgreb-Hagele T, Senanayake U, Chong-Morrison V, Thongjuea S, Repapi E, Mead A, Sauka-Spengler T. 2018. From Pioneer to Repressor: Bimodal foxd3 Activity Dynamically Remodels Neural Crest Regulatory Landscape *In vivo*. Developmental Cell. 47(5):608-628.e6. doi:10.1016/j.devcel.2018.11.009.

Ma Y, McKay DJ, Buttitta L. 2019. Changes in chromatin accessibility ensure robust cell cycle exit in terminally differentiated cells. PLoS Biology. 17(9). doi:10.1371/journal.pbio.3000378.

McKay DJ, Lieb JD. 2013. A Common Set of DNA Regulatory Elements Shapes *Drosophila* Appendages. Developmental Cell. 27(3):306–318. doi:10.1016/j.devcel.2013.10.009.

Michael AK, Thomä NH. 2021. Reading the chromatinized genome. Cell. 184(14):3599–3611. doi:10.1016/j.cell.2021.05.029.

Mou X, Duncan DM, Baehrecke EH, Duncan I. 2012. Control of target gene specificity during metamorphosis by the steroid response gene E93. Proceedings of the National Academy of Sciences of the United States of America. 109(8):2949–2954. doi:10.1073/pnas.1117559109.

Niederhuber MJ, McKay DJ. 2020. Mechanisms underlying the control of dynamic regulatory element activity and chromatin accessibility during metamorphosis. Curr Opin Insect Sci. 43:21–28. doi:10.1016/j.cois.2020.08.007.

Nodelman IM, Bowman GD. 2021. Biophysics of Chromatin Remodeling. Annu Rev Biophys. 50:73–93. doi:10.1146/annurev-biophys-082520-080201.

Parker DS, White MA, Ramos AI, Cohen BA, Barolo S. 2011. The *cis*-Regulatory Logic of Hedgehog Gradient Responses: Key Roles for Gli Binding Affinity, Competition, and Cooperativity. Sci Signal. 4(176):ra38. doi:10.1126/scisignal.2002077.

Requena D, Álvarez JA, Gabilondo H, Loker R, Mann RS, Estella C. 2017. Origins and Specification of the *Drosophila* Wing. Current Biology. 27(24):3826-3836.e5. doi:10.1016/j.cub.2017.11.023.

Respuela P, Nikolić M, Tan M, Frommolt P, Zhao Y, Wysocka J, Rada-Iglesias A. 2016. Foxd3 Promotes Exit from Naive Pluripotency through Enhancer Decommissioning and Inhibits Germline Specification. Cell Stem Cell. 18(1):118–133. doi:10.1016/j.stem.2015.09.010.

Rickels R, Shilatifard A. 2018. Enhancer Logic and Mechanics in Development and Disease. Trends in Cell Biology. 28(8):608–630. doi:10.1016/j.tcb.2018.04.003.

Schulz KN, Bondra ER, Moshe A, Villalta JE, Lieb JD, Kaplan T, McKay DJ, Harrison MM. 2015. Zelda is differentially required for chromatin accessibility, transcription factor binding, and gene expression in the early *Drosophila* embryo. Genome Research. 25(11):1715–1726. doi:10.1101/gr.192682.115.

Segert JA, Gisselbrecht SS, Bulyk ML. 2021. Transcriptional Silencers: Driving Gene Expression with the Brakes On. Trends Genet. 37(6):514–527. doi:10.1016/j.tig.2021.02.002.

Shlyueva D, Stampfel G, Stark A. 2014. Transcriptional enhancers: From properties to genome-wide predictions. Nature Reviews Genetics. 15(4):272–286. doi:10.1038/nrg3682.

Soufi A, Garcia MF, Jaroszewicz A, Osman N, Pellegrini M, Zaret KS. 2015. Pioneer transcription factors target partial DNA motifs on nucleosomes to initiate reprogramming. Cell. 161(3):555–568. doi:10.1016/j.cell.2015.03.017.

Spitz F, Furlong EEM. 2012. Transcription factors: From enhancer binding to developmental control. Nature Reviews Genetics. 13(9):613–626. doi:10.1038/nrg3207.

Stergachis AB, Neph S, Reynolds A, Humbert R, Miller B, Paige SL, Vernot B, Cheng JB, Thurman RE, Sandstrom R, *et al*. 2013. Developmental fate and cellular maturity encoded in human regulatory DNA landscapes. Cell. 154(4):888–903. doi:10.1016/j.cell.2013.07.020.

Sur I, Taipale J. 2016. The role of enhancers in cancer. Nat Rev Cancer. 16(8):483–493. doi:10.1038/nrc.2016.62.

Swanson CI, Schwimmer DB, Barolo S. 2011. Rapid Evolutionary Rewiring of a Structurally Constrained Eye Enhancer. Current Biology. 21(14):1186–1196. doi:10.1016/j.cub.2011.05.056.

Taylor J, Adler PN. 2008. Cell rearrangement and cell division during the tissue level morphogenesis of evaginating *Drosophila* imaginal discs. Dev Biol. 313(2):739–751. doi:10.1016/j.ydbio.2007.11.009.

Thomas S, Li XY, Sabo PJ, Sandstrom R, Thurman RE, Canfield TK, Giste E, Fisher W, Hammonds A, Celniker SE, *et al*. 2011. Dynamic reprogramming of chromatin accessibility during *Drosophila* embryo development. Genome Biology. 12(5). doi:10.1186/gb-2011-12-5-r43.

Thummel CS. 1996. Flies on steroids - *Drosophila* metamorphosis and the mechanisms of steroid hormone action. Trends in Genetics. 12(8):306–310. doi:10.1016/0168-9525(96)10032-9.

Tripathi BK, Irvine KD. 2022. The wing imaginal disc. Genetics. 220(4):iyac020.

doi:10.1093/genetics/iyac020.

Tyagi M, Imam N, Verma K, Patel AK. 2016. Chromatin remodelers: We are the drivers!! Nucleus. 7(4):388–404. doi:10.1080/19491034.2016.1211217.

Ureña E, Manjón C, Franch-Marro X, Martín D. 2014. Transcription factor E93 specifies adult metamorphosis in hemimetabolous and holometabolous insects. Proceedings of the National Academy of Sciences of the United States of America. 111(19):7024–7029. doi:10.1073/pnas.1401478111.

Uyehara CM, Nystrom SL, Niederhuber MJ, Leatham-Jensen M, Ma Y, Buttitta LA, McKay DJ. 2017. Hormone-dependent control of developmental timing through regulation of chromatin accessibility. Genes and Development. 31(9):862–875. doi:10.1101/gad.298182.117.

Vincent BJ, Estrada J, DePace AH. 2016. The appeasement of Doug: a synthetic approach to enhancer biology. Integrative Biology (United Kingdom). 8(4):475–484. doi:10.1039/c5ib00321k.

Vincent BJ, Staller MV, Lopez-Rivera F, Bragdon MDJ, Pym ECG, Biette KM, Wunderlich Z, Harden TT, Estrada J, DePace AH. 2018. Hunchback is counter-repressed to regulate even-skipped stripe 2 expression in *Drosophila* embryos. PLoS Genetics. 14(9):1–21. doi:10.1371/journal.pgen.1007644.

Waddington CH. 1940. The genetic control of wing development in*Drosophila*. Journ of Genetics. 41(1):75–113. doi:10.1007/BF02982977.

Wang J, Zhuang J, Iyer S, Lin X, Whitfield TW, Greven MC, Pierce BG, Dong X, Kundaje A, Cheng Y, et al. 2012. Sequence features and chromatin structure around the genomic regions bound by 119 human transcription factors. Genome Res. 22(9):1798–1812. doi:10.1101/gr.139105.112.

Weirauch MT, Yang A, Albu M, Cote AG, Montenegro-Montero A, Drewe P, Najafabadi HS, Lambert SA, Mann I, Cook K, *et al*. 2014. Determination and Inference of Eukaryotic Transcription Factor Sequence Specificity. Cell. 158(6):1431–1443. doi:10.1016/j.cell.2014.08.009.

Wu Xiaotong, Wu Xi, Xie W. 2023 May 21. Activation, decommissioning, and dememorization: enhancers in a life cycle. Trends Biochem Sci.:S0968-0004(23)00110-X. doi:10.1016/j.tibs.2023.04.005.

Yamanaka N, Rewitz KF, O'Connor MB. 2013. Ecdysone Control of Developmental Transitions: Lessons from *Drosophila* Research. Annual Review of Entomology. 58(1):497–516. doi:10.1146/annurev-ento-120811-153608.

Yu X, Buck MJ. 2019. Defining TP53 pioneering capabilities with competitive nucleosome binding assays. Genome Res. 29(1):107–115. doi:10.1101/gr.234104.117.

Zaret KS. 2020. Pioneer Transcription Factors Initiating Gene Network Changes. Annu Rev Genet. 54:367–385. doi:10.1146/annurev-genet-030220-015007.

Zaret KS, Mango SE. 2016. Pioneer transcription factors, chromatin dynamics, and cell fate control. Current Opinion in Genetics and Development. 37:76–81. doi:10.1016/j.gde.2015.12.003.

Zhu F, Farnung L, Kaasinen E, Sahu B, Yin Y, Wei B, Dodonova SO, Nitta KR, Morgunova E, Taipale M, *et al*. 2018. The interaction landscape between transcription factors and the nucleosome. Nature. 562(7725):76–81. doi:10.1038/s41586-018-0549-5.

Zhu LJ, Christensen RG, Kazemian M, Hull CJ, Enuameh MS, Basciotta MD, Brasefield JA, Zhu C,

Asriyan Y, Lapointe DS, *et al*. 2011. FlyFactorSurvey: a database of *Drosophila* transcription factor binding specificities determined using the bacterial one-hybrid system. Nucleic Acids Research. 39(suppl_1):D111–D117. doi:10.1093/nar/gkq858.

Zirin JD, Mann RS. 2007. Nubbin and Teashirt mark barriers to clonal growth along the proximal-distal axis of the *Drosophila* wing. Developmental Biology. 304(2):745–758. doi:10.1016/j.ydbio.2007.01.025.

CHAPTER 2: MECHANISMS UNDERLYING THE CONTROL OF DYNAMIC REGULATORY ELEMENT ACTIVITY AND CHROMATIN ACCESSIBILITY DURING METAMORPHOSIS

2.1 Dynamic gene expression drives development

Gene expression programs are highly dynamic during animal development. This is necessary in order to orchestrate the progression from the initial specification of cell fates and body axes, to the final expression of effector proteins that determine the characteristics of terminally differentiated tissues. Numerous transcriptome-profiling studies have captured the remarkable degree of dynamic gene expression that occurs during various developmental programs in *Drosophila* and other insects [1–4] (**Figure 2.1A, B**). The regulation that makes these transcriptional dynamics possible involves both *cis* and trans components. Trans components include transcription factors (TFs) and the protein machinery they recruit to target loci to affect gene transcription. *Cis* elements include non-coding regions of the genome such as promoters, enhancers, and silencers. These *cis* elements contain clusters of TF binding motifs and can act over large genomic distances to drive spatiotemporal-specific patterns of transcription [5–7] (**Figure 2.1C**). In recognition that *cis*-elements function as discrete units that can both activate and repress gene transcription, we refer to them here as *cis*-regulatory modules (CRMs).

CRMs integrate spatial and temporal information by virtue of the TF binding sites they contain. TFs provide spatial information in the form of master regulators that define the cell and regional identities that compose the body plan, as well as the effectors of signal transduction pathways. TFs also provide temporal information about developmental stage, often in the form of hormone signaling. The combined input of spatial and temporal information at CRMs makes it possible for relatively few TFs to produce the requisite variety of gene expression programs that underlie organismal complexity [8,9]. While this combinatorial model provides a framework to explain CRM-mediated spatiotemporal gene regulation, TF's are often reused in different developmental contexts, and yet they only bind and activate target CRMs in select settings [10]. A classic example of this is the cell-type and temporal-specific effects of Notch signaling [11–13]. The answer to this complication may lie in the additional layer of control that is provided

by the packaging of DNA into chromatin.

In eukaryotic organisms, DNA is complexed with histone octamers to form nucleosomes, which are the repeating units of the higher-order structure, chromatin. Long thought to only be necessary for packaging a large chromosome into the nucleus, we now understand that chromatin plays a significant role in gene regulation and CRM activity. Early evidence of this came from invitro experiments that showed that the DNA binding affinity of some TFs was significantly reduced when the DNA binding site was contained within a nucleosome [14,15]. It is now generally accepted that the absence of nucleosomes favors TF binding, while the presence of nucleosomes acts as a barrier to TF binding (**Figure 2.1D**).

2.2 Insect metamorphosis as a system to study spatiotemporal gene control mechanisms

Insect metamorphosis has proven to be a powerful experimental system to study the molecular and genetic mechanisms of spatiotemporal gene regulation. This is particularly the case in *Drosophila melanogaster* due to the elegant and sophisticated genetic methods available for testing gene function. During *Drosophila* metamorphosis, nearly all larval structures are destroyed and replaced with adult tissues, and the central nervous system (CNS) undergoes extensive remodeling [16,17]. Like the CNS, the larval imaginal discs are not destroyed, but are instead dramatically transformed to produce the adult appendages and body wall (**Figure 2.1B**) [18]. The appendages, which we focus on here, are an especially powerful experimental system because the inputs that determine their identity, pattern their morphology, and direct their metamorphic transformation have been extensively characterized. Furthermore, the effects of genetic manipulations are easily visualized in the final pattern of the adult structures.

The conserved steroid hormone 20-hydroxyecdysone (ecdysone) coordinates initiation of insect metamorphosis and the orchestration of subsequent metamorphic events. In *Drosophila*, ecdysone is secreted from the prothoracic gland at stereotypical times during development. From there it spreads through the hemolymph to induce gene expression changes in physically separated tissues [16,19]. Ecdysone controls gene activity by binding to its nuclear hormone receptor, a heterodimer of Ecdysone

Receptor (EcR) and Ultraspiracle (Usp). EcR/Usp regulate gene expression in an ecdysone-dependent manner, activating ecdysone-responsive genes in the presence of hormone, but repressing many of the same genes when ecdysone is absent [19]. Foundational work in *Drosophila* by Michael Ashburner established the central model of the ecdysone-mediated transcriptional response. The Ashburner Model proposes that ecdysone triggers two phases of gene transcription. An initial phase in which "early genes" respond directly to hormone, and a larger secondary phase of "late gene" expression that requires transcription of the early genes for effective activation [20]. Importantly, the ecdysone-induced transcriptional cascade varies significantly between different target tissues, such as the midgut and the wing. Thus, a longstanding question in the field is how ecdysone elicits these tissue-specific transcriptional responses.

2.3 Recent advances in genomics technologies have provided new insight into gene regulation during metamorphosis

In *Drosophila*, recent genomics studies have contributed to the emerging picture of a highly dynamic regulatory landscape that involves sequential activation and deactivation of CRMs genome-wide during metamorphosis. Open chromatin profiling has proved to be a key method for identifying putative CRMs in developing tissues [21–24]. Because TFs compete with nucleosomes to bind DNA, active CRMs are typically depleted of nucleosomes, thus creating a local "open" chromatin site. Assays that map open chromatin include FAIRE-seq and ATAC-seq, both of which have been successfully employed in insects (see Box 1).

The decapentaplegic (*dpp*) locus in *Drosophila* is emblematic of the dynamic *cis*-regulatory developmental landscape. Dpp is a member of the TGF-β superfamily and its patterned expression is necessary for proper development at each of the embryonic, larval, and pupal stages. The *dpp* locus spans over 60kb and harbors multiple *cis*-regulatory regions that control its spatiotemporal expression (**Figure 2.2A**) [31]. In embryos, dpp is necessary for dorsal-ventral patterning and midgut development, and is initially expressed in the dorsal half of the blastoderm [32,33]. In the larval wing disc, Dpp is expressed in a stripe of cells adjacent to the anterior-posterior boundary where it functions

as a morphogen to control patterning and tissue growth [34,35,36]. As metamorphosis proceeds in the pupal wing, *dpp* transcription at the anterior-posterior boundary decays, and it is newly transcribed in the developing longitudinal veins where it promotes vein identity (**Figure 2.2B**) [37,38]. These distinct patterns of *dpp* expression are regulated by several dynamically active CRMs, including the early embryo-specific (dpp^{BDE}) [32], the imaginal disc-specific ($dpp^{BS3.23}$) [39], and pupal wing vein-specific ($dpp^{1.65KpnI/XhoI}$) [37] CRMs. Notably, classical mutations that disrupt these regions, such as dpp^{ho} and dpp^{shv}, lead to stage-specific wing phenotypes, such as the failure to properly form veins [37,39,40]. Moreover, open chromatin profiling indicates that accessibility of these stage-specific CRMs is strikingly dynamic over the course of wing development, with regions opening and closing as CRMs switch on and off over time [21,22,41–43].

The strong correlation between regulatory activity and accessibility has led to the identification of new CRMs in *Drosophila* and other insects, including butterflies and beetles [24,44]. One study in *Tribolium casteneum* employed FAIRE-seq at several stages of embryogenesis and in developing appendages to identify open chromatin sites with *cis* regulatory potential. These candidates were then used to establish a new transgenic reporter system for characterizing spatiotemporal patterns of CRM activity in *Tribolium*, further facilitating investigations into the evolution of morphological diversity [23]. A separate study in *Drosophila* used open chromatin profiling to provide insight into the mechanisms linking terminal differentiation and cell cycle exit. The authors found that entry into a robust post-mitotic state in the pupal wing is ensured by chromatin closing at loci encoding key rate-limiting cell cycle regulators such as Cyclin E and E2F [22]. Another recent study in *Drosophila* applied CATaDa to profile changes in chromatin accessibility within developing neuronal and midgut cell lineages. Notably, this work leveraged the use of cell-type specific GAL4 drivers to profile specific cell lineages at progressive developmental stages. The authors found that patterns of accessibility are dynamic within these lineages and sites of accessibility are strong predictors of active CRMs [59]. Taken together, these studies have begun to reveal the interplay between changes in chromatin state, dynamic CRM activity, and the regulation of gene expression in developing tissues.

2.4 What factors are involved in temporally dynamic CRM usage?

Exactly how changes in CRM accessibility and activity are regulated during metamorphosis remains an open question. Some enticing clues have come from comparisons of chromatin accessibility patterns between *Drosophila* leg, wing, and haltere tissues of late larvae and pharate adults [21]. Analysis of these data revealed that the patterns of open chromatin were nearly identical between these tissues, despite their being defined by distinct master regulator TFs and having tissue-specific gene expression programs. Even more striking, the shared patterns of accessibility changed in concert with one another over time. That is, accessibility was highly similar between appendages of the same stage, but it was highly dissimilar in the same tissue at different stages [21]. Highly similar chromatin landscapes between thoracic appendages have also been observed in wing and elytra of *Tribolium* [23], as well as between forewing and hindwing of *Heliconius* [24,44] and *Junonia* [45] butterflies, revealing this to be a conserved characteristic.

Coordinated changes in chromatin accessibility between spatially separated tissues suggests the involvement of a systemic signal. Ecdysone's role in coordinating developmental timing makes it an attractive candidate pathway for regulating the temporal dynamics of chromatin accessibility and CRM activity. A new genomics method for mapping TF binding, termed CUT&RUN, has recently provided insight into the role ecdysone plays in regulating temporal changes in CRM activity during appendage metamorphosis (see Box 1). CUT&RUN for EcR in late larval and early pupal wings revealed that EcR binds throughout the genome before and after the major ecdysone pulse that triggers pupariation in *Drosophila* [42]. EcR binding was observed at many genes that encode core components of the ecdysone response, including *broad*, *Eip93F*, and *Eip75B*. Surprisingly however, the majority of EcR binding sites were found at genes with appendage-specific functions that are not canonical members of the core ecdysone cascade. This suggests that EcR plays a direct role in tissue-specific ecdysone responses, a hypothesis the authors supported by demonstrating that EcR-bound CRMs require EcR/Usp for their normal patterns of activity in the wing disc. This study also demonstrated that EcR binding is temporally dynamic between larval and pupal stages, suggesting that in addition to its involvement in tissue-specific CRM activity, EcR may also function in shaping distinct responses to ecdysone at different

times. What role, if any, EcR plays in the regulation of dynamic chromatin accessibility remains to be determined, as well as how its binding profiles and regulatory function may change later in *Drosophila* pupal development. In contrast to temporally dynamic EcR binding reported in *Drosophila*, a recent ChIP-seq study found few changes in EcR binding between larval and pupal time points in butterfly wings [45]. It is not clear whether these contrasting results are due to divergent gene regulatory strategies between species, or if they stem from differences in the sensitivities of the assays used to profile EcR (ChIP vs CUT&RUN). Of note, the authors found a correlation between binding of the basic helix-loop-helix TF, Spineless, with temporal changes in open chromatin, suggesting that tissue-specific TFs may contribute to sequential use of developmental CRMs.

A series of studies in *Drosophila* have provided evidence for a central role of another ecdysone-regulated TF in dynamic control of chromatin accessibility during wing metamorphosis. The ecdysone-induced TF Eip93F (E93), which was classically identified as an “early gene” in the ecdysone signaling response, has since been found to be an evolutionarily conserved factor required for specifying adult identity in insects [17,46,47]. In *Drosophila* wings, E93 is induced to high levels during the prepupal to pupal transition around 12h after the initiation of metamorphosis. E93 is required for proper terminal differentiation of cell fates such as specification of the pigmented bract cells in legs and vein differentiation in the wing [48,49]. A time course of open chromatin profiling in wild-type wings found that many CRMs with pupal-specific activity are inaccessible in larval wing discs before opening at later stages. By contrast, CRMs with larval-specific activity are accessible in larval wing discs and subsequently close at later stages. Open chromatin profiling in an E93 loss-of-function (E93 LOF) background revealed that thousands of late-acting sites fail to open. Conversely, thousands of early-acting sites fail to close in E93 mutant wings [41]. Thus, E93 is required to both open and close chromatin over time. Characterization of E93-bound CRMs with dynamic accessibility in transgenic reporter assays showed the timing of their activity correlated with accessibility, and that when accessibility changes failed in E93 LOF wings (both opening and closing sites), these CRMs failed to activate or deactivate respectively (**Figure 2.3**). Tests of E93 sufficiency, in which E93 was precociously expressed early in larval wings, demonstrated this TF was sufficient to bind and institute changes to accessibility at many of its target sites, including those

validated as functional CRMs with dynamic activity. These CRMs also exhibited precocious activation or deactivation in the presence of precocious E93 [50]. Notably, the patterns of precocious activity indicated that E93 targets responded to the same spatial cues that normally control these CRMs later in pupal stages, suggesting that E93 expression regulates the competence of CRMs to respond to existing spatial information. These results implicate E93, and ecdysone signaling by proxy, as a general regulator of dynamic chromatin accessibility during wing metamorphosis.

In the model that emerges from these studies, E93 functions as a temporal cue by controlling CRM accessibility. This in turn controls CRM competence to respond to spatial input. Temporally restricted expression of E93 may establish stage-specific windows of competent CRMs, such that only certain regulatory sites are responsive to spatial inputs at certain times. A corollary of this model is that control of CRM competence allows for spatial inputs to be reutilized during development without compromising their context-specific activity [51,52]. E93 has been shown to function as a temporal cue across insects [47,49,54–56] and in multiple tissues [41,48], suggesting E93-dependent control of stage-specific CRM accessibility may be a general feature of developmental gene regulation.

While the molecular mechanisms of hormone-regulated changes in CRM activity and accessibility have yet to be fully uncovered, one recent study offered a connection between the ATP-dependent nucleosome remodeler dMi-2 and ecdysone signaling. This work showed that dMi-2 complexes with EcR and tunes the ecdysone response by reducing chromatin accessibility at ecdysone target genes [53]. Still, a significant outstanding question is how regulators like E93 are capable of cueing both opening and closing of chromatin, coincident with CRM activation and deactivation, in the same cells during the same stage. Whether temporal control of chromatin accessibility involves combined action of spatial factors, and what those combinatorial inputs may be, also remains to be determined.

2.5 Concluding remarks

The progression and increased affordability of high-throughput sequencing technologies has accelerated genome-wide characterization of TF binding, histone modifications, chromatin accessibility, and 3D genome topology over the last decade. These advances have enabled the global identification of CRMs in developing tissues across insects, thereby opening new windows into the mechanisms

underlying developmental gene regulation and morphological evolution.

2.6 Acknowledgements

This work was supported by the National Science Foundation (GRFP Award No. 1650116), the American Cancer Society (RSG-17-164-01-DDC), and the National Institute of General Medical Sciences of the NIH (R35GM128851).

2.7 Figures

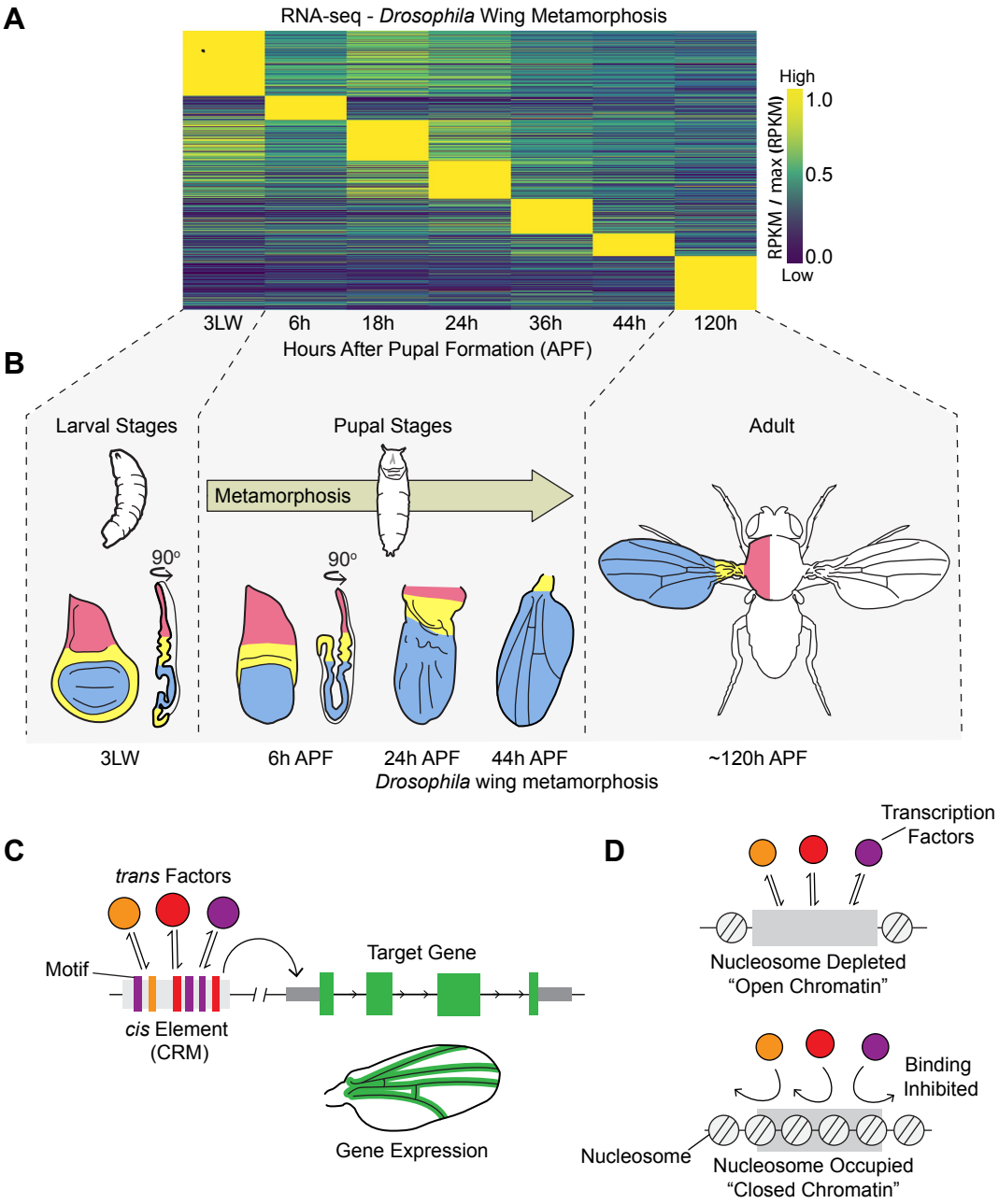

Figure 2.1: *Cis*-regulatory modules mediate dynamic gene expression during development. (a) Heatmap of RNA-seq time course in *Drosophila* wings spanning late-larval (3LW) to mid-pupal (44h APF) stages [3]. Normalized reads are plotted as a fraction of the maximum for each gene. (b) Schematic depicting morphological changes that reorganize the late larval wing imaginal disc to create the adult wing, hinge, and notum. (c) Schematic of cis and trans components regulating target gene expression. (d) Schematic depicting the inhibitory effect of nucleosomes on TFs physically accessing their DNA binding sites.

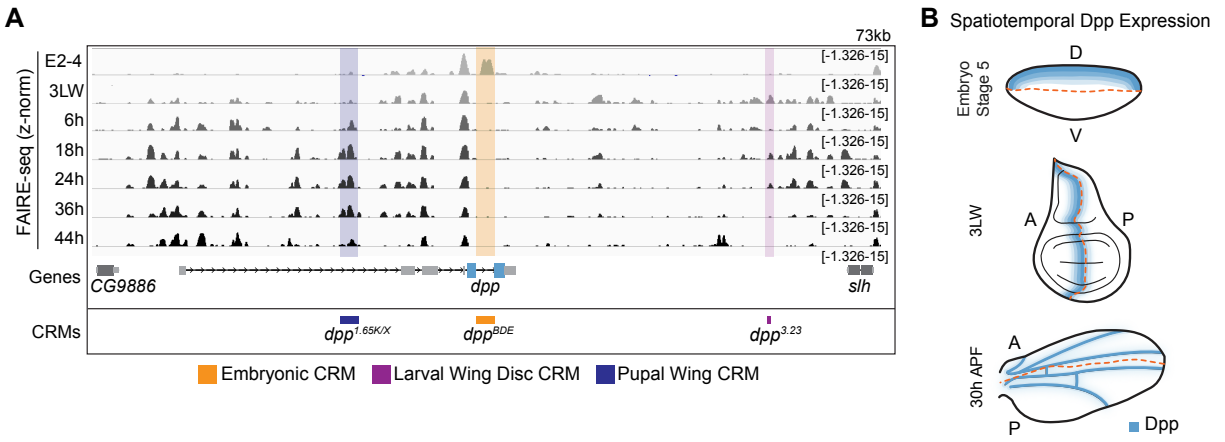

Figure 2.2: Genes are regulated by distinct sets of CRMs that have stage-specific activity and chromatin accessibility. (a) Browser tracks of FAIRE-seq timecourse during *Drosophila* development at the *decapentaplegic* (*dpp*) locus. 2-4 hour embryos (E2-4) are shown, as well as six time points of wing development: 3LW denotes 3rd larval wandering stage, all other times indicate hours after puparium formation. Selected CRMs with stage-specific activity are shown. dpp^{BDE} is active in embryos [32], $dpp^{BS3.23}$ is active in imaginal discs [39], and $dpp^{1.65KpnI/XhoI}$ is active in the pupal wing [37]. Several open chromatin sites at this locus remain uncharacterized. (b) Illustrations of the spatiotemporal changes in Dpp expression (blue) from early-stage embryos, through wing metamorphosis. Orange dashed line indicates approximate dorsal/ventral boundary in embryos and anterior/posterior boundary in wings. The single stripe of Dpp along the anterior-posterior boundary in wings is lost shortly after the onset of metamorphosis, and a new pattern along the developing longitudinal veins is gained.

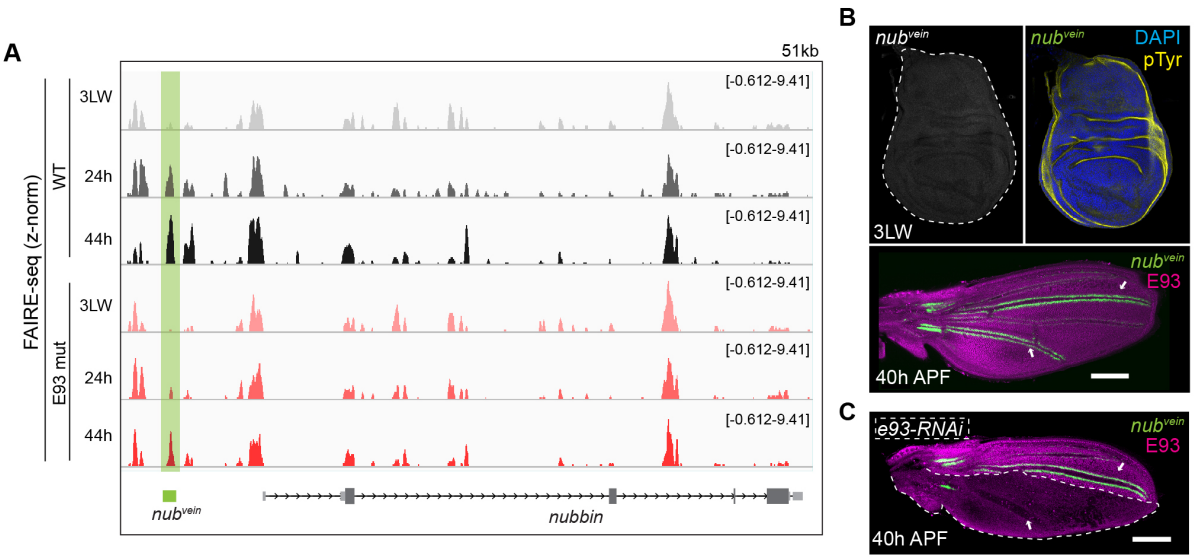

Figure 2.3: Ecdysone signaling regulates a temporal shift in CRM accessibility and activity during wing development. (a) Genome browser tracks of *Drosophila* wing FAIRE-seq in wild-type (WT) and E93 mutant (*E93*^{4}*/Df(3R)93Fx2*) animals. The *nub*^{vein} CRM (green box), which is active only in pupal wings, fails to fully open in an E93 mutant background. (b) The transgenic *nub*^{vein}*-nlsGFP* reporter is inactive in late larval wing discs, when the CRM is closed. This CRM activates later in cells flanking the developing pupal veins, most strongly along L3 and L5 (white arrows), corresponding with a significant increase of CRM accessibility (WT 24h and 44h FAIRE). Dashed-white line indicates tissue boundary. (c) *nub*^{vein} fails to activate in the context of E93 knockdown (*e93-RNAi*) in the posterior half of the pupal wing. Dashed white line outlines region of knockdown. White arrows highlight WT activity in top (anterior) half versus inactivity in lower (posterior) half. Scale bars = 100µm.

REFERENCES

1. Li T-R, White KP: Tissue-specific gene expression and ecdysone-regulated genomic networks in *Drosophila* the two major types of cells in the larval. Dev Cell 2003, 5:59-72.

2. Graveley BR, Brooks AN, Carlson JW, Duff MO, Landolin JM, Yang L, Artieri CG, Van Baren MJ, Boley N, Booth BW, *et al*.: The developmental transcriptome of *Drosophila melanogaster*. Nat 2011, 471:473-479.

3. Guo Y, Flegel K, Kumar J, McKay DJ, Buttitta LA: Ecdysone signaling induces two phases of cell cycle exit in *Drosophila* cells. Biol Open 2016, 5:1648-1661.

4. Ou J, Deng HM, Zheng SC, Huang LH, Feng QL, Liu L: Transcriptomic analysis of developmental features of *Bombyx mori* wing disc during metamorphosis. BMC Genom 2014, 15:1–15.

5. Buecker C, Wysocka J: Enhancers as information integration hubs in development: lessons from genomics. Cell Rev 2012, 28(6):276-284.

6. Spitz F, Furlong EEM: Transcription factors: from enhancer binding to developmental control. Nat Rev Genet 2012, 13:613–626.

7. Shlyueva D, Stampfel G, Stark A: Transcriptional enhancers: from properties to genome-wide predictions. Nat Rev Genet 2014, 15:272-286.

8. Farley EK, Olson KM, Levine MS: Regulatory principles governing tissue specificity of developmental enhancers. CSHL Press 2016, 80:27–32.

9. Levine M, Cattoglio C, Tjian R: Leading edge review looping back to leap forward: transcription enters a new era. Cell 2014, 157:13-25.

10. Sandmann T, Jensen LJ, Jakobsen JS, Karzynski MM, Eichenlaub MP, Bork P, Furlong EEM: A temporal map of transcription factor activity: Mef2 directly regulates target genes at all stages of muscle development. Dev Cell 2006, 10:797–807.

11. Terriente-Felix A, Li J, Collins S, Mulligan A, Reekie I, Bernard F, Krejci A, Bray S: Notch cooperates with Lozenge/Runx to lock haemocytes into a differentiation programme. Dev 2013, 140:926–937.

12. Bray SJ, Gomez-Lamarca M: Notch after cleavage. Curr Opin Cell Biol 2018, 51:103–109.

13. Skalska L, Stojnic R, Li J, Fischer B, Cerda-Moya G, Sakai H, Tajbakhsh S, Russell S, Adryan B, Bray SJ: Chromatin signatures at Notch-regulated enhancers reveal large-scale changes in H3K56ac upon activation. EMBO J 2015, 34:1889–1904.

14. Taylor ICA, Workman JL, Schuetz TJ, Kingston RE: Facilitated binding of GAL4 and heat shock factor to nucleosomal templates: differential function of DNA-binding domains. Genes Dev 1991, 5:1285-1298.

15. Workman JL, Kingston RE: Alteration of nucleosome structure as a mechanism of transcriptional regulation. Annu Rev Biochem 1998, 67:545–579.

16. Truman JW: The evolution of insect metamorphosis. Curr Biol 2019, 29:R1252–R1268.

17. Truman JW: Metamorphosis of the central nervous system of *Drosophila*. J Neurobiol 1990, 21:1072–1084.

18. Beira J V, Paro R: The legacy of *Drosophila* imaginal discs. Chrom 2016, 125:573-592.

19. Yamanaka N, Rewitz KF, O'connor MB: Ecdysone control of developmental transitions: lessons from *Drosophila* research. Annu Rev Entomol 2013, 58:497-516.

20. Ashburner M: Puffs, genes, and hormones revisited. Cell 1990, 61:1-3.

21. McKay DJ, Lieb JD: A common set of DNA regulatory elements shapes *Drosophila* appendages. Dev Cell 2013, 27:306–318.

22. Ma Y, McKay DJ, Buttitta L: Changes in chromatin accessibility ensure robust cell cycle exit in terminally differentiated cells. PloS Biol 2019, 17.

23. Lai YT, Deem KD, Borràs-Castells F, Sambrani N, Rudolf H, Suryamohan K, El-Sherif E, Halfon MS, McKay DJ, Tomoyasu Y: Enhancer identification and activity evaluation in the red flour beetle, *Tribolium castaneum*. Dev 2018, 145.

24. Lewis JJ, Geltman RC, Pollak PC, Rondem KE, van Belleghem SM, Hubisz MJ, Munn PR, Zhang L, Benson C, Mazo-Vargas A, *et al*.: Parallel evolution of ancient, pleiotropic enhancers underlies butterfly wing pattern mimicry. Proc Natl Acad Sci 2019, 116:24174–24183.

25. Giresi PG, Kim J, McDaniell RM, Iyer VR, Lieb JD: FAIRE (Formaldehyde-Assisted Isolation of Regulatory Elements) isolates active regulatory elements from human chromatin. Genome Res 2007, 17:877–885.

26. Mckay DJ: Using Formaldehyde-Assisted Isolation of Regulatory Elements (FAIRE) to identify functional regulatory DNA in insect genomes. Met Mol Biol 2019, 1858:89-97.

27. Buenrostro JD, Giresi PG, Zaba LC, Chang HY, Greenleaf WJ: Transposition of native chromatin for fast and sensitive epigenomic profiling of open chromatin, DNA-binding proteins and nucleosome position. Nat Methods 2013, 10:1213–1218.

28. Buenrostro JD, Wu B, Litzenburger UM, Ruff D, Gonzales ML, Snyder MP, Chang HY, Greenleaf WJ: Single-cell chromatin accessibility reveals principles of regulatory variation. Nat 2015, 5 23:486–490.

29. Skene PJ, Henikoff S: An efficient targeted nuclease strategy for high-resolution mapping of DNA binding sites. Elife 2017, 6:1–35.

30. Skene PJ, Henikoff JG, Henikoff S: Targeted *in situ* genome-wide profiling with high efficiency for low cell numbers. Nat Protoc 2018, 13:1006–1019.

31. Affolter M, Basler K: The Decapentaplegic morphogen gradient: from pattern formation to growth regulation. Nat Rev Genet 2007, 8:663–674.

32. Jackson PD and Hoffmann FM: Embryonic expression patterns of the *Drosophila decapentaplegic* gene: separate regulatory elements control blastoderm expression and lateral ectodermal expression. Dev Dyn 1994, 199:28-44.

33. Capovilla M, Brand& M, Betas J: Direct regulation of decapentaplegic by Ultrabithorax and its role in *Drosophila* midgut morphogenesis. Cell 1994, 76:461-475.

34. Blackman RK, Sanicola M, Raftery LA, Gillevet T, Gelbart WM: An extensive 3' *cis*-regulatory region directs the imaginal disk expression of decapentaplegic, a member of the TGF-beta family in *Drosophila*. Dev 1991, 111:657-665.

35. Bosch PS, Ziukaite R, Alexandre C, Basler K, Vincent JP: Dpp controls growth and patterning in *Drosophila* wing precursors through distinct modes of action. Elife 2017, 6:1–16.

36. Johnston RD, Hoffmann FM, Blackman RK, Segal D, Grimaila R, Padgett RW, Irick HA, Gelbart WM: Molecular organization of the decapentaplegic gene in *Drosophila melanogaster*. Gene Dev 1990, 4:1114-112.

37. Sotillos S, de Celis JF: Regulation of decapentaplegic expression during *Drosophila* wing veins pupal development. Mech Dev 2006, 123:241–251.

38. O'Keefe DD, Thomas S, Edgar BA, Buttitta L: Temporal regulation of Dpp signaling output in the *Drosophila* wing. Dev Dyn 2014, 243:818–832.

39. Hepker J, Blackman RK, Holmgren R: Cubitus interruptus is necessary but not sufficient for direct activation of a wing-specific *decapentaplegic* enhancer. Dev 1999, 126:3669-3677.

40. Spencer FA, Hoffmann FM, Gelbart WM: Decapentaplegic: a gene complex affecting morphogenesis in *Drosophila melanogaster*. Cell 1982, 28:451-461.

41. Uyehara CM, Nystrom SL, Niederhuber MJ, Leatham-Jensen M, Ma Y, Buttitta LA, McKay DJ: Hormone-dependent control of developmental timing through regulation of chromatin accessibility. Genes Dev 2017, 31:862–875.

42. Uyehara CM, McKay DJ: Direct and widespread role for the nuclear receptor EcR in mediating the response to ecdysone in *Drosophila*. Proc Natl Acad Sci 2019, 116:9893–9902.

43. Wang W, Peng J, Li Z, Wang P, Guo M, Zhang T, Qian W, Xia Q, Cheng D: Transcription factor E93 regulates wing development by directly promoting Dpp signaling in *Drosophila*. Biochem Biophys Res Commun 2019, 513:280–286.

44. Lewis JJ, Reed RD: Genome-wide regulatory adaptation shapes population-level genomic landscapes in *Heliconius*. Mol Biol Evol 2018, 36:159-173.

45. Van der Burg KRL, Lewis JJ, Martin A, Nijhout HF, Danko CG, Reed RD: Contrasting roles of transcription factors Spineless and EcR in the highly dynamic chromatin landscape of butterfly wing metamorphosis. Cell Rep 2019, 27:1027-1038.

46. Baehrecke EH, Thummel CS: The *Drosophila E93* gene from the 93F early puff displays stage- and tissue-specific regulation by 20-Hydroxyecdysone. Dev Biol 1995, 171:85–97.

47. Ureña E, Manjón C, Franch-Marro X, Martín D: Transcription factor E93 specifies adult metamorphosis in hemimetabolous and holometabolous insects. Proc Natl Acad Sci 2014, 111:7024–7029.

48. Mou X, Duncan DM, Baehrecke EH, Duncan I: Control of target gene specificity during metamorphosis by the steroid response gene *E93*. Proc Natl Acad Sci 2012, 109:2949–2954.

49. Chafino S, Ureñ E, Casanova J, Casacuberta E, Franch-Marro X, Martín D: Upregulation of *E93* gene expression acts as the trigger for metamorphosis independently of the threshold size in the beetle *Tribolium castaneum*. Cell Rep 2019, 27:1039-1049.

50. Nystrom SL, Niederhuber MJ, McKay DJ: Expression of E93 provides an instructive cue to control dynamic enhancer activity and chromatin accessibility during development. Dev 2020, 147.

51. Sen SQ, Chanchani S, Southall TD, Doe CQ: Neuroblast-specific open chromatin allows the temporal transcription factor, Hunchback, to bind neuroblast-specific loci. Elife 2019, 8:1–26.

52. Erclik T, Li X, Courgeon M, Bertet C, Chen Z, Baumert R, Ng J, Koo C, Arain U, Behnia R, *et al*.: Integration of temporal and spatial patterning generates neural diversity. Nat 2017, 541:365-370.

53. Kreher J, Kovač K, Bouazoune K, MačInković I, Ernst AL, Engelen E, Pahl R, Finkernagel F, Murawska M, Ullah I, *et al*.: EcR recruits dMi-2 and increases efficiency of dMi-2-mediated remodelling to constrain transcription of hormone-regulated genes. Nat Commun 2017, 8.

54. Xi L, Dai F, Guo E, Li K, Ma L, Tian L, Cao Y, Zhang G, Palli S, Li S: 20-hydroxyecdysone (20E) primary response gene *E93* modulates 20E signaling to promote *Bombyx* larval-pupal metamorphosis. J Biol Chem 2015, 290(45):27370-27383.

55. Chafino S, López-Escardó, Benelli G, Kovac H, Casacuberta E, Franch-Marro X, Kathirithamby J, Martín D: Differential expression of the adult specifier E93 in the strepsipteran *Xenos vesparum* Rossi suggests a role in female neoteny. Nat Sci Rep 2018, 8.

56. Gujar H and Palli SR, Krüppel homolog 1 and E93 mediate Juvenile hormone regulation of metamorphosis in the common bed bug, *Cimex lectularius*. Nat Sci Rep 2016, 6.

CHAPTER 3: EXPRESSION OF E93 PROVIDES AN INSTRUCTIVE CUE TO CONTROL DYNAMIC ENHANCER ACTIVITY AND CHROMATIN ACCESSIBILITY DURING DEVELOPMENT

3.0 Contributions

The work presented in this chapter is the result of a collaboration between Matthew J. Niederhuber (MJN) and Spencer L. Nystrom (SLN), who were co-first authors. MJN and SLN both contributed to conceptualization, methodology, validation, formal analysis, investigation, data curation, and writing. MJN specifically performed all enhancer reporter experiments, associated microscopy, image analysis, and designed figure illustrations. The work was published in the journal Development in 2020 (Nystrom *et al.,* 2020). .

3.1 Introduction

Cis-regulatory regions such as enhancers and promoters interpret multiple types of inputs to control gene expression during development. These inputs come in the form of both spatial and temporal cues. Spatial cues are often provided by transcription factors, which can contribute information on cell identity (e.g. MyoD), organ identity, (e.g. Pha-4), and regional identity (e.g. Hox factors). Additional spatial cues are provided by the activity of signaling pathways such as the Wnt, BMP, and EGFR families, which contribute information on distance relative to the source of the signal through their downstream transcriptional effectors. Remarkably, many of these spatial cues are used reiteratively over the course of development, often with different effects on target gene expression. For example, the Hox factor Ubx controls different sets of target genes at different times in *Drosophila* appendage development, as does the intestine-specifying factor CDX2 during gut development in mouse and humans (Kumar *et al.,* 2019; Pavlopoulos and Akam, 2011). Similarly, EGFR signaling promotes wing vein formation early in *Drosophila* larval development, whereas later in pupal stages, EGFR represses vein formation and instead promotes differentiation of the complementary intervein cells (Mart´ın-Blanco *et al.,* 1999). Thus, spatial inputs alone are insufficient to account for the sequence of gene expression and cell state changes that occur during development.

Temporal cues provide an additional axis of information that can increase the range of gene expression responses to spatial inputs. Some temporal cues come in the form of post-transcriptional regulators, such as lin-4, lin-28, and let-7 in *C. elegans*, which control transitions between developmental stages through regulation of RNA stability and translation efficiency (Pasquinelli and Ruvkun, 2002). Other temporal cues come in the form of developmentally restricted expression of transcription factors. For example, in mammals and in *Drosophila*, the diversity of cell types found in the adult nervous system depends on a temporal cascade of transcription factor expression in neural progenitor cells (Doe, 2017; Holguera and Desplan, 2018). Yet another means of temporal gene regulation involves systemically secreted signals that coordinate the timing of gene expression programs between distant tissues. Ecdysone signaling in insects and thyroid hormone-dependent metamorphosis in amphibians are classic examples of systemic signals that trigger temporal-specific gene expression changes during development.

Although it is clear that both spatial and temporal inputs are necessary for proper gene regulation during development, the mechanisms by which these inputs combine to control target enhancer activity are poorly understood. One potential mechanism for control of the responsiveness of enhancers to transcriptional inputs is regulation of chromatin accessibility. *In vivo*, the genome is packaged into chromatin. DNA that is wrapped around histone proteins to form nucleosomes is less accessible to transcription factor binding relative to free DNA. For many transcription factors to access their target sequences, nucleosomes must be depleted or remodeled. In principle, the relative accessibility of an enhancer could determine whether it is competent to respond to transcription factor input and thereby help to explain how transcription factors can be re-utilized during development with different transcriptional outcomes.

Recently, support for the role of chromatin accessibility in the integration of spatial and temporal factor inputs has emerged from examination of tissues at two different stages of development in *Drosophila*: neural diversification in the embryo and specification of appendage cell fates in the pupa (Sen *et al.,* 2019; Uyehara *et al.,* 2017). In the embryo, distinct neural stem cell lineages are determined by differential expression of spatial transcription factors. Within a given lineage, neural stem cells utilize

sequential expression of temporal transcription factors to produce progeny with distinct identities over time. Importantly, different neural lineages use the same set of temporal transcription factors to specify progeny identities. Using a lineage-specific method of generating genome-wide DNA binding profiles, the temporal transcription factor Hunchback was found to bind different target sites in different neural lineages. Moreover, these target sites correspond to lineage-specific patterns of open chromatin (Sen *et al.,* 2019). These findings indicate that the temporal factor Hunchback does not control open chromatin profiles and does not determine where it binds in the genome. Instead, they suggest that the spatial transcription factors expressed in neuroblasts control open chromatin profiles to drive lineage-specific binding of temporal transcription factors.

The ecdysone-induced transcription factor E93 provides a contrasting example of temporal transcription factor function. Similar to Hunchback's role in the embryonic nervous system, E93 functions as a temporal identity factor. E93 is activated during the transition from prepupal to pupal stages of metamorphosis, and E93 loss-of-function mutations exhibit defects in cell fates that are specified during this time (Baehrecke and Thummel, 1995; Mou *et al.,* 2012). Also similar to Hunchback, E93 combines with spatial cues to pattern cell fates. During specification of the pigmented bract cells during pupal leg development, E93 expression makes the Distal-less gene competent to respond to EGFR signaling (Mou *et al.,* 2012). However, in contrast to Hunchback, recent work from pupal wings suggest an essential role for E93 in regulating chromatin accessibility (Uyehara *et al.,* 2017). During metamorphosis, the wing undergoes dramatic morphological, cell fate, and gene expression changes to form the notum (back), hinge, and wing blade of the adult. Gene expression and chromatin accessibility profiling of larval wing imaginal discs and pupal wings 24-hours and 44-hours after puparium formation revealed that these changes coincide with sequential changes in open chromatin genome-wide (Guo *et al.,* 2016; Uyehara *et al.,* 2017). These chromatin accessibility changes strongly correlate with enhancer activity. Sites that open with time correspond to late-acting enhancers switching on, and sites that close with time correspond to early acting enhancers switching off. E93 binds many temporally dynamic open chromatin sites in pupal wings. Moreover, chromatin accessibility profiling of E93 mutants determined that E93 is required for temporal changes in chromatin accessibility and enhancer activity. In the absence of E93, early acting

target enhancers fail to close and fail to turn off. Conversely, late-acting target enhancers fail to open and fail to turn on (**Figure 3.1A**). These findings support a model in which E93 functions as a temporal identity factor by acting as a gatekeeper to the genome. In this model, E93 makes late-acting enhancers competent to respond to spatial inputs by increasing their accessibility, whereas it makes early acting enhancers refractory to spatial inputs by decreasing their accessibility, thus allowing for reutilization of spatial inputs.

In this study, we sought to address two major unanswered questions regarding E93-dependent control of enhancer activity. First, E93 appears to simultaneously coordinate the opening and activation of certain target enhancers while closing and deactivating others, however, the determinants of this context-specific activity are unknown. Second, we sought to determine the sufficiency of E93 expression to regulate target enhancers. Although E93 is required for sequential changes in chromatin accessibility, it is not known if E93 simply maintains accessibility changes initiated by other factors, or if it initiates these changes itself.

We took advantage of the temporal sequence of *Drosophila* wing development to investigate the limits of E93 function by expressing it at an earlier stage of wing development, prior to the endogenous E93 expression window. We find that precocious E93 expression alters the activity and accessibility of target enhancers, and that it can simultaneously trigger the activation and deactivation of different enhancers in the same cells. Genome-wide profiling demonstrates these findings are generalizable, and that precocious E93 expression accelerates the wild-type chromatin accessibility program. Finally, we find that not all E93 target enhancers respond to premature E93 expression in wing imaginal discs, even after prolonged exposure. However, these target enhancers become responsive to premature E93 later in prepupal wings, suggesting the requirement of additional temporal inputs that are independent of E93. Together, this work supports a model in which E93 expression defines a broad temporal window, providing competence of genes to respond to inductive signals by regulating chromatin accessibility at target enhancers.

3.2 Results

To help define the limits of E93's abilities to regulate enhancer activity and chromatin accessibility

we expressed E93 outside of its normal developmental context. In wild-type animals E93 expression is temporally regulated. E93 is off early in wing development, including third instar larvae. It is not until later during pupal stages that ecdysone signaling induces E93, with transcript levels peaking by 24-hours after the larval-to-pupal transition (24hr after puparium formation, 24hAPF) (**Figure 3.1B**, Uyehara *et al.,* 2017). Using tissue-specific GAL4 drivers in combination with a *UAS-E93* transgene and a ubiquitously expressed temperature-sensitive GAL4 repressor ($GAL80^{ts}$), we induced E93 in the wing imaginal disc of third instar wandering larvae (3rd Larval Wandering, 3LW), prior to when E93 is normally expressed (**Figure 3.1B**, **3.S1**, Bischof *et al.,* 2013). By switching between the permissive (22°C) and restrictive temperatures (29°C) for $GAL80^{ts}$, we limited the duration of exogenous E93 expression to 15–24 hours at the end of larval development. We refer to this as "precocious" or "premature" E93 expression. Immunofluorescence experiments with E93 antibodies indicated that precocious E93 levels in 3LW wing imaginal discs are approximately two-fold greater than endogenous E93 levels in pupal wings (**Figure 3.S1**). Thus, this experimental design allows us to determine the impact of near-physiological levels of E93 on enhancer activity and chromatin accessibility.

3.2.1 Precocious E93 expression is sufficient to deactivate a target enhancer

We first examined whether premature expression of E93 is capable of regulating target enhancer activity using a previously identified E93-bound enhancer from the *broad* (*br*) locus, which encodes a zinc-finger transcription factor. In wild-type larvae, the br^{disc} enhancer is active throughout the wing imaginal disc epithelium, with stronger activity in the pouch (**Figure 3.2A**). Later in pupal wings (24-40h APF), br^{disc} has turned off (**Figure 3.2A**). In E93 mutant wings the br^{disc} enhancer fails to turn off (Uyehara *et al.,* 2017). To test the impact of precocious E93 expression on br^{disc} activity, we expressed E93 in the anterior half of the wing imaginal disc with *ci-GAL4*. We found that br^{disc} activity is strongly reduced in E93-expressing cells relative to the wild-type posterior half of 3LW discs (**Figure 3.2B**). Control wing discs from larvae subjected to identical experimental conditions, but lacking the UAS-E93 transgene, showed no change in br^{disc} activity (**Figure 3.2B**). Similarly, discs from larvae of the experimental genotype, but not subjected to a 29°C shift, showed no induction of the E93 transgene or change in enhancer activity

(**Figure 3.S2**). We reasoned that E93-dependent repression of *br^{disc}* could result either from E93 blocking the initial activation of *br^{disc}*, or from E93 turning off *br^{disc}* after its initial activation. To discriminate between these possibilities, we assessed enhancer activity shortly after E93 induction. After only 5-hours at 29°C we observe induction of E93 in the anterior half of the disc, but no change in *br^{disc}* activity in E93-expressing cells relative to E93-nonexpressing cells (**Figure 3.2B**). Thus, precocious E93 triggers *br^{disc}* enhancer deactivation instead of simply blocking its activation. *En-GAL4* driven E93 expression in the posterior wing compartment resulted in similar *br^{disc}* deactivation (**Figure 3.S2**). Together, these findings demonstrate that E93 is capable of deactivating a target enhancer even when expressed at an earlier developmental stage.

3.2.2 Precocious E93 expression is sufficient to activate target enhancers

In addition to *br^{disc}*, we examined two E93-bound enhancers from the *tenectin* (*tnc*) locus that depend on E93 for proper activation in pupal wings (Uyehara *et al.,* 2017). *Tnc* encodes a constituent of the extracellular matrix that binds integrins (Fraichard *et al.,* 2010). In wild-type flies, the *tnc^{blade}* enhancer is inactive in larval wing imaginal discs. Later in pupal wings, *tnc^{blade}* is active in the tissue between the developing longitudinal wing veins (**Figure 3.2C**). It is also active at high levels in the body wall adjacent to the wing hinge. *Tnc^{blade}* activity co-localizes with expression of the proximal patterning factor Teashirt (Tsh) in these cells (**Figure 3.2C**). Precocious expression of E93 with *ci-GAL4* resulted in premature activation of *tnc^{blade}* in 3LW wing discs in a cluster of cells perpendicular to the anterior-posterior (AP) axis outside the pouch (**Figure 3.2D**). Staining for Tsh and Wingless (Wg) revealed that cells with premature *tnc^{blade}* activity are located in the proximal hinge and neighboring notum (**Figure 3.2D**, **3.S2**, Zirin and Mann, 2007). Similar activation of *tnc^{blade}* occurred in the posterior wing compartment upon precocious E93 expression using *en-GAL4* (**Figure 3.S2**). Control wing discs lacking the *UAS-E93* transgene showed no change in *tnc^{blade}* activity despite being shifted to 29^{o}C for 24-hours (**Figure 3.2D**). Discs with the *UAS-E93* transgene, but not shifted to 29^{o}C, likewise showed no change in enhancer activity (**Figure 3.S2**). Thus, premature E93 expression leads to activation of the *tnc^{blade}* enhancer in the presumptive proximal hinge and notum of wing imaginal discs. Notably, the pattern of precocious *tnc^{blade}* activation

resembles its wild-type pattern in pupal wings, indicating that the spatial inputs controlling *tnc^{blade}* in its normal developmental context are similar to those that control the enhancer when E93 is prematurely expressed.

We observed similar outcomes with a second enhancer from the *tnc* locus, the *tnc^{wv}* enhancer. In wild-type pupal wings, *tnc^{wv}* is active in 10-20 cells surrounding the developing veins, as indicated by phosphorylated Mothers Against Decapentaplegic (pMad) staining, a marker of active Dpp signaling (**Figure 3.2E**; de Celis, 1997). Like *tnc^{blade}*, *tnc^{wv}* is also dependent on E93 for activation (Uyehara *et al.,* 2017). Precocious expression of E93 with *ci-GAL4* resulted in premature activation of *tnc^{wv}* in E93-expressing cells flanking the dorsal-ventral (DV) boundary, adjacent to the AP boundary in the pouch of 3LW wing imaginal discs (**Figure 3.2F**). Notably, the pattern of precociously activated *tnc^{wv}* showed a high degree of overlap with strong pMad signal in these discs, similar to the overlap of *tnc^{wv}* with pMad in wild-type pupal wings (**Figure 3.2F**). Using *en-GAL4* to drive precocious E93 expression in the posterior compartment resulted in a similar pattern of precocious *tnc^{wv}* activity and similar overlap with active Dpp signaling (**Figure 3.S2**). Control larvae subjected to the same 29^{o}C shift, but without the *UAS-E93* transgene, showed no change in enhancer activity, as did larvae with the transgene that were kept at room-temperature (**Figure 3.2F**, **3.S2**). Thus, similar to our observations with the *tnc^{blade}* enhancer, these findings demonstrate that precocious E93 expression prematurely switches on late-acting pupal wing enhancers. Moreover, the pattern of premature enhancer activity appears to be guided by similar spatial signals as the wild-type pattern of activity observed later in development, consistent with the proposed role of E93 as a temporal competence factor.

3.2.3 Precocious E93 expression is not sufficient for activation of the *nub^{vein}* enhancer

Our observations with the br and tnc enhancers suggest that premature expression of E93 accelerates the developmental program active in pupal wings. However, not all E93 target enhancers are sensitive to precocious E93 expression. We previously identified the E93-bound *nub^{vein}* enhancer, which is normally inactive in early wings and becomes active in 24-hour pupal wings in an E93-dependent manner (**Figure 3.2G**; Uyehara *et al.,* 2017). However, in contrast to the tnc enhancers, precocious expression

of E93 with en-GAL4 does not activate *nub*^{vein} in wing imaginal discs (**Figure 3.2H**). We observed no difference in reporter activity in E93-expressing cells relative to their wild-type counterparts in the anterior compartment. Thus, for a subset of target enhancers, E93 expression can support activation outside of their normal developmental context. However, other target enhancers require regulatory inputs in addition to E93 for premature activation.

3.2.4 Precocious E93 binds late targets genome wide

To expand our understanding of E93's ability to regulate target enhancers outside of its normal developmental context, we next performed a series of genome-wide profiling experiments in which E93 was prematurely expressed throughout the 3LW wing imaginal disc (**Figure 3.S1**). We first performed ChIP-seq to define the DNA binding profiles of precocious E93. Comparison of ChIP-seq profiles for precocious E93 in early wings and endogenous E93 in 24-hour pupal wings (late E93 targets) revealed three distinct binding site categories: precocious E93 binding sites that overlap late E93 targets (entopic sites), precocious E93 binding sites that do not overlap late E93 targets (ectopic sites), and late E93 binding sites that do not overlap precocious E93 targets (orphan sites) (**Figure 3.3A**). 81% of endogenous late targets are bound by precocious E93, suggesting that the ability of E93 to recognize and bind most of its target sites is not dependent on a late-wing developmental context (**Figure 3.3B**). Notably, the *br*^{disc}, *tnc*^{blade}, and *tnc*^{wv} enhancers are all bound by precocious E93, consistent with their responsiveness in reporter assays (**Figure 3.4D-E**). By contrast, the *nub*^{vein} enhancer exhibits low-level binding of precocious E93, indicating that its failure to respond may be due to the inability of E93 to bind *nub*^{vein} in early wings (**Figure 3.5E**).

The presence of ectopic and orphan binding sites suggests E93 binds to these sites in a context- specific manner. We first compared the levels of E93 ChIP-seq signal between these peak categories. Precocious E93 exhibits increased signal at entopic sites relative to ectopic sites in 3LW wing imaginal discs (**Figure 3.3C**). Additionally, endogenous E93 exhibits decreased signal at orphan sites relative to entopic sites in 24h pupal wings. We therefore sought to define the features that may explain these differences in E93 binding. We observed no difference in the distribution of E93 peaks

between binding site categories, demonstrating that localization to specific genomic regions is not a feature that discriminates orphan and ectopic binding sites from entopic sites (**Figure 3.S3A**). By contrast, examination of chromatin accessibility at these sites during wild-type development revealed differences between peak categories. Orphan sites are less accessible in early wings but increase in accessibility in late wings (**Figure 3.3B, C**), suggesting that low accessibility may prevent E93 binding in 3LW wing discs. However, many ectopic sites also exhibit low accessibility in 3LW wing discs. Thus, chromatin accessibility may explain some, but not all of the observed differences in E93 binding.

We next sought to determine whether the different E93 binding categories reflect differences in DNA sequence. First, we examined the E93 motif itself and detected no differences in E93 motif enrichment, quality, or positioning in ectopic and orphan sites relative to entopic sites (**Figure 3.3D, E, Figure 3.S4**). Consistent with these findings, position-weight matrices (PWM's) derived from E93 motifs within each binding category are nearly identical to each other (Pearson's R > 0.98) (**Figure 3.S4B, C**). We conclude that the E93 motif is not the primary determinant of the observed differences in binding. We also performed both de novo and directed motif analyses to determine whether other DNA sequence motifs distinguish ectopic, entopic, and orphan categories (**Figure 3.S5**). We observed very few differences in motif content between E93 peak categories. Orphan peaks exhibit modest enrichment for homeodomain factor motifs, ectopic peaks are weakly enriched for motifs for the paralogous transcription factors Nub and Pdm2, and entopic peaks exhibit weak enrichment for the zinc finger factors Crol and Pad. While the functional significance of these motifs is unclear, the overall assessment is that DNA sequences within each E93 binding site category are highly similar. Only a small amount of differential E93 binding can be explained by the presence of particular transcription factor motifs. Other reasons for the existence of ectopic and orphan peaks include the use of different antibodies in the precocious E93 experiments relative to the endogenous E93 ChIP-seq performed in 24h pupal wings, and the higher levels of E93 expression in the precocious experimental system.

3.2.5 Precocious E93 expression is sufficient to regulate chromatin accessibility

The ChIP-seq data described above demonstrate that a large majority of targets bound by

endogenous E93 in late wings are also bound by precocious E93 in early wings. We next sought to determine the impact of precocious E93 binding on chromatin accessibility. Our prior findings from E93 mutant wings suggested that E93 may function as a competence factor by controlling chromatin accessibility at target enhancers. To further test this model, we performed FAIRE-seq to generate genome-wide open chromatin profiles in wing imaginal discs precociously expressing E93. Comparison of these profiles with wild-type wing imaginal disc FAIRE-seq profiles revealed extensive changes in open chromatin. Using conservative thresholds to define differentially accessible sites bound by E93 (DESeq2 adjusted p value < 0.05 and $\log_2$ fold change 1), we identified 282 sites that decrease in accessibility, 846 sites that increase in accessibility, and 7,376 sites that remain static in response to premature E93 expression (**Figure 3.4 A-C**). Notably, the ratio of sites that open relative to those that close in precocious E93 early wings is similar to the ratio of sites that depend on E93 for opening and closing in wild-type late wings previously identified in E93 loss-of-function experiments (Uyehara *et al.,* 2017). This indicates that the ability of precociously expressed E93 to open chromatin relative to its ability to close chromatin is similar to the abilities of endogenous E93 to regulate chromatin accessibility, despite being expressed outside of its normal developmental context.

To determine the impact of the observed changes in chromatin accessibility induced by premature E93 expression on transcriptional regulation, we examined FAIRE-seq profiles at E93 target enhancers described above. Accessibility of the br^{disc} enhancer strongly decreases in precocious E93 wing discs (**Figure 3.4D**), consistent with its deactivation in transgenic reporter assays. The br^{disc} enhancer normally closes between L3 and 24-hour pupae, raising the question as to whether any of the other 281 sites that decrease in accessibility in response to premature E93 expression also close over time in wild-type wings. Remarkably, 95% of sites that decrease in accessibility in precocious E93 wing discs also decrease in accessibility during wild-type development (**Figure 3.4G**), suggesting that premature E93 expression recapitulates the normal sequence of enhancer closing. Examination of FAIRE-seq profiles at the tnc enhancers revealed changes in chromatin accessibility that were also consistent with the effects of precocious E93 expression on transgenic reporter activity. Tnc^{wv} and to a lesser extent tnc^{blade} increase in accessibility in response to precocious E93, consistent with the activation of both enhancers

in transgenic reporter assays (**Figure 3.4E**). At the genome-wide level, 73% of the sites that increase in response to precocious E93 expression also increase in accessibility during wild-type development (**Figure 3.4H**). Thus, the directionality of chromatin accessibility changes in wings prematurely expressing E93 is preserved relative to the sequential changes in accessibility that normally occur in wild-type wings. This indicates that E93 expression functions as an instructive cue that triggers a response in enhancer accessibility. However, the directionality of this response is not determined by E93.

3.2.6 DNA sequence partially explains differential effects on chromatin accessibility

Although E93 expression is sufficient to change chromatin accessibility at a subset of its target sites (hereafter, E93 “sensitive” sites), E93 does not determine whether target sites increase or decrease in accessibility. The concordance in accessibility changes between precocious E93 and wild-type development suggests the accessibility determinant is either pre-existing on the chromatin or is encoded in the DNA sequence of target enhancers. To test for pre-existing regulatory information, we examined histone post-translational modifications (PTMs) from wild-type 3LW wings (Schertel *et al.,* 2015). We find that specific histone PTMs do not closely correlate with chromatin accessibility changes at E93 target sites (**Figure 3.S6**). E93-sensitive sites that decrease in accessibility (“decreasing E93-sensitive” sites) exhibit modestly higher average levels of histone PTMs correlated with active transcription (**Figure 3.S6A**), such as H3K4me1 and H3K27ac, consistent with these sites being open and active regulatory elements in 3LW wings. However, many decreasing E93-sensitive sites do not exhibit high levels of these PTMs (**Figure 3.S6A–C**), indicating that active histone PTMs are not required for E93 to close chromatin. Conversely, high levels of active histone PTMs are found at many E93 binding sites that do not change in accessibility in precocious E93 wings (E93 “insensitive” sites), indicating that the presence of active histone PTMs does not necessitate closing of chromatin upon E93 binding. Sites that increase in accessibility upon E93 binding (“increasing E93-sensitive” sites) likewise do not exhibit a clear correlation with histone PTMs. Most increasing E93-sensitive sites lack enrichment of histone PTMs, indicating they are not pre-marked for activation at this stage. However, the absence of histone PTMs does not necessitate opening of chromatin upon E93 binding because many decreasing E93-sensitive

and insensitive sites also lack histone PTM enrichment. We conclude that histone PTMs are not the main determinants controlling the differential effects of E93 on chromatin accessibility. Instead, histone PTMs likely reflect the regulatory state of the DNA.

We next examined the DNA sequence of E93-sensitive sites relative to E93-insensitive sites by de novo motif discovery. Decreasing E93-sensitive sites are enriched > 2-fold for E93 binding site motifs relative to E93-insensitive sites (**Figure 3.S7A, B**). Targeted E93 motif analysis revealed that decreasing sites exhibit both greater motif quality and a greater number of E93 motifs relative to increasing E93-sensitive sites or E93-insensitive sites (**Figure 3.S8A-C**). We do not detect enrichment of the E93 motif within increasing E93-sensitive sites relative to E93-insensitive sites, likely due to equal enrichment of the E93 motif observed between increasing and static sites (**Figure 3.S8A**). Instead, increasing E93-sensitive sites are enriched for motifs matching the zinc finger transcription factors Br-Z2 (1.4-fold enriched), and Crol (1.3-fold enriched) (**Figure 3.S9A, B**). Both br and crol are ecdysone target genes with essential roles in wing development (D'Avino and Thummel, 2000; Schubiger *et al.,* 2005). Br expression is high in larval wings when these sites exhibit low accessibility, and it decreases during the larval-to-pupal transition when these sites increase in accessibility in wild-type wings (Guo *et al.,* 2016). Thus, over-representation of Br motifs in increasing E93-sensitive sites suggests a role for Br in keeping pupal regulatory element chromatin inaccessible in larval wings. Crol is expressed at similar levels in both 3LW and pupal wings, and the enrichment of Crol motifs in both entopic E93 sites and increasing E93-sensitive sites suggests Crol may work with E93 to bind DNA (**Figure 3.S5, 3.S9, 3.S10**, Uyehara *et al.,* 2017). Supporting a potential combinatorial role for E93 and Crol in pupal gene regulation, E93 and crol mutants exhibit similar wing defects, including loss of adhesion and abnormal venation (D'Avino and Thummel, 2000; Mou *et al.,* 2012). Together, these analyses indicate that the differential effects of precocious E93 on chromatin accessibility are at least partially explained by differences in DNA sequence composition of E93 target sites.

3.2.7 Developmental context informs the response of *nub^{vein}* to precocious E93

Although approximately 1,100 sites change in accessibility in response to premature E93

expression, the majority of E93-bound sites do not change in accessibility in early wings even though many are dynamic during wild-type development (**Figure 3.4C,F,I**). The *nub*^{vein} enhancer is representative of this category in that it depends on E93 for opening in pupal wings, but it fails to activate or open in response to precocious E93 expression in larval wing discs (**Figure 3.2G, 3.5E**, Uyehara *et al.,* 2017). We considered the possibility that *nub*^{vein} requires prolonged E93 exposure, relative to E93-sensitive enhancers such as *tnc*^{blade}, in order to become responsive. Prolonged exposure might allow time for E93-initiated events to occur, such as induction of a coregulator. To test this hypothesis, we doubled the duration of *nub*^{vein} exposure to E93 (from 24-hours to 48-hours) by inducing E93 expression earlier in wing development and then dissecting at the same developmental stage as before (3LW) (**Figure 3.5A**). Despite the prolonged exposure to E93, we still observed no change in *nub*^{vein} reporter activity (**Figure 3.5B**). We next examined the possibility that E93 may require additional developmental inputs in order to activate the *nub*^{vein} enhancer. To test this hypothesis, we precociously expressed E93 for the same duration as in our initial experiments (24-hours), but instead of dissecting at 3LW, we dissected 12-hours later (mid-prepupal wings at 5hAPF). Using this experimental design, we detected clear activation of the *nub*^{vein} reporter in a subset of E93-expressing cells (**Figure 3.5D**). Thus, the ability of the *nub*^{vein} enhancer to respond to precocious E93 is dependent on developmental context. It does not respond to E93 in third instar larvae regardless of the duration of E93 expression. However, it does respond to E93 in prepupal wings, suggesting a change in the regulatory environment during the larval-to-prepupal transition makes *nub*^{vein} competent to respond to E93.

3.2.8 Temporal dynamics of chromatin accessibility indicate context-dependent roles for E93

The findings described above indicate that precocious E93 expression controls accessibility and activity of some target sites, but other targets require additional developmentally regulated inputs in order to respond to E93. To gain insight into the extent to which developmental context influences E93 target site responsivity, we examined the timing of chromatin accessibility changes in wild-type wings. Clustering of FAIRE-seq data for E93-bound sites across six time points in wild-type wing development revealed eight distinct temporal chromatin accessibility profiles (**Figure 3.6A**). Notably, the *br*^{disc}, *nub*^{vein},

and tnc enhancers fall into different clusters. Br^{disc} falls into cluster 2 with other E93 targets that close between 6 and 18-hours hAPF (**Figure 3.6B**). The tnc^{blade} and tnc^{wv} enhancers fall into cluster 3 with other E93 targets that open between 6 and 18hAPF (**Figure 3.6B**). Finally, the nub^{vein} enhancer falls into cluster 5 with other E93 targets that open even later in pupal wing development (**Figure 3.6B**). Since each of these enhancers is a bona fide E93 target, their separation into different clusters suggests that E93 regulates target enhancers over a relatively wide range of prepupal and pupal wing development. Supporting this interpretation, western blotting of wild-type wings at six-hour intervals surrounding the larval-to-pupal transition demonstrate that E93 expression overlaps the time points that exhibit changes in chromatin accessibility (**Figure 3.6C**). These findings indicate that E93 functions over a broad window of development to control enhancer activity and accessibility, and that this broad window is subdivided into narrower windows through interactions with other developmentally regulated factors.

To identify potential coregulators that subdivide E93 activity during wild-type development, we looked for enrichment of transcription factor motifs in each temporally dynamic cluster (clusters 1–5) relative to all other dynamic clusters. Targeted motif scanning identified motifs with differential enrichment across clusters (**Figure 3.S10**). Several of these transcription factors have documented roles in controlling developmental timing. For example, Br motifs are enriched in clusters 3, 4, and 5, which contain E93 targets that open at sequential times after the larval-to-pupal transition. As discussed above, Br expression drops during the larval-to-pupal transition, supporting a potential role for Br in keeping pupal regulatory DNA inaccessible in larval and prepupal wings. Differential motif enrichment for other transcription factors involved in coordinating developmental timing include Ultraspiracle, E74, and Abrupt. We also detect differential enrichment of motifs for transcription factors downstream of signaling pathways, including Enhancer of Split, Pointed, and Mad, as well as wing patterning factors such as Mirror, Nubbin, Scalloped, and Rotund. Finally, we identify strong motif enrichment for Zelda (Zld) in cluster 1, which contains sites that are accessible only in larval wing discs. Zld is a putative pioneer factor required for chromatin accessibility in early *Drosophila* embryos (Schulz *et al.,* 2015). Intriguingly, Zld is also expressed in the larval wing, and its transcript levels drop 8-fold during the larval-to-prepupal transition (**Figure 3.S11**, Hamm *et al.,* 2017). The coincident decrease in accessibility of cluster 1 peaks

suggests Zld may also have a role in wing development. Thus, a combination of temporal and spatial transcription factors may work with E93 to control accessibility and activity of target enhancers at distinct stages of wing development.

3.3 Discussion

3.3.1 Temporal transcription factors as determinants of developmental competence

Spatial cues are iteratively used during development to produce distinct transcriptional outcomes. Many of these spatial inputs come in the form of transcription factors that are expressed at multiple stages of development. However, it is unclear how these factors regulate their given targets only at select times. The findings presented in this study indicate that E93 expression provides competence for target enhancers to respond to spatially restricted inputs. Premature expression of E93 in larval wings switches on the *tnc*^{blade} enhancer in Tsh-expressing cells of the proximal hinge, similar to its wild-type activity pattern in the hinge later in pupal wings. Likewise, larval E93 expression switches on the *tnc*^{wv} enhancer in cells with high pMad levels, similar to its wild-type pattern in pupal wing veins. Notably, neither of these enhancers becomes active in all cells that precociously express E93. Instead, precocious E93 expression activates these enhancers only in populations of cells that appear to receive similar spatial inputs as those in which they normally become active later in development. This suggests that E93 is the limiting factor that enables these enhancers to respond to spatial cues that are used at multiple stages of development. This interpretation is consistent with prior demonstration that E93 expression makes the Distal-less gene competent to respond to EGFR signaling in the leg (Mou *et al.,* 2012). Importantly, like the spatial cues that regulate the tnc enhancers, the EGFR pathway is active in both early and late legs, and yet EGFR is only capable of activating Distal-less in the presence of E93. Thus, the spatial cues present prior to E93 expression are insufficient to activate their target enhancers, indicating that E93 is the key determinant for unlocking their activities.

The findings presented here provide new insight into the means by which E93 controls enhancer competence. ChIP-seq demonstrates that E93 binds directly to target enhancers. FAIRE-seq in wings precociously expressing E93 reveals that E93 binding results in chromatin accessibility changes.

Together, these findings support a model in which E93 functions as a temporal cue by binding target enhancers and triggering local changes to the chromatin accessibility landscape. Importantly, we observe that E93 initiates distinct effects on chromatin accessibility depending on the target enhancer. At a subset of targets, E93 expression results in increased chromatin accessibility, which may enable binding of other transcription factors that control the spatial pattern of enhancer activity. However, at a different subset of enhancers that is already accessible, E93 expression results in decreased chromatin accessibility. Loss of accessibility may make these enhancers refractory to transcription factor binding and enable redeployment of spatial inputs to other targets. Thus, by controlling the accessibility and consequently the competence of *cis*-regulatory elements to respond to spatial inputs, temporal transcription factors like E93 help to control the sequence of gene expression changes that drive development forward in time.

3.3.2 Does E93 control chromatin accessibility on its own, or in combination with other factors?

Although E93 binds directly to target enhancers, this does not mean that E93 controls chromatin accessibility independently of coregulators. The findings presented in this study suggest a model in which other transcription factors influence the ability of E93 to regulate target enhancer accessibility. Several lines of evidence support this interpretation. First, only a fraction of E93-bound sites exhibit a change in accessibility in response to precocious E93 expression, even though many of them exhibit temporal changes in accessibility that are dependent on E93 later in development. Our motif analyses raise the intriguing possibility that some of E93's effects on target chromatin may be limited by other transcription factors in the ecdysone cascade. Motifs for the temporal transcription factor Br are enriched in E93 targets that open during pupal stages. In wild-type wings, br is induced by ecdysone to high levels during larval stages when these sites are inaccessible. Br levels subsequently drop as pupal development progresses, coincident with these sites increasing in accessibility (Guo *et al.,* 2016). Thus, it is possible that Br antagonizes E93 function by maintaining pupal enhancers in an inaccessible chromatin state during larval stages. Since E93 deactivates the br^{disc} enhancer, E93-mediated repression may contribute to the drop in Br levels in prepupal wings. Examples of cross-regulation between ecdysone-induced transcription factors have been previously reported (Mao *et al.,* 2019; Uren˜a *et al.,* 2016). Thus, some

effects of E93 on chromatin accessibility may be indirectly mediated by cross-regulatory interactions between temporal transcription factors.

A second observation supporting a role for coregulators in E93-dependent control of chromatin accessibility is that the *nub*^{vein} enhancer only responds to E93 after the larval-to-prepupal transition. Although *nub*^{vein} depends on E93 for opening and activation in wild-type pupal wings, precocious E93 expression in larval wings does not result in *nub*^{vein} activation or in increased chromatin accessibility. *Nub*^{vein} remains inactive even with prolonged exposure to E93 at larval stages, suggesting that its activation is not dependent on a downstream effector of E93 activity. Instead, *nub*^{vein} exhibits precocious activity only after progression through the larval-to-prepupal transition. This switch in responsivity of *nub*^{vein} as a function of developmental stage rather than duration of E93 exposure indicates that there is a change in the trans-regulatory environment that occurs independent of E93 activity. One potential trans-regulatory change is fluctuating titers of ecdysone. In Bombyx, E93 binds the ecdysone hormone receptor, EcR/Usp, through its LXXLL nuclear receptor interaction motif (Liu *et al.,* 2015). Hormone binding triggers conformational changes in nuclear receptors that result in differential recruitment of coregulatory proteins (Glass and Rosenfeld, 2000), and decreasing ecdysone levels during the larval-to-prepupal transition could cause differential association of E93 with EcR/Usp complexes, thus making target enhancers such as *nub*^{vein} dependent on circulating ecdysone titers.

An additional observation suggesting E93 works with other factors to control chromatin accessibility is the finding that E93 targets do not all experience changes in accessibility at the same time. Clustering of FAIRE-seq data at E93 binding sites from six stages of wild-type wing development revealed distinct temporal patterns of accessibility change. Moreover, these temporal clusters exhibit differential enrichment of transcription factor DNA binding motifs that correspond to transcription factors with varied spatial and temporal functions. This suggests that E93 works in combination with a diverse and dynamic set of coregulators during pupal wing development to trigger multiple phases of chromatin accessibility regulation. Overall, we envision a model wherein E93 expression functions as a temporal cue that makes target enhancers competent to respond to spatial gene regulatory inputs; other transcription factors that bind with E93 at target enhancers dictate the effect E93 has on chromatin accessibility (**Figure 7**).

3.3.3 Activation and deactivation by E93

While it is clear that transcription factors often possess both activating and repressing roles, the determinants of this context-specific function are poorly understood. In this study, we find that E93 expression both activates and represses different target enhancers in the same cells at the same time. The br^{disc} enhancer is active across larval wing discs. This enhancer is closed and deactivated in response to precocious E93 expression. Conversely, the tnc^{blade} and tnc^{wv} enhancers are opened and activated in response to precocious E93 expression. The pattern of br^{disc} overlaps the activity pattern of both tnc enhancers, thus strongly indicating that E93 expression is able to enact two opposing transcriptional outputs (activation and deactivation) simultaneously during development. Chromatin accessibility profiling indicates that E93 opens and closes chromatin at hundreds of loci when expressed in larval wings. Thus, the E93-mediated cue to increase or decrease accessibility at target enhancers is not exclusively due to stage-specific expression of coregulators or a temporally regulated modification of E93 that makes it a dedicated activator or repressor. Instead, how a site responds to E93 is target specific. This is supported by the observation that sites which open or close in response to precocious E93 largely replicate the accessibility changes they normally exhibit during wild-type development. Thus, premature expression of E93 accelerates a regulatory program that is encoded in the DNA sequence of target enhancers. To gain insight into how E93 differentially regulates enhancer accessibility, we examined the DNA sequence of E93-sensitive sites. This analysis revealed that sites that decrease in accessibility in response to E93 binding contain higher quality as well as a greater number of E93 motifs relative to increasing E93-sensitive sites or E93-insensitive sites. Characteristics such as motif quality and quantity can determine whether a transcription factor activates or represses target enhancers (Parker *et al.,* 2011; Scully, 2000; White *et al.,* 2016). Thus, differential E93 motif composition could serve as a key determinant for the opposing effects E93 has on target chromatin. Increased E93 motif content in decreasing E93-sensitive sites could indicate that control of chromatin accessibility at these sites occurs independently of other transcription factors. However, we disfavor this hypothesis because it predicts that decreasing sites would be disproportionately enriched relative increasing sites amongst E93-sensitive regions. Comparing the ratio of decreasing to increasing sites reveals no differences in E93-sensitive

sites relative to E93-dependent sites. Thus, E93 is no more likely to close chromatin as it is to open, suggesting both types of target are equally dependent on coregulators. Further studies are necessary to identify the coregulator proteins used by E93 to differentially control chromatin accessibility. Identifying these factors will help reveal the mechanisms controlling enhancer competence in development.

3.4 Materials & Methods

3.4.1 *Drosophila* culture and genetics

Either ci-GAL4 or en-GAL4 lines were used for enhancer experiments with similar effects on reporter activity. Crosses were raised at 22ºC and vials were shifted to 29ºC for 24-hours to induce E93 expression, unless otherwise indicated. For the experiments presented in **Figure 3.2B** (Early L3), larvae were dissected 5-hours after the shift to 29°C. For the experiments presented in **Figure 3.5B**, larvae were dissected 48-hours after the shift to 29ºC. Wandering third instar larvae were dissected for all experiments, except for the experiments presented in **Figure 3.5D**, in which mid-prepupae (5-7h APF) were collected after 24-hours of E93 induction. The vg-GAL4, Tub>CD2>GAL4, UAS-GFP, UAS-FLP; GAL80ts driver was used for FAIRE-seq and ChIP-seq. Embryos were collected for 6-hours on apple plates at 25ºC and then transferred to 29ºC for 36-hours. GFP-positive larvae then were picked, transferred to vials, and raised for 4.5 days at 18ºC. Vials were then switched back to 29ºC for 15-hours to induce E93 expression. Wandering third instar larvae were dissected.

3.4.2 Fly stocks used:

w; Tub-GAL80ts; tm2/tm6b (BDSC 7108)

w; Tub-GAL80ts; tm2/tm6b (BDSC 7108)

yw; UAS-E93-3xHA (FlyORF F000587, Bischof *et al.,* 2013)

yw; vg-GAL4, UAS-FLP, UAS-GFP, Tub>CD2>GAL4 / CyO (Crickmore and Mann, 2006)

yw; en-GAL4 (Gift of Greg Matera)

yw; ci-GAL4 (Gift of Robert Duronio)

yw; broad^{disc}-tdTomato (Uyehara *et al.,* 2017)

yw; nub^{vein}-nlsGFP (Uyehara *et al.,* 2017)

yw; tnc^{wv}-tdTomato (Uyehara *et al.,* 2017)

yw; tnc^{blade}-tdTomato (Uyehara et al., 2017)

3.4.3 Immunofluorescence and image analysis

Immunofluorescence experiments and confocal imaging were performed as previously described (McKay and Lieb, 2013). The following antibodies were used: rabbit anti-E93 (1:2500, Uyehara *et al.,* 2017), mouse anti-HA (1:1000, Sigma H3663), rabbit anti-HA (1:500, Abcam ab9110), guinea pig anti-Teashirt (1:1000, Zirin and Mann, 2007), mouse anti-Wingless (1:25, DSHB 4D4), rabbit anti-Smad3 (phospho S423 + S425) (pMad, 1:200, Abcam ab52903). Alexafluor secondary antibodies (Invitrogen) were used at 1:1000. Precociously expressed E93 and endogenous E93 at ˜30h APF were quantified by immunofluorescence using anti-E93 and Alexa 633 secondary. Fluorescent intensity was measured using ImageJ (Schindelin *et al.,* 2012). WT 30h APF pupal wings were combined with 3LW wing imaginal discs precociously expressing E93 in the same tube for antibody incubations, then mounted on the same slide and imaged with identical settings (Leica Confocal SP5). E93 levels were quantified by measuring mean grey value in 25x25 pixel selections (10 selections per wing and 3 wings each). E93 signal was normalized by dividing by the mean background, which was calculated from 9 25x25 pixel selections in E93-negative portions of tissue in each experiment.

3.4.4 High throughput sequencing & data analysis

FAIRE-seq and ChIP-seq were performed as previously described (Uyehara 2017). Briefly, ChIP experiments were performed in duplicate using a minimum of 200 wings for each replicate. Control genotypes contained the GAL4 driver but lacked the UAS-E93-3xHA transgene. Immunoprecipitation was performed using 5 µg of Rabbit anti-HA (Abcam, ab9110). FAIRE-seq in precocious E93- expressing wings was performed using 45–60 wings in duplicate. Reads were aligned to the dm3 reference genome with Bowtie2 (Langmead and Salzberg, 2012). ChIP peaks were called with MACS2 (Zhang *et al.,* 2008) on each replicate using as background reads from the control genotype (precocious E93 experiments) or from a sonicated genomic DNA library (wild-type 24hAPF E93). ChIP peaks that overlapped between

biological replicates were used for analysis. E93 binding categories were identified by intersecting the resulting peak lists from precocious E93 ChIP and wild-type E93 ChIP using the ChIPpeakAnno package from bioconductor (Gentleman *et al.,* 2004; R Core Team, 2017). Summits from the resulting union ChIP peak list were recomputed from aligned reads from pooled replicates using FunChip (setting d = 125) (v1.0.0) (Parodi *et al.,* 2017). Summits from entopic and orphan sites were computed from wild-type late E93 ChIP-seq, while summits from ectopic sites were computed from precocious E93 ChIP. Chromatin accessibility differences within precocious E93 ChIP peaks were identified by counting FAIRE-seq reads within the union set of E93 ChIP peaks using featureCounts (setting allowMultioverlap = T) from Rsubread and testing for differential accessibility with DESeq2 using an adjusted p value < 0.05 and an absolute $\log_2$FoldChange > 1 (Liao *et al.,* 2019; Love *et al.,* 2014). Concordance of precocious chromatin accessibility changes with wild-type chromatin accessibility changes was determined using DESeq2, using an adjusted p value < 0.05. Average signal line plots were generated using seqplots and ggplot2 from z-score normalized bigwig files at 10 base-pair resolution (Stempor and Ahringer, 2016; Wickham, 2009). Signal tracks were rendered in R with Gviz and cowplot (Hahne and Ivanek, 2016; Wilke, 2017). Overlap of ChIP peaks with genomic feature annotations was performed with ChIPseeker (v1.5.1), using the TxDb.D*melanogaster*.UCSC.dm3.ensGene annotation package from Bioconductor (Carlson, 2015).

3.4.5 Motif scanning

The dm3 assembly of the *Drosophila melanogaster* genome was scanned for the E93 motif from the FlyFactor Survey database using FIMO v4.12.0 (setting –thresh 0.01 –max-strand –text –skip-matched-sequence) (Grant *et al.,* 2011; Zhu *et al.,* 2011). Motifs overlapping a 20-base pair window around ChIP peak summits were identified using GenomicRanges findOverlaps (Lawrence *et al.,* 2013). Motif number per window was quantified by directly counting these overlaps. For each peak category, motif quality within these windows was compared by using the ‘oneway.test’ function in R. Motif centrality within peaks was compared by computing the distance from each peak summit to the nearest E93 motif, then comparing the distribution of distances between binding categories using the ks.test function in R. PWMs of matched E93 motifs from within binding categories were derived by returning the DNA sequence

matching each E93 motif detected within each peak. Sequences were converted to PWMs using the ‘PWM‘ function from Biostrings, then converted to PFMs using the toPFM function from PWMEnrich (v4.10.0) (Page`s *et al*.; Stojnic and Diez, 2016). Sequence logos were rendered using ggseqlogo (Wagih, 2017). Similarity of rederived E93 motifs was compared using a version of the TFBSTools PWMPearson internal function modified to accept PFMs (Tan and Lenhard, 2016). Motif similarity heatmaps in S4D were rendered using ComplexHeatmap (Gu *et al.,* 2016).

3.4.6 De novo motif analysis

DREME (v4.12.0) was used to scan a 100bp region around each E93 ChIP peak summit within each E93 binding category using shuffled input sequences as background (using: dreme-py3 -dna -e 0.05 -m 10 -mink 3 -maxk 8) (Bailey, 2011). For analysis within E93 sensitive sites, the same analysis was performed within a 200bp window around peak summits. Discovered motifs were imported into R using the importMatrix function from motifStack (v1.29.8) (Ou *et al.,* 2018). Similarity values for discovered motifs were determined using the motifSimilarity function from PWMEnrich on all pairwise combinations of discovered motif(Stojnic and Diez, 2016). Clustering of PWM similarity was also performed by heirarcical clustering of motif distances computed using MotIV (v1.30.0) functions ‘motifDistances‘ and ‘motifHclust‘ (Mercier and Gottardo, 2014). Clustered tree was rendered using ggdendro, ggseqlogo, and cowplot (de Vries and Ripley, 2016; Wagih, 2017; Wilke, 2017). Discovered motifs were matched to motifs from the Fly Factor Survey using TOMTOM (v4.12.0, using: tomtom -no-ssc -min-overlap 5 -dist “pearson” -evalue -thresh 10.0), displayed matches represent those corresponding to the top hit from this analysis (Gupta *et al.,* 2007).

3.4.7 Targeted motif analysis

Directed motif searches were performed using AME (v5.1.0, setting: ame –scoring avg –method fisher –hit-lo-fraction 0.25 –evalue-report-threshold 10) to scan a 200 bp region around E93 binding category summits (using all ChIP peaks as background) and E93 sensitive summits (insensitive sites used as background). Searches within dynamic clusters were performed using a 100bp window around the summit of each dynamic cluster, using all other dynamic clusters as background. For all analyses PWMs from the entire Fly Factor Survey were used for detection. All results were first filtered to remove

any motifs from TFs with FPKM values < 5 in wings during our wild-type RNAseq timecourse, reasoning that TFs passing this threshold are more likely to be functional during wing development (GSE77562).

3.4.8 Analysis of histone modifications

Data from GSE59769 were processed as described above for ChIP-seq (Schertel *et al.,* 2015). Bigwigs were generated at 10bp resolution and z-score normalized for analysis. Signal within target regions was extracted using seqPlots for heatmaps and average signal plots (Stempor and Ahringer, 2016). Heatmaps were generated using EnrichedHeatmap (Gu *et al.,* 2018).

3.4.9 Western blotting

Wing discs were dissected from E93-GFSTF animals at 6-hour intervals relative to puparium formation by staging animals as white prepupae (3LW larvae were used as the –6h timepoint). Western blots were performed as previously described, with the following changes. 20 wings were collected per timepoint and stored at -80 °C. Samples were lysed in hot Laemmli sample buffer (Leatham-Jensen *et al.,* 2019; Uyehara and McKay, 2019). Samples were run for 60-minutes at 100 V on a 7.5% Biorad stain-free TGX gel. Total protein stains were collected by laying the PAGE gel directly onto a UV transilluminator for 3 minutes and imaged on an Amersham Imager 600; the gel was kept hydrated with distilled water during all total protein crosslinking and imaging steps. After imaging the total protein stain, protein was transferred to a 0.2 µm nitrocellulose membrane at 100 V for 60 minutes. E93-GFSTF protein was detected using rabbit-anti-GFP (1:5000, abcam ab290), HRP-conjugated secondary (1:10000 donkey anti-Rabbit-HRP, GE Healthcare #NA934V) and Amersham ECL prime detection kit (GE healthcare, RPN2232). Blots were imaged on an Amersham Imager 600. Signals were quantified with FIJI. Each of three replicates were scaled first to total protein then relative to the maximum E93 signal (24h APF) for quantification.

3.5 Acknowledgements

We thank Daphne Knudsen for assistance with E93 western blots, Mary Leatham-Jensen for help with FAIRE and ChIP experiments, Jill Dowen and Greg Matera for critical reading of the manuscript, and members of the McKay and Dowen labs for useful discussions. The Wg antibody, developed by Steve Cohen, was obtained from the Developmental Studies Hybridoma Bank, created by the NICHD of the NIH

and maintained at The University of Iowa, Department of Biology, Iowa City, IA 52242. Stocks obtained from the Bloomington *Drosophila* Stock Center (NIH Grant P40OD018537) were used in this study.

3.6 Competing Interests

No competing interests declared

3.7 Funding

M.J.N. was supported in part by NIH Grant T32GM007092 and an NSF GRFP Award. This work was supported in part by Research Scholar Grant RSG-17-164-01-DDC to D.J.M from the American Cancer Society, and in part by Grant R35-GM128851 to D.J.M. from the National Institute of General Medical Sciences of the NIH (https://www.nigms.nih.gov/).

3.8 Data availability

Data generated from this study can be found using GEO accession number GSE141738. All code used for data processing and analysis will be made available upon request.

3.9 Figures

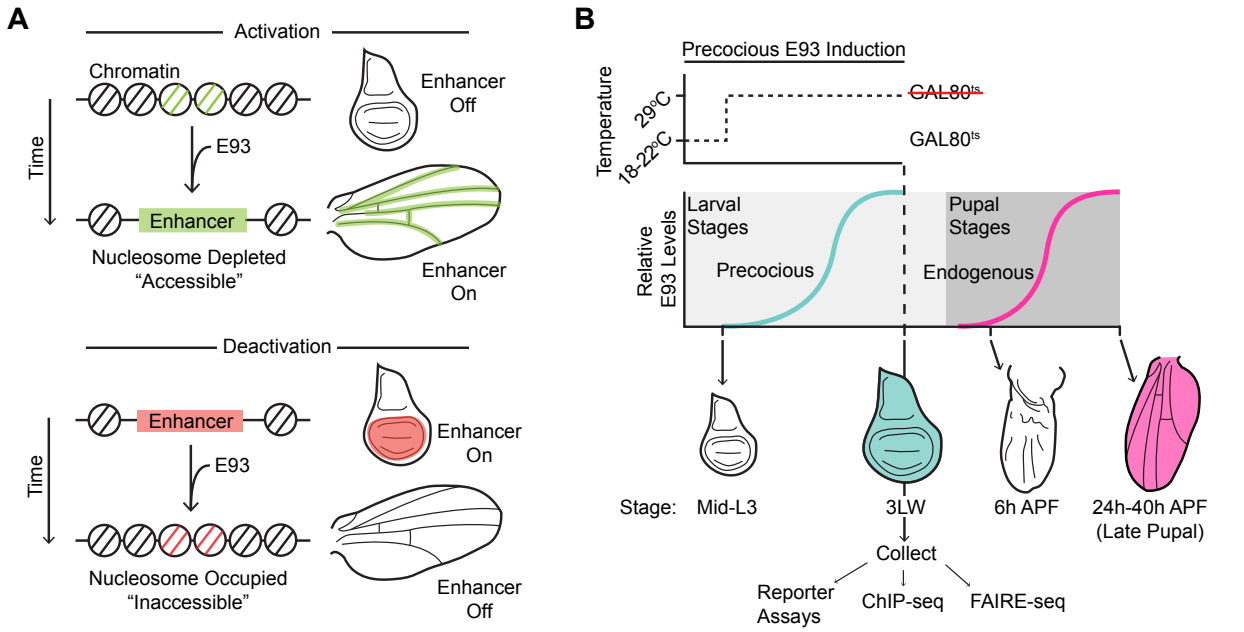

Figure 3.1: (A) Illustrations of larval wing imaginal discs and late pupal wings depicting that E93-dependent changes in chromatin accessibility correlate with temporal changes in the activity of two target enhancers (expression patterns indicated in green and red). (B) Schematic of E93 induction and relative timing of precocious E93 expression (teal) versus endogenous E93 expression (magenta). GAL4 drivers in combination with GAL80^{ts} were used to initiate precocious E93 expression in mid-third instar larvae (L3) for subsequent dissection in wandering third instar larvae (3LW).

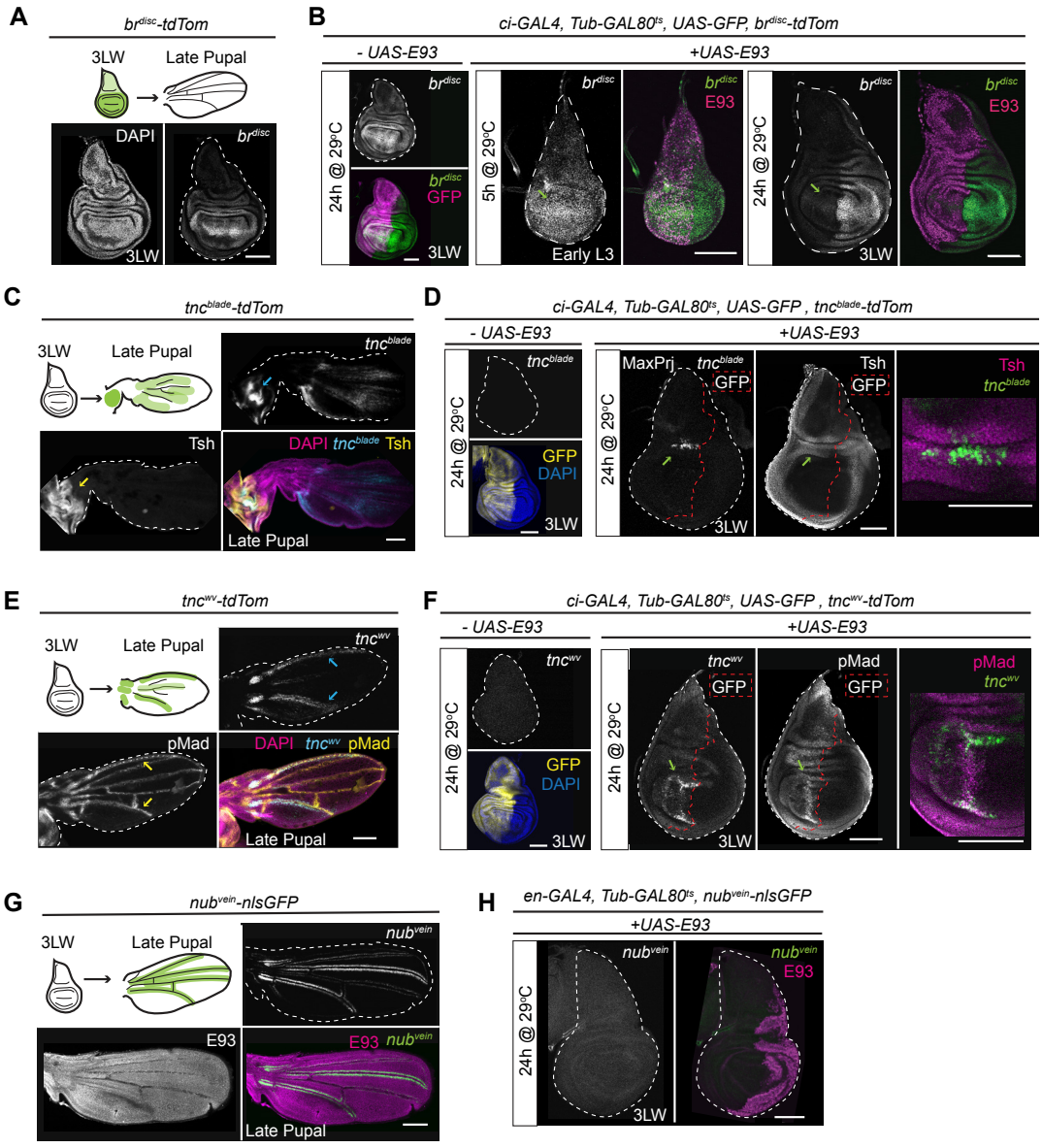

Figure 3.2: (A, C, E, G) Schematic of spatiotemporal enhancer activity alongside immunofluorescence examples. (A) *br*^{disc} is active in wing discs and inactive in pupal wings. (B) (left panels) Confocal image depicting *br*^{disc} activity (green) in control genotypes lacking the *UAS-E93* trans-gene. (middle panels) *br*^{disc} remains active (green) after a 5-hour E93 (magenta) induction. (right panels) *br*^{disc} activity (green) is lost in E93-expressing cells (magenta) after a 24-hour induction. (C) *tnc*^{blade} (cyan) is inactive in wing discs but is active in pupal wings in the body wall (arrows) marked by Tsh (yellow), and in intervein cells of the blade. (D) (left panels) *tnc*^{blade} is inactive in control genotypes lacking the *UAS-E9*3 transgene. *ci-GAL4* pattern is indicated in yellow. (right panels) *tnc*^{blade} is active (green) in E93-expressing cells (left of red dashed line) also expressing Tsh (magenta). (E) *tnc*^{wv} (cyan) is inactive in wing discs but is active in pupal wings along longitudinal veins marked by pMad (yellow). Cyan arrows indicate high level *tnc*^{wv} activity in the marginal and L5 veins. (F) (left panels) *tnc*^{wv} is inactive in control genotypes lacking the UAS-E93 transgene. *ci-GAL4* pattern is indicated in yellow. (right panels) *tnc*^{wv} is active (green) in E93-expressing cells (left of dashed red line) with high pMad levels (magenta). (G) *nub*^{vein} (green) is inactive in wing discs, but is active in pupal wings along the longitudinal veins. E93 expression is shown in magenta (H) *nub*^{vein} (green) is inactive in wing discs regardless of E93 expression (magenta). Scale bars = 100μm

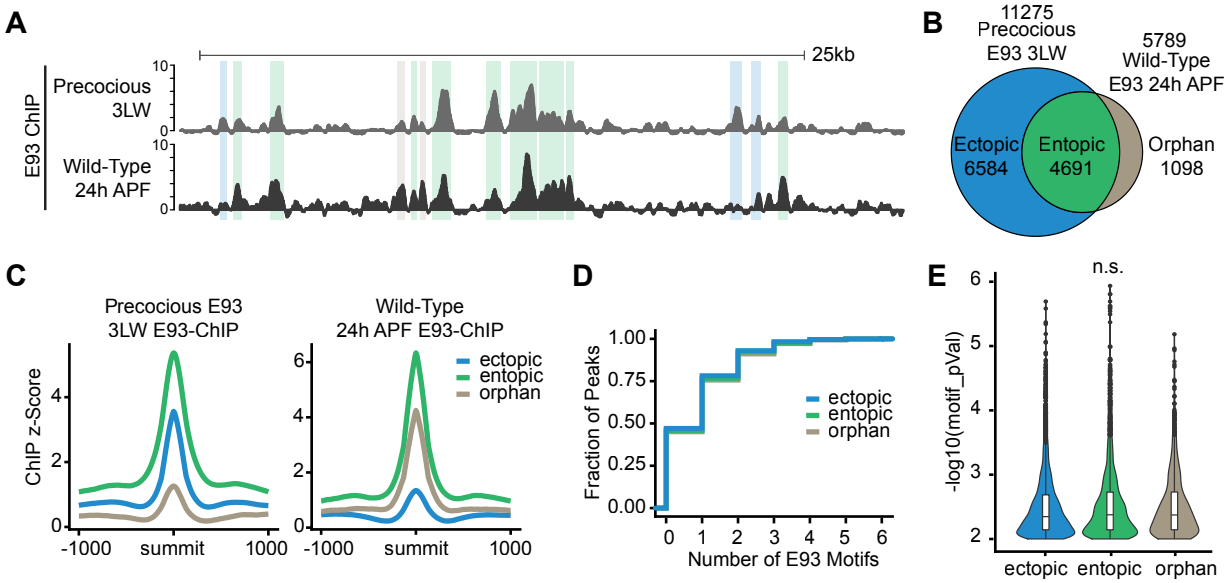

Figure 3.3: (A) Browser shot of ChIP-seq data for WT and precocious E93 wings. Colored highlights correspond to ectopic (blue), entopic (green), and orphan (brown) sites. (B) Venn diagram of peak overlaps between WT and precocious E93 ChIP-seq datasets. (C) Average signal plots of ChIP-seq z-score within each binding category for WT and precocious E93 ChIP. (D) Cumulative distribution of the number of E93 motifs within 20bp of the summit for each binding category. (E) Violin plots depicting motif quality ($-\log_{10}$ p-value) for all E93 motifs within 20bp of E93 ChIP peak summits for each binding category ($p > 0.05$, one-way analysis of means, not assuming equal variance).

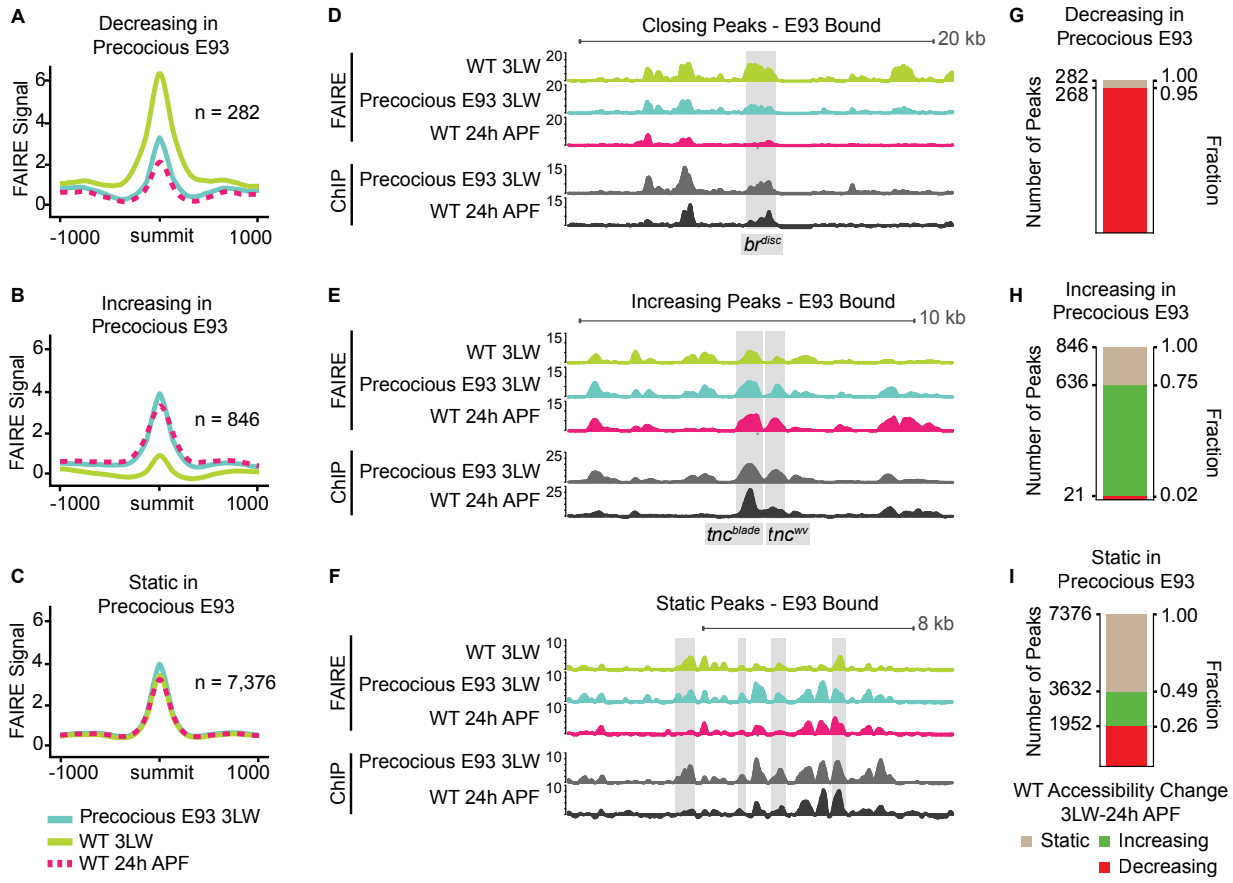

Figure 3.4: (A–C) Average FAIRE-seq signal (z-score) from WT 3LW wings (green), WT 24hAPF wings (dashed red), and precocious E93 3LW wings (teal) at precocious E93 binding sites that decrease accessibility (A), increase in accessibility (B), or remain static (C) in response to precocious E93 expression. (D–E) Browser shots of FAIRE-seq and ChIP-seq signal (z-scores) at the *br*^{disc} enhancer (D) and the *tnc*^{wv} and *tnc*^{blade} enhancers (E). (F) Browser shot of static sites bound by precocious E93. (G–I) Stacked bar charts indicating the changes in chromatin accessibility that occur in wild-type development for each of the three E93 binding site categories.

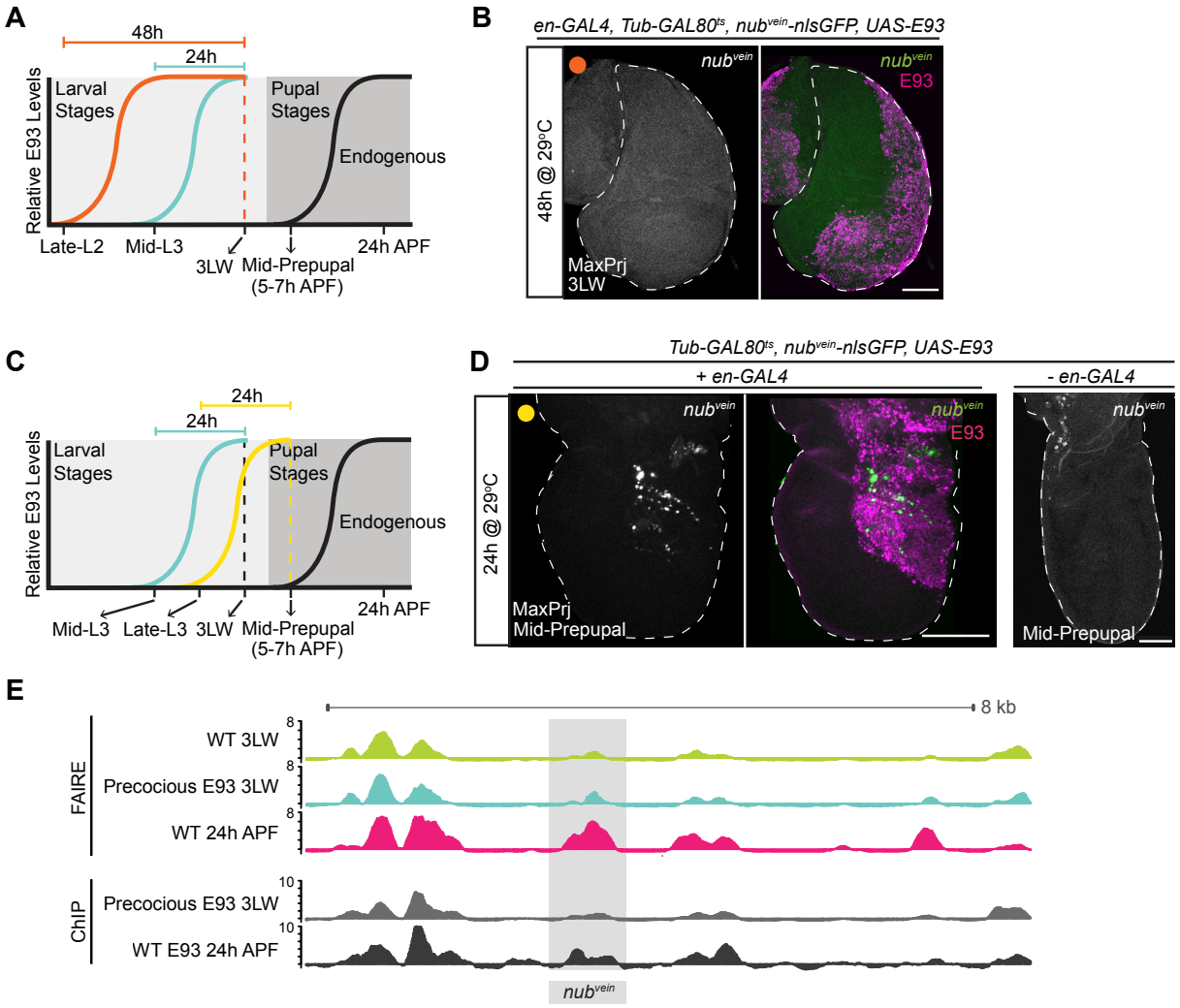

Figure 3.5: (A) Schematic depicting timing of prolonged E93 induction (orange), prior precocious E93-induction (teal), and endogenous E93 expression (black). Dashed vertical line indicates time of dissection. (B) Confocal image of *nub*^{vein} activity (green) in 3LW wing disc precociously expressing E93 (magenta) for 48-hours. (C) Schematic depicting timing of E93 induction for mid-prepupal wings (yellow), prior precocious E93-induction (teal), and wild-type E93 expression (black). (D) Confocal images of *nub*^{vein} activity (green) in mid-prepupal wings precociously expressing E93 (magenta) for 24-hours. Control wing lacking *en-GAL4* is shown at the right. (E) Browser shot showing FAIRE-seq and ChIP-seq signal (z-scores) at the *nub*^{vein} enhancer (shaded region). Scale bars = 100μm.

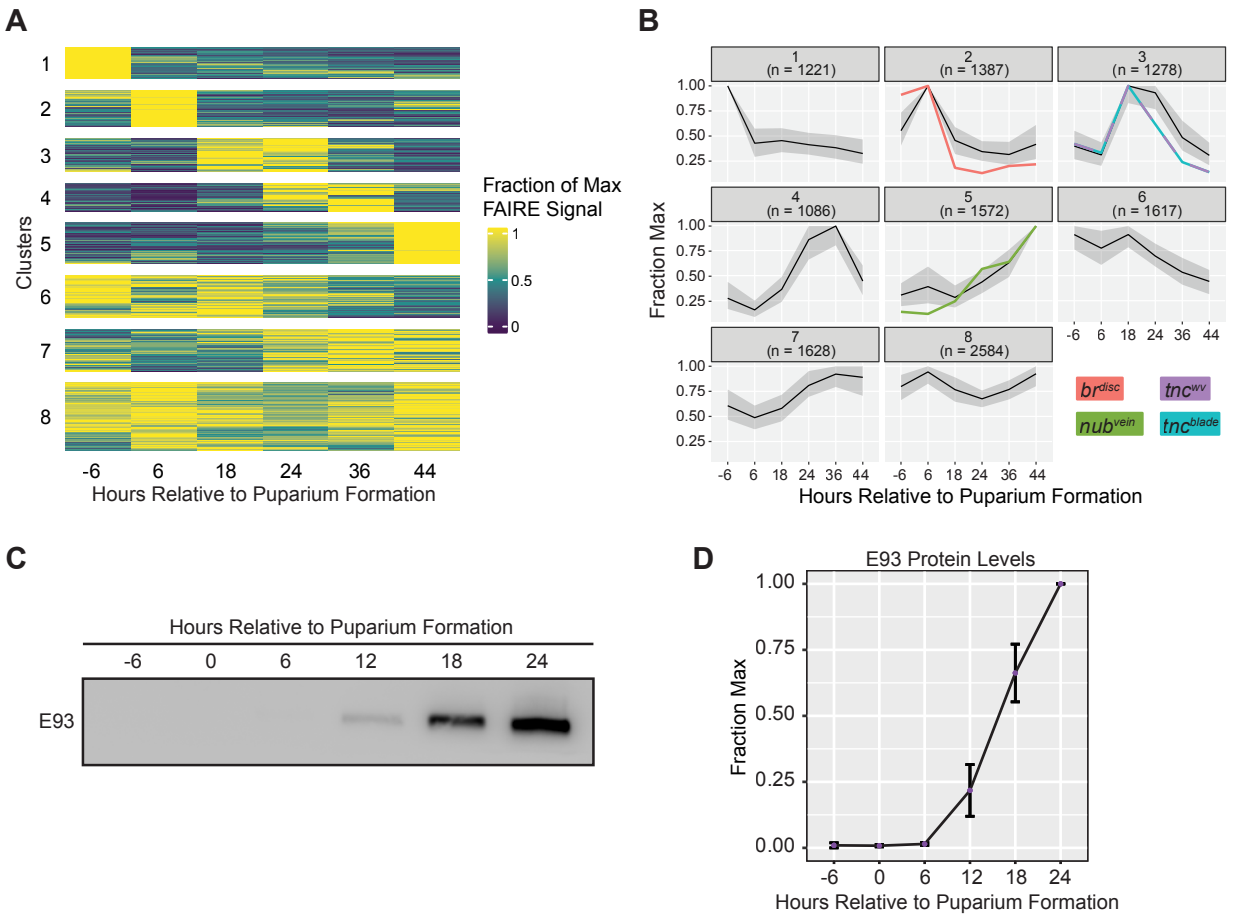

Figure 3.6: (A) Heatmap of chromatin accessibility over time within E93 ChIP peaks represented as fraction of maximum accessibility clustered using k-means (k=8). (B) Line plots depicting FAIRE signal for each cluster in A. Black lines: median fraction of max FAIRE signal. Grey area: interquartile range. Accessibility within ChIP-peaks overlapping enhancers is plotted in color indicated by inset labels. (C) Western blot of E93 levels in WT wings over time. (D) Quantification of E93 protein levels. Error bars = SE of Mean.

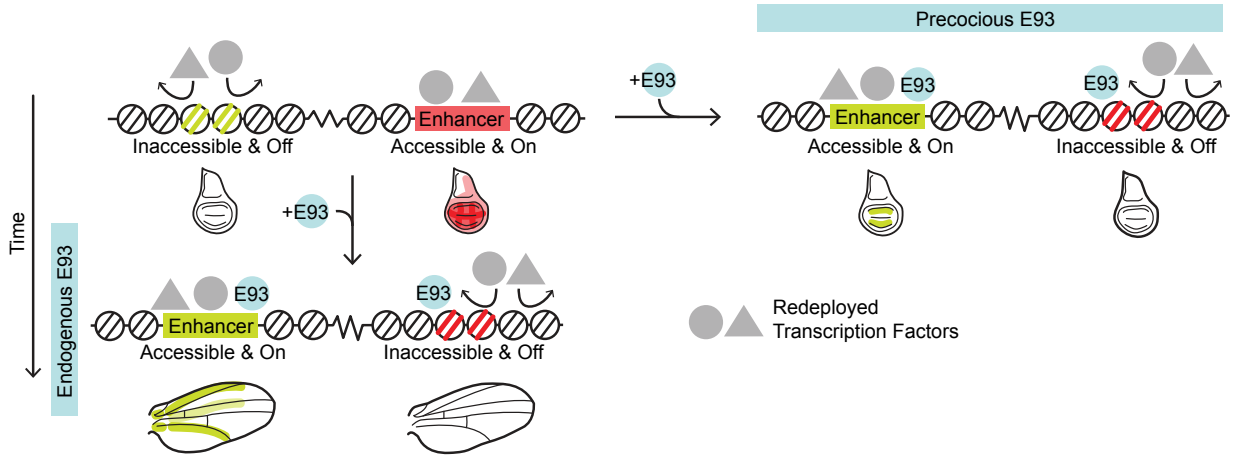

Figure 3.7: E93 expression defines a temporal window of enhancer competency by instructing changes to chromatin accessibility at a subset of sites to which it binds. Transcription factors that bind with E93 at target enhancers determine whether E93 opens or closes chromatin. Regulation of chromatin accessibility by temporal transcription factors may enable redeployment of spatial patterning factors to produce distinct transcriptional responses at different developmental times.

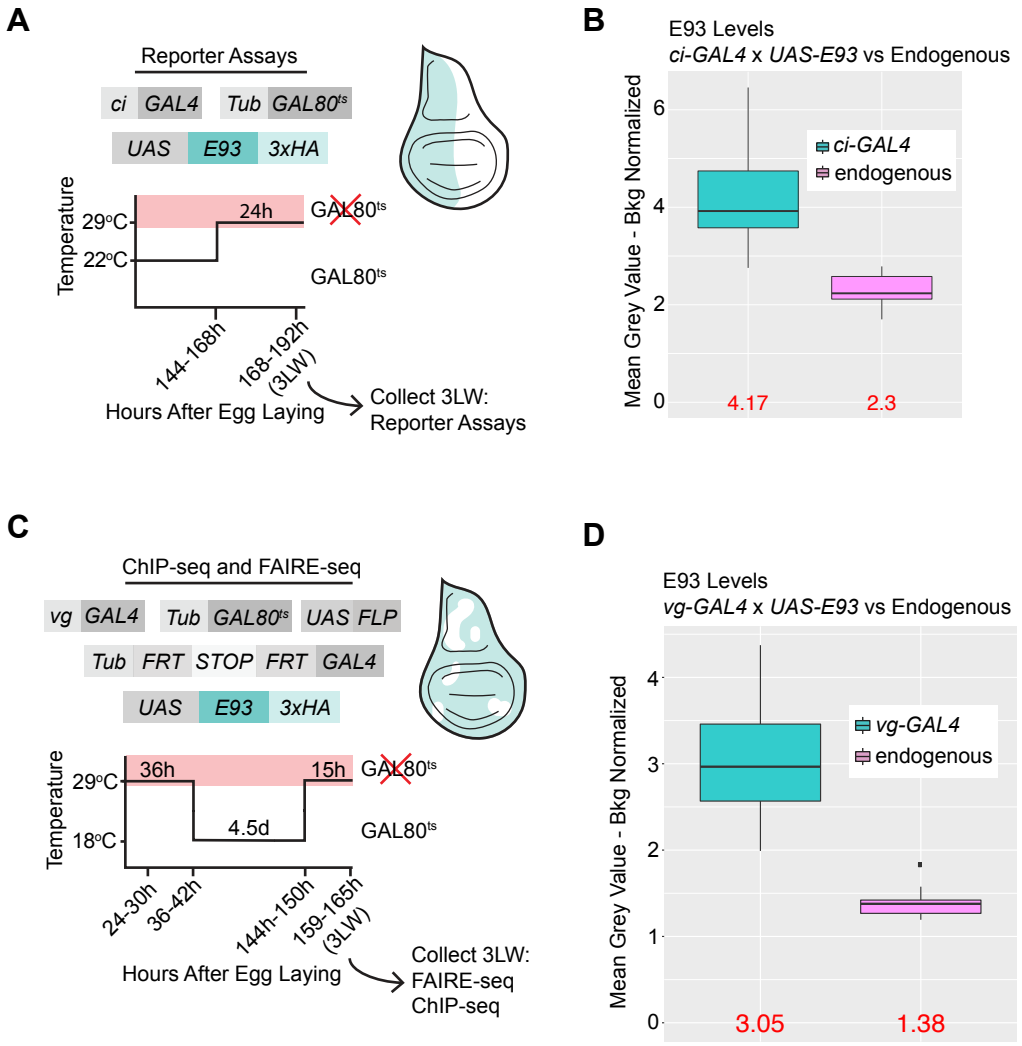

Figure 3.S1: (A) Experimental details of *ci-GAL4/GAL80^{ts}* control of the *UAS-E93-3xHA* transgene. Crosses were raised at room temperature (22°C), at which temperature *GAL80^{ts}* is stable and can repress GAL4 activity, until mid-third instar (144h-168h). They were then switched to 29°C, at which temperature *GAL80^{ts}* is inactive, thereby inducing E93 expression. Wandering third-instar larvae (3LW) were dissected twenty-four hours later for immunostaining. (B) Box plots depicting quantification of E93 levels driven by *ci-GAL4* in 3LW wing discs relative to endogenous E93 levels in pupal wings 30h after puparium formation (APF) using anti-E93 antibodies. (C) Experimental details of the *vg-GAL4* lineage tracing experiments. Crosses were maintained at 29°C for thirty-six hours to permit *vg-GAL4* driven flip-out of the stop cassette. Crosses were then shifted to 18°C for 4.5 days. Finally, crosses were shifted back to 29°C for fifteen hours before dissecting wandering third-instar larvae (3LW). Due to the inefficiency of flip-out, some portion of each disc remains WT (white regions). (D) Box plots depicting quantification of E93 levels driven using the *vg-GAL4* system in 3LW wings relative to endogenous E93 in pupal wings 30hAPF using anti-E93 antibodies. Averages noted in red. n = 30 (10 measurements across 3 wings) per condition.

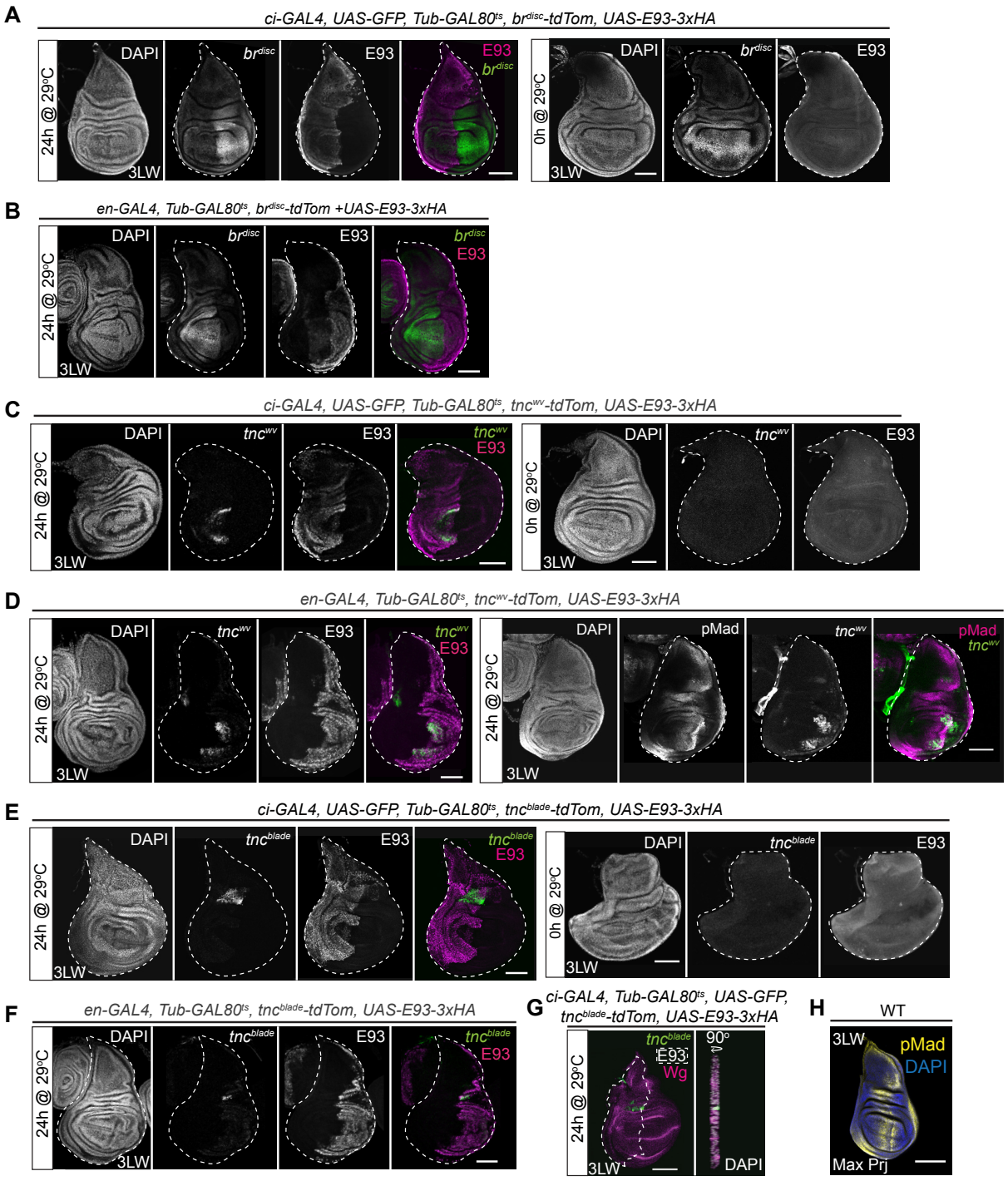

Figure 3.S2: (A, C, E) Precocious expression of E93 (magenta) in the anterior compartment using *ci-GAL4* deactivates the discenhancer, and activates the *tnc*^{wv} and *tnc*^{blade} enhancers (green). In control experiments lacking a 29°C shift (right panels), E93 was not expressed and no change in enhancer activity was observed. (B, D, F) Precocious expression of E93 (magenta) in the posterior compartment with *en-GAL4* deactivates the discenhancer and activates the *tnc*^{blade} and *tnc*^{wv} enhancers similarly to their response to E93 expression with *ci-GAL4*. (G) *tnc*^{blade} (green) is precociously activated by ectopic E93 expression in cells proximal to the outer ring of Wg (magenta). (H) Wild-type pMad pattern (yellow) in 3LW wing discs. Scale bars = 100m.

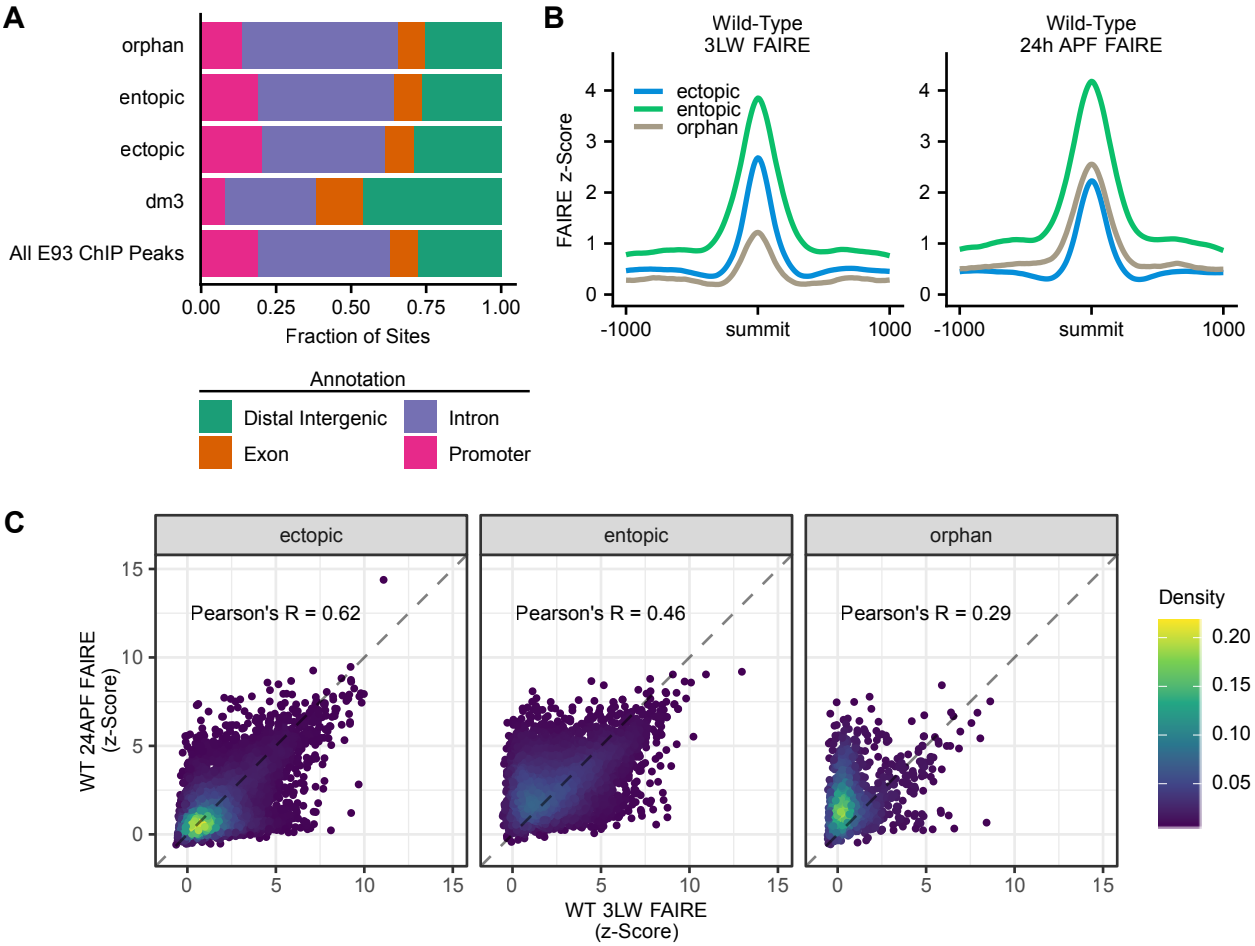

Figure 3.S3: (A) Stacked bar chart plotting the fraction of total sites present at annotated genomic regions. Distributions are shown for the full set of E93 chip peaks, the mappable dm3 assembly, and each E93 binding category separately. (B) Average signal plot of FAIRE-seq signal within each binding category during wild-type 3LW and wild-type 24h APF wings. (C) Scatter plots of FAIRE signal (z-score) in wild-type 3LW and wild-type 24APF wings for each E93 binding category. Colors represent point density. Pearson's R values are reported for each category reflecting the correlation of FAIRE-seq z-scores between two timepoints.

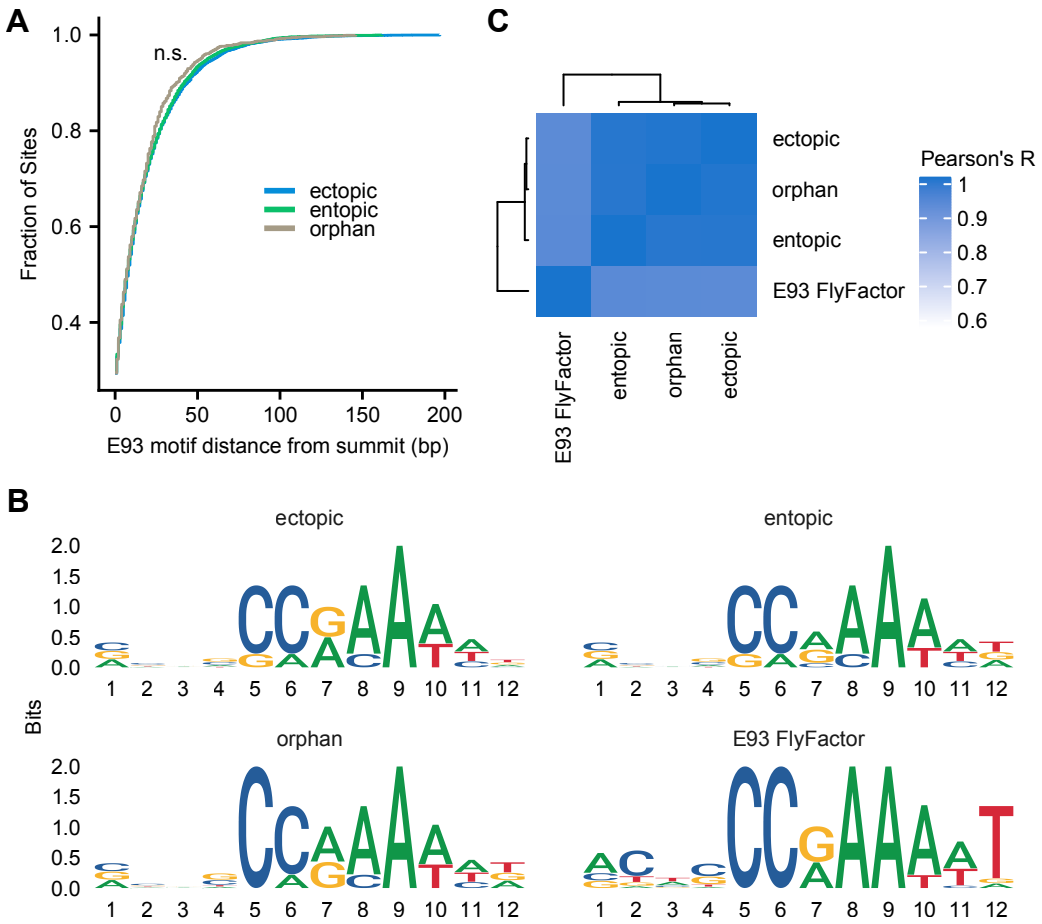

Figure 3.S4: (A) Cumulative distribution plot showing the distance from the summit to the nearest E93 motif. n.s. = p > 0.05 KS-test. (B) PWMs derived from E93 motifs within E93 binding categories compared to the E93 motif from the Fly Factor Survey database. (C) Heatmap of Pearson correlation values between the PWMs shown in (B) values are hierarchically clustered.

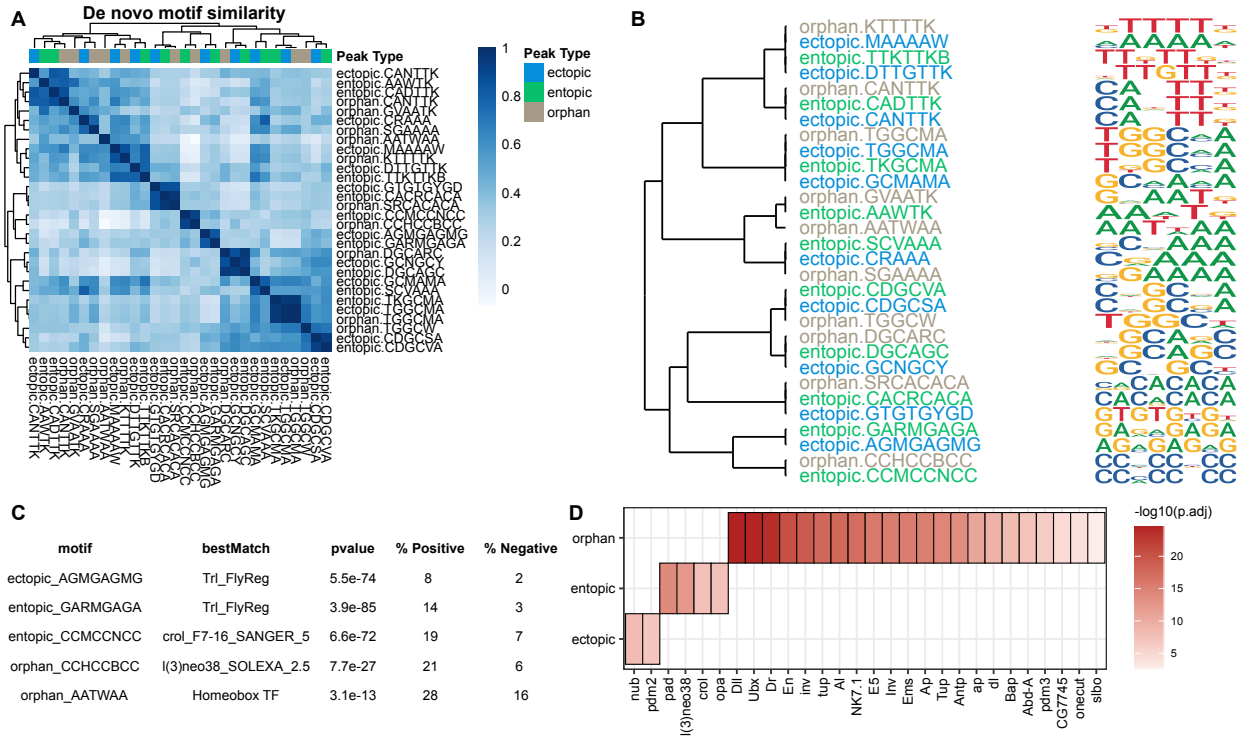

motif	bestMatch	pvalue	% Positive	% Negative
ectopic_AGMGAGMG	Trl_FlyReg	5.5e-74	8	2
entopic_GARMGAGA	Trl_FlyReg	3.9e-85	14	3
entopic_CCMCCNCC	crol_F7-16_SANGER_5	6.6e-72	19	7
orphan_CCHCCBCC	l(3)neo38_SOLEXA_2.5	7.7e-27	21	6
orphan_AATWAA	Homeobox TF	3.1e-13	28	16

Figure 3.S5: (A) Heatmap of PWM correlations for de novo discovered motifs within each E93 binding category. Color represents Pearson's R value. Heatmap is clustered by hierarchical clustering of correlation coefficients. (B) Clustering based on PWM distances. (C) Table displaying characteristics of de novo discovered motifs not found in all 3 binding categories. Best Match indicates the top matched Fly Factor Survey motif for the discovered PWM. Pvalue indicates the DREME p-value. % Positive and % Negative indicate the fraction of sites in foreground vs background sequences that contain a match to the de novo PWM. (D) Heatmap showing the top hits following directed motif scanning within each E93 binding category. Color represents -$\log_{10}$(adjusted p-value) of enrichment.

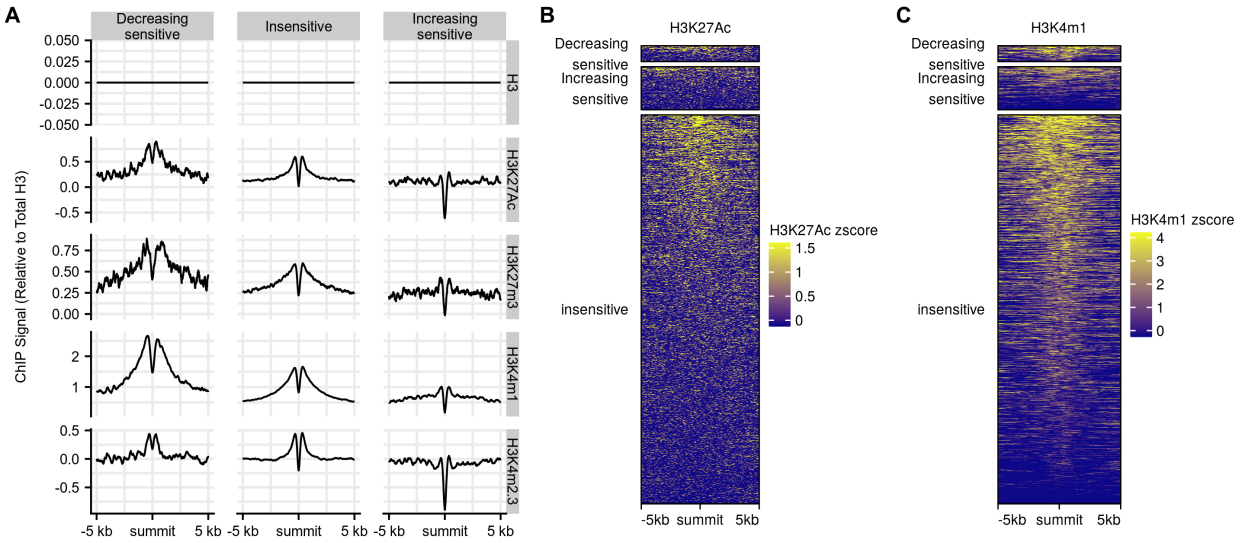

Figure 3.S6: (A) Average signal plots of histone PTM ChIP-seq z-scores (normalized to total H3 signal) at E93 sensitive and insensitive sites in wild-type 3LW wings. (B) Heatmap of H3K27Ac signal inside E93 sensitive sites. (C) Heatmap of H3K4m1 signal within E93 sensitive sites.

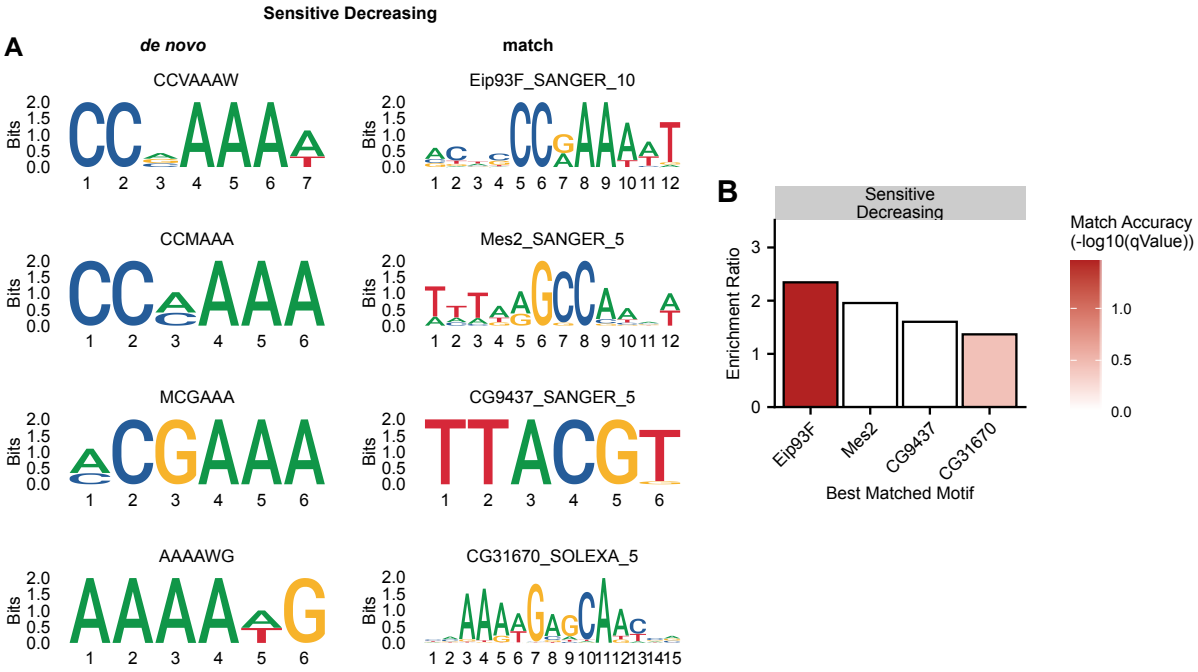

Figure 3.S7: (A) PWMs of de novo discovered motifs within decreasing E93-sensitive sites compared to their corresponding best matched motif. The motif matching Mes2 strongly resembles the E93 motif. (B) Bar plot of enrichment ratio for de novo discovered motifs from (A) within E93 sensitive decreasing sites. Color of bar represents confidence that this PWM is the correct match to the de novo PWM.

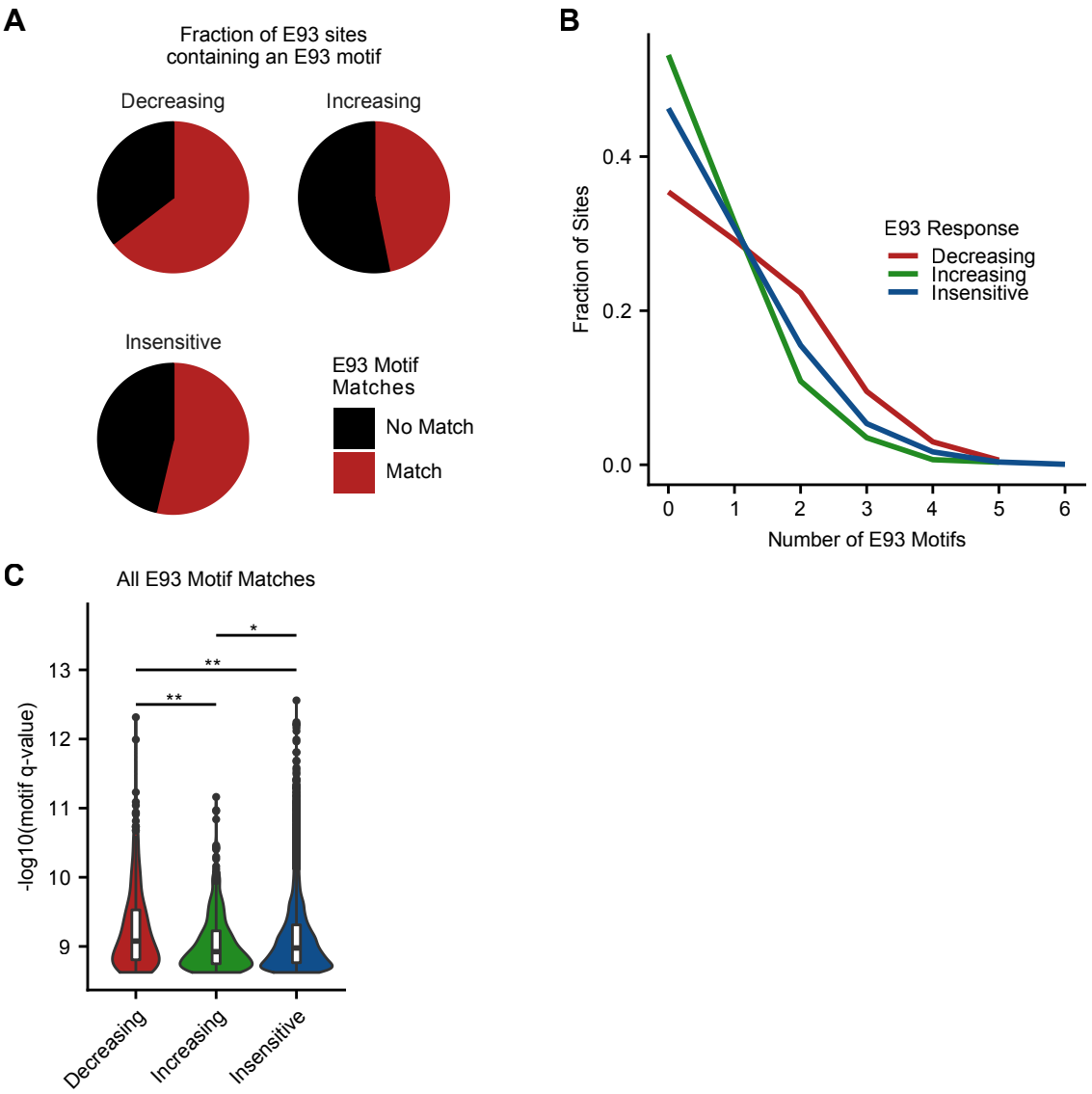

Figure 3.S8: (A) Pie charts showing the fraction of E93 binding sites containing at least 1 match to the E93 motif. (B) Lineplot showing the fraction of E93 binding sites containing a given number of E93 motifs. (C) Violin plots depicting E93 motif quality within E93 binding sites. * = $p < 0.05$, ** = $p < 0.015$, oneway anova followed by TukeyHSD test.

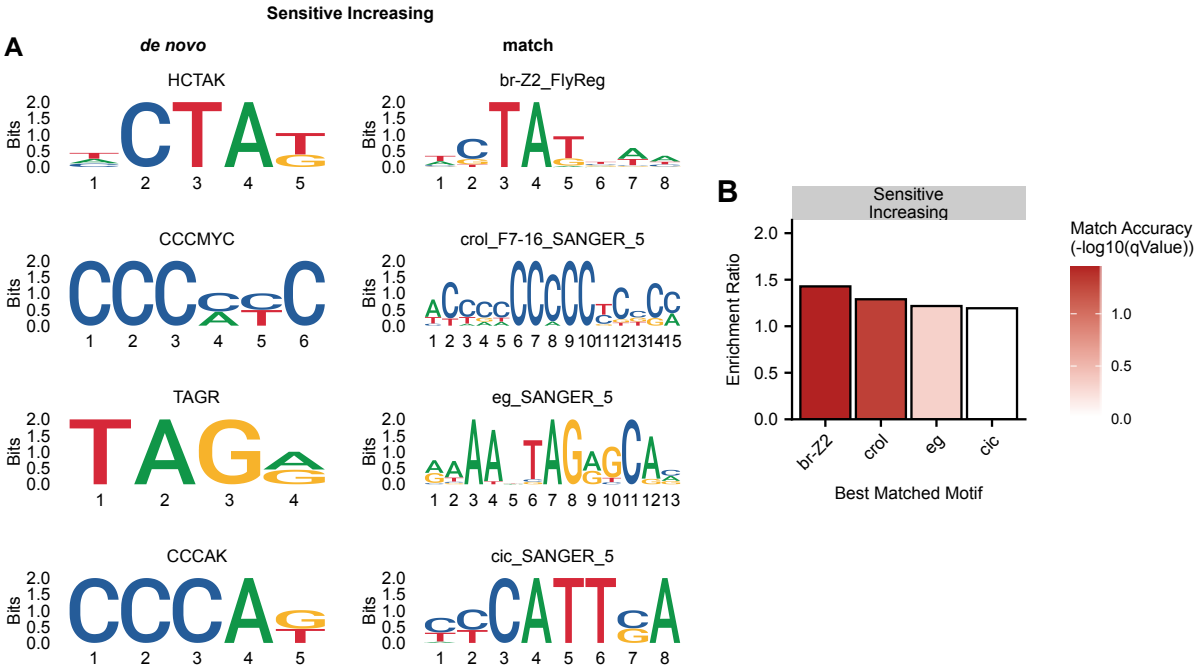

Figure 3.S9: (A) PWMs of de novo discovered motifs within increasing E93-sensitive sites compared to their corresponding best matched motif. (B) Bar plot of enrichment ratio for de novo discovered motifs (from (A)) within increasing E93-sensitive sites. Color of bar represents confidence that this PWM is the correct match to the de novo PWM.

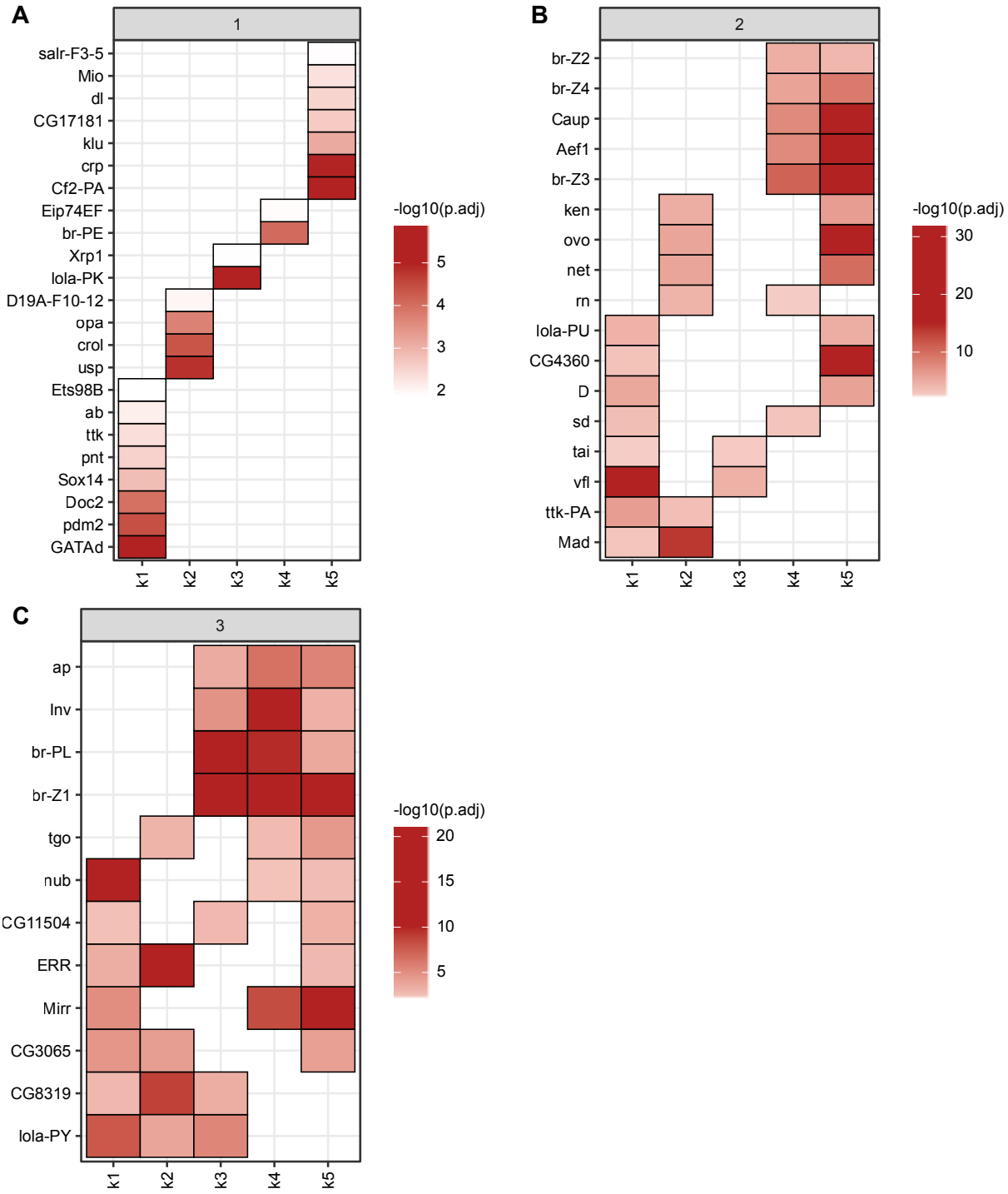

Figure 3.S10: Heatmaps of motifs detected in each temporal cluster. Facets represent motifs which are shared between 1, 2, or 3 clusters, (AC) respectively. Color represents -log10(adjusted p-value) of enrichment.

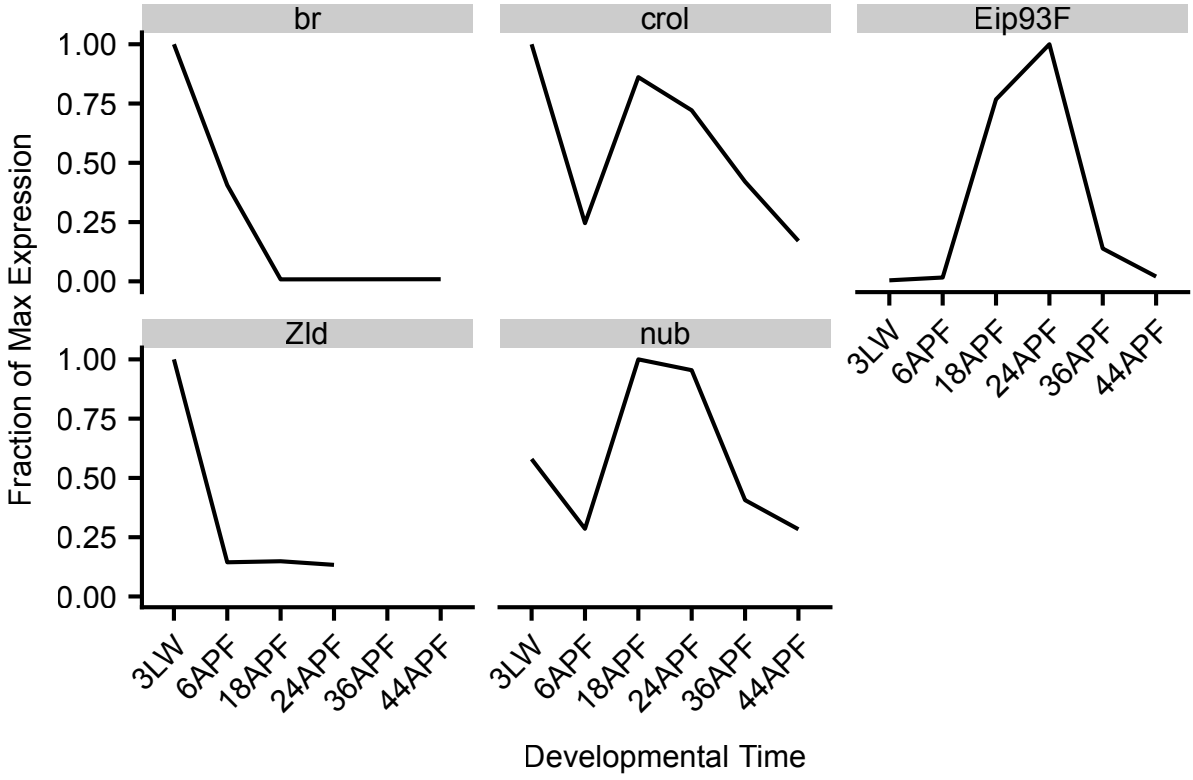

Figure 3.S11: mRNA levels of transcription factors identified in motif analyses plotted as the fraction of maximum signal during a wild-type wing developmental timecourse.

REFERENCES

Baehrecke, E. H. and Thummel, C. S. (1995). The *Drosophila* E93 Gene from the 93F Early Puff Displays Stage- and Tissue-Specific Regulation by 20-Hydroxyecdysone. Dev. Biol. 171, 85–97.

Bischof, J., Bjorklund, M., Furger, E., Schertel, C., Taipale, J. and Basler, K. (2013). A versatile platform for creating a comprehensive UAS-ORFeome library in *Drosophila*. Development 140, 2434–2442.

Broadus, J., McCabe, J. R., Endrizzi, B., Thummel, C. S. and Woodard, C. T. (1999). The *Drosophila* beta FTZ-F1 orphan nuclear receptor provides competence for stage-specific responses to the steroid hormone ecdysone. Mol. Cell 3, 143–9.

Crickmore, M. A. and Mann, R. S. (2006). Hox Control of Organ Size by Regulation of Morphogen Production and Mobility. Science (80-.). 313, 63–68.

Crossgrove, K., Bayer, C. A., Fristrom, J. W. and Guild, G. M. (1996). The *Drosophila* Broad-Complex early gene directly regulates late gene transcription during the ecdysone-induced puffing cascade. Dev. Biol. 180, 745–58.

De Celis, J. F. (1997). Expression and function of decapentaplegic and thick veins during the differentiation of the veins in the *Drosophila* wing. Development 124, 1007–18.

Doe, C. Q. (2017). Temporal Patterning in the *Drosophila* CNS. Annu. Rev. Cell Dev. Biol. 33, 219–240.

Fraichard, S., Bougé, A.-L., Kendall, T., Chauvel, I., Bouhin, H. and Bunch, T. A. (2010). Tenectin is a novel αPS2βPS integrin ligand required for wing morphogenesis and male genital looping in *Drosophila*. Dev. Biol. 340, 504–517.

Gentleman, R. C., Carey, V. J., Bates, D. M., Bolstad, B., Dettling, M., Dudoit, S., Ellis, B., Gautier, L., Ge, Y., Gentry, J., *et al*. (2004). Bioconductor: open software development for computational biology and bioinformatics. Genome Biol. 5, R80.

Grant, C. E., Bailey, T. L. and Noble, W. S. (2011). FIMO: scanning for occurrences of a given motif. Bioinformatics 27, 1017–1018.

Guo, Y., Flegel, K., Kumar, J., McKay, D. J. and Buttitta, L. A. (2016). Ecdysone signaling induces two phases of cell cycle exit in *Drosophila* cells. Biol. Open 5, 1648–1661.

Hahne, F. and Ivanek, R. (2016). Visualizing Genomic Data Using Gviz and Bioconductor. In Methods in molecular biology (Clifton, N.J.), pp. 335–351.

Holguera, I. and Desplan, C. (2018). Neuronal specification in space and time. Science (80-.). 362, 176–180.

Karim, F. D., Guild, G. M. and Thummel, C. S. (1993). The *Drosophila* Broad-Complex plays a key role in controlling ecdysone-regulated gene expression at the onset of metamorphosis. Development 118, 977–88.

Kumar, N., Tsai, Y.-H., Chen, L., Zhou, A., Banerjee, K. K., Saxena, M., Huang, S., Toke, N. H., Xing, J., Shivdasani, R. A., *et al*. (2019). The lineage-specific transcription factor CDX2 navigates dynamic chromatin to control distinct stages of intestine development. Development 146, dev172189.

Langmead, B. and Salzberg, S. L. (2012). Fast gapped-read alignment with Bowtie 2. Nat. Methods 9, 357–359.

Lawrence, M., Huber, W., Pagès, H., Aboyoun, P., Carlson, M., Gentleman, R., Morgan, M. T. and Carey, V. J. (2013). Software for Computing and Annotating Genomic Ranges. PLoS Comput. Biol. 9, e1003118.

Leatham-Jensen, M., Uyehara, C. M., Strahl, B. D., Matera, A. G., Duronio, R. J. and McKay, D. J. (2019). Lysine 27 of replication-independent histone H3.3 is required for Polycomb target gene silencing but not for gene activation. PLOS Genet. 15, e1007932.

Liu, X., Dai, F., Guo, E., Li, K., Ma, L., Tian, L., Cao, Y., Zhang, G., Palli, S. R. and Li, S. (2015). 20-Hydroxyecdysone (20E) Primary Response Gene E93 Modulates 20E Signaling to Promote Bombyx Larval-Pupal Metamorphosis. J. Biol. Chem. 290, 27370–83.

Martín-Blanco, E., Roch, F., Noll, E., Baonza, A., Duffy, J. B. and Perrimon, N. (1999). A temporal switch in DER signaling controls the specification and differentiation of veins and interveins in the *Drosophila* wing. Development 126, 5739–47.

McKay, D. J. and Lieb, J. D. (2013). A common set of DNA regulatory elements shapes *Drosophila* appendages. Dev. Cell 27, 306–18.

Mou, X., Duncan, D. M., Baehrecke, E. H. and Duncan, I. (2012). Control of target gene specificity during metamorphosis by the steroid response gene E93. Proc. Natl. Acad. Sci. U. S. A. 109, 2949–54.

O'Keefe, D. D., Thomas, S., Edgar, B. A. and Buttitta, L. (2014). Temporal regulation of Dpp signaling output in the *Drosophila* wing. Dev. Dyn. 243, 818–832.

Parodi, A. C. L., Sangalli, L. M., Vantini, S., Amati, B., Secchi, P. and Morelli, M. J. (2017). FunChIP: an R/Bioconductor package for functional classification of ChIP-seq shapes. Bioinformatics 33, 2570–2572.

Pasquinelli, A. E. and Ruvkun, G. (2002). Control of Developmental Timing by MicroRNAs and Their Targets. Annu. Rev. Cell Dev. Biol. 18, 495–513.

Pavlopoulos, A. and Akam, M. (2011). Hox gene Ultrabithorax regulates distinct sets of target genes at successive stages of *Drosophila* haltere morphogenesis. Proc. Natl. Acad. Sci. 108, 2855–2860. R Core Team (2017). R: A Language and Environment for Statistical Computing.

Schertel, C., Albarca, M., Rockel-Bauer, C., Kelley, N. W., Bischof, J., Hens, K., van Nimwegen, E., Basler, K. and Deplancke, B. (2015). A large-scale, *in vivo* transcription factor screen defines bivalent chromatin as a key property of regulatory factors mediating *Drosophila* wing development. Genome Res. 25, 514–23.

Schindelin, J., Arganda-Carreras, I., Frise, E., Kaynig, V., Longair, M., Pietzsch, T., Preibisch, S., Rueden, C., Saalfeld, S., Schmid, B., *et al*. (2012). Fiji: an open-source platform for biological-image analysis. Nat. Methods 9, 676–682.

Sen, S. Q., Chanchani, S., Southall, T. D. and Doe, C. Q. (2019). Neuroblast-specific open chromatin allows the temporal transcription factor, Hunchback, to bind neuroblast-specific loci. Elife 8,.

Stempor, P. and Ahringer, J. (2016). SeqPlots - Interactive software for exploratory data analyses, pattern discovery and visualization in genomics. Wellcome Open Res. 1, 14.

Uyehara, C. M. and McKay, D. J. (2019). Direct and widespread role for the nuclear receptor EcR in mediating the response to ecdysone in *Drosophila*. Proc. Natl. Acad. Sci. U. S. A. 116, 9893–9902.

Uyehara, C. M., Nystrom, S. L., Niederhuber, M. J., Leatham-Jensen, M., Ma, Y., Buttitta, L. A. and McKay, D. J. (2017). Hormone-dependent control of developmental timing through regulation of chromatin accessibility. Genes Dev. 31, 862–875.

Wickham, H. (2009). ggplot2 : elegant graphics for data analysis. Springer.

Wilke, C. O. (2017). cowplot: Streamlined Plot Theme and Plot Annotations for “ggplot2”. R package version 0.9.4. https://CRAN.R-project.org/package=cowplot. R Packag. version 0.9.2 https://cran.r–project.org/package=cowplot.

Yao, T.-P., Forman, B. M., Jiang, Z., Cherbas, L., Chen, J.-D., McKeown, M., Cherbas, P. and Evans, R. M. (1993). Functional ecdysone receptor is the product of EcR and Ultraspiracle genes. Nature 366, 476–479.

Zhang, Y., Liu, T., Meyer, C. A., Eeckhoute, J., Johnson, D. S., Bernstein, B. E., Nusbaum, C., Myers, R. M., Brown, M., Li, W., *et al*. (2008). Model-based analysis of ChIP-Seq (MACS). Genome Biol. 9, R137.

Zhu, L. J., Christensen, R. G., Kazemian, M., Hull, C. J., Enuameh, M. S., Basciotta, M. D., Brasefield, J. A., Zhu, C., Asriyan, Y., Lapointe, D. S., *et al*. (2011). FlyFactorSurvey: a database of *Drosophila* transcription factor binding specificities determined using the bacterial one-hybrid system. Nucleic Acids Res. 39, D111–7.

Zirin, J. D. and Mann, R. S. (2007). Nubbin and Teashirt mark barriers to clonal growth along the proximal-distal axis of the *Drosophila* wing. Dev. Biol. 304, 745–58.

CHAPTER 4: THE SWI/SNF NUCLEOSOME REMODELER CONSTRAINS ENHANCER ACTIVITY DURING WING DEVELOPMENT

4.1 Introduction

Animal development requires robust control over the spatial patterns, magnitude, and temporal dynamics of gene expression. Dysregulation in any of these regulatory dimensions is known to contribute to developmental disorders and acquired disease states. Spatial control refers to the selective patterns of gene expression across a field of cells. For instance, the spatially restricted expression of Hox genes in animals is essential for specification of regional identities along the developing body axis (Mallo *et al.,* 2013). Both loss of expression and ectopic expression of Hox genes beyond their normal spatial domains can lead to homeotic transformations. The magnitude of gene expression must also be tightly controlled for proper development, and both excessive and insufficient gene expression can be detrimental. For instance, duplication of the *APP* gene is associated with early onset alzheimer's disease and is thought to be a driver of Alzheimer's in individuals with Trisomy 21 (Tang *et al.,* 2013). Conversely, heterozygosity of Notch pathway components, including the Notch receptor itself, is associated with several developmental syndromes (Falo-Sanjuan and Bray, 2020). This dose-dependency is conserved in *Drosophila*, which exhibit defects in sensory organ development when genes encoding Notch pathway components are mutated, as well as in genotypes with extra copies of Notch pathway genes (Hartenstein and Posakony, 1990; Parks and Muskavitch, 1993; Doherty *et al.,* 1996; Elfring *et al.,* 1998; Armstrong *et al.,* 2005). The spatial patterns and levels of gene expression are also temporally dynamic, as cells transition through intermediate identities over developmental time. A classic example of temporal regulation is ecdysone hormone signaling in insects, which triggers changes in stage-specific gene expression programs across body parts that are not in close physical contact (Yamanaka *et al.,* 2013). Despite their importance, the factors and mechanisms coordinating these three dimensions of developmental gene regulation remain incompletely understood.

A primary layer of gene regulation lies at the level of *cis*-acting DNA regulatory elements and

the trans-acting factors that bind them. Enhancers are relatively short (~0.5-2kb) non-coding regions of DNA that function as integration points for the spatiotemporal information transmitted by sequence-specific transcription factors, which typically bind short DNA sequences 6-10bp in length (Spitz and Furlong, 2012; Uyehara and Apostolou, 2023). Additional layers of information come in the form of the packaging and chemical modification of chromatin. Histone post-translational modifications directly and indirectly control chromatin structure and help propagate cellular memory (Millán-Zambrano *et al.,* 2022). Access to DNA-encoded information is also influenced by the positioning, stability, and occupancy of nucleosomes. Nucleosomes are inhibitory to transcription factor binding and thus must be remodeled or removed for an enhancer to become active (Brahma and Henikoff, 2020; Niederhuber and McKay, 2020; Isbel *et al.,* 2022). Genome-wide patterns of chromatin accessibility are predictive of enhancer activity. Moreover, temporal changes in chromatin accessibility profiles are correlated with stage-specific changes in gene expression during development (Uyehara *et al.,* 2017). Recent studies in *Drosophila* have provided insight into the mechanisms controlling developmentally programmed changes in chromatin accessibility. A number of transcription factors have been identified that open chromatin in early stage embryos to promote activation of the zygotic genome (Gaskill *et al.,* 2021). Likewise, the ecdysone-induced transcription factor E93 has been found to be required for promoting accessibility of enhancers active later in pupal stages of development (Nystrom *et al.,* 2020). Interestingly, E93 is also necessary for closing and deactivating early acting enhancers (Uyehara *et al.,* 2017; Nystrom *et al.,* 2020). Returning accessible enhancers to a closed chromatin state is important for rendering them refractory to transcription factor binding, thereby allowing regulatory inputs to be utilized at distinct targets over the course of development. However, the mechanisms of closing chromatin to repress enhancers during development are poorly understood relative to those controlling chromatin opening.

Here, we examine the contribution of nucleosome remodelers in control of a developmentally dynamic enhancer in *Drosophila*. Nucleosome remodelers use ATP hydrolysis to disrupt histone-DNA interactions, and by doing so, occlude or make accessible short stretches of DNA to transcription factors. Through mechanisms that remain unclear, disruption of short stretches of histone-DNA contacts by nucleosome remodelers can result in accessibility of enhancers that are often orders of magnitude

greater in length (Clapier *et al.,* 2017). Through an *in vivo* RNAi screen, we identified the *Drosophila* BAP complex, which is orthologous to yeast and human SWI/SNF, as being required for repression of a developmentally dynamic enhancer. Contrary to expectations, we find that BAP is dispensable for developmentally programmed changes in chromatin accessibility during wing metamorphosis. Instead, we find that the BAP subunit Osa is required to constrain activity when the enhancer is in the on state. Using CUT&RUN, we find that Osa directly binds thousands of regions that have signatures of active enhancers, including multiple genes in the Notch signaling pathway. Lastly, we find that loss of BAP function results in upregulation of a direct Osa target gene, *Delta*, which encodes the Notch ligand. Together these data suggest a model in which the BAP complex directly constrains enhancer activity to ensure correctly measured responses to developmental signals like Notch signaling and cell specification programs during wing development.

4.2 Results

4.2.1 The *br^{disc}* enhancer is a model of a developmentally dynamic regulatory element

In order to interrogate the role of nucleosome remodelers in developmentally dynamic enhancer regulation, we selected a previously identified enhancer known to respond to temporal inputs from the ecdysone hormone pathway (Uyehara *et al.,* 2017; Nystrom *et al.,* 2020). The *br^{disc}* enhancer is a ~2kb region on the X chromosome that lies approximately 9kb upstream of the gene *broad* (*br*). Prior studies of *br^{disc}* activity using transgenic reporters indicated that it switches on prior to the 3rd larval instar stage in the precursors of the adult appendages, including the wing (Uyehara *et al.,* 2017). *Br^{disc}* is then deactivated during the first 24 hours of pupal development, thus making it a good model for studying temporally dynamic enhancer control.

We first sought to improve the temporal resolution of *br^{disc}* transgenic reporter activity. Traditional enhancer reporters optimize rapid fluorophore maturation, brightness, and stability. Although these optimizations are useful for sensitive detection of enhancer activity patterns, they are problematic when monitoring dynamic enhancer behavior because persistent fluorescent protein interferes with determining when enhancer activity shuts off. To mitigate these effects, we developed two new fluorescent reporters.

The first is a dual fluorophore reporter system, which we refer to as *br^{disc}-switch*. This reporter was designed to drive expression of a tandem tomato fluorophore (tdTomato) that could be inducibly switched via FLP/FRT-meditated recombination to transcribe a myristoylated GFP (myr-GFP, **Fig 4.1A**). The switch reporter system allows for better temporal resolution of enhancer dynamics relative to conventional reporters because GFP detected after reporter switching indicates the enhancer was active after recombination was induced. Conversely, a lack of GFP detected after reporter switching demonstrates that the enhancer was inactive at the time of recombination or later. Examination of *br^{disc}-switch* activity revealed that the reporter is highly active in third larval wandering (3LW) wing imaginal discs, but there is little to no detectable nascent GFP in young pupal wings aged <40 hours after puparium formation (APF) (**Fig 4.1B**). By contrast, tdTomato signal remains high in this same wing (**Fig 4.1B**). Interestingly, the *br^{disc}-switch* reporter exhibits new GFP signal in older (>40h APF) wings, in bristle shafts located along the wing margin and in cells of the posterior cross vein (PCV), indicating that it is reactivated in a subset of pupal wing cells after its initial deactivation. Closer inspection of another transgenic *br^{disc}* reporter integrated at a separate genomic locus, and which employs a different minimal promoter, revealed similar late enhancer activity along the wing margin (**Fig 4.S1A**). Thus, the observed spatiotemporal changes in reporter expression are likely driven by the enhancer rather than DNA sequences in the vector or surrounding genomic regions.

Comparison of temporal changes in *br^{disc}* reporter activity and a chromatin accessibility time course performed in developing wild-type wings revealed a strong correlation between reporter activity and endogenous enhancer accessibility. *Br^{disc}* exhibits high accessibility in 3LW wing discs, remains in an open state during the prepupal stage at 6h APF, and subsequently loses most of its accessibility by 18h APF, shortly after the prepupal to pupal transition (Uyehara *et al.,* 2017; **Fig 4.1C**). These accessibility profiles are congruent with changes in reporter activity. We note that the later reactivation of *br^{disc}* along the pupal wing margin does not coincide with a detectable increase in accessibility. This may be due to a lack of sensitivity to detect changes in a small number of cells using whole-wing FAIRE-seq. Alternatively, the small amount of accessibility that remains at later stages may derive from this population of cells. Together these observations demonstrate that *br^{disc}* is dynamically active and accessible during wing

development, thus making it a useful model for studying the mechanisms of dynamic enhancer regulation.

4.2.2 The *Drosophila* BAP nucleosome remodeling complex is required to repress br^{disc}

To identify factors that contribute to the developmental dynamics of br^{disc} enhancer activity during wing metamorphosis we performed an *in vivo* RNAi screen. As described above, conventional fluorescent reporters are engineered to be highly stable, making them poorly suited for detecting changes in enhancer activity. While the switch reporter corrects for this problem by using a two-fluorophore output, it is too technically cumbersome for use in a larger scale screen. To circumvent this limitation while optimizing screen throughput, we created a second new transgenic fluorescent reporter in which the br^{disc} enhancer drives tdTomato fused to a C-terminal PEST degradation tag (*br^{disc}-tdT-PEST*; Li *et al.,*, 1998; Nern *et al.,*, 2011). This design yielded increased sensitivity for detecting br^{disc} dysregulation, as determined by comparing reporter levels in the presence and absence of the PEST tag upon knockdown of a known br^{disc} repressor (**Fig 4.S2A**). We interpret the increase in sensitivity to be due to increased tdTomato turnover relative to the non-tagged version. Despite addition of the PEST tag, a low but detectable level of tdTomato expression was observed in wild-type pupal wing cells, which we interpret as residual fluorophore expression from earlier times in development when the enhancer is active (**Fig 4.S2A**). RNAi expression was controlled by the UAS/GAL4 system via the cubitus interruptus anterior compartment GAL4 driver (*ci-GAL4*). A ubiquitously expressed temperature-sensitive allele of the GAL4 repressor GAL80 (*tub-$GAL80^{ts}$*) was used to restrict RNAi expression to later stages of development (ci^{ts}; **Fig 4.2A**). We envisioned two potential outcomes upon RNAi knockdown of br^{disc} regulators: loss of an activator would yield decreased levels of tdTomato relative to control cells, and loss of a repressor would yield increased levels of tdTomato relative to control cells. We reasoned that by screening for tdTomato levels in pupal wings, we would potentially capture two types of repressors, those that deactivate br^{disc} over time and those that constrain the levels of br^{disc} activity while it is on in larval stages (**Fig 4.2B**). Knockdown of the transcription factor Eip93F (E93), a known negative regulator of br^{disc} expressed during pupal stages, resulted in increased br^{disc} reporter activity in pupal wings, whereas expression of a negative control *lexA-RNAi* failed to impact br^{disc} activity, confirming the sensitivity of our reporter screen

design to detect changes in enhancer activity (**Fig 4.2C**).

We focused our RNAi screen on nucleosome remodelers, reasoning that the functions of these enzymatic complexes in controlling nucleosome occupancy, positioning, and stability may contribute to developmentally programmed changes in enhancer accessibility. We tested a total of 49 RNAi lines corresponding to 31 genes encoding components of major ATP-dependent nucleosome remodeling complexes (Clapier *et al.,* 2017; **Table 4.S1**). These include members of all four families of remodeling complexes: Imitation Switch (ISWI), Switch/Sucrose Non-Fermenting (SWI/SNF), Chromodomain Helicase DNA-binding (CHD), and Inositol requiring 80 (INO80). Specific *Drosophila* nucleosome remodeling complexes include members of the ACF complex, the Brahma Complex (BAP and PBAP), the Chromatin Accessibility Complex (CAC), the Domino Complex, the INO80 complex, the Nucleosome Remodeling Deacetylase (NuRD) complex, the Nucleosome Remodeling Factor (NURF) complex, the Toutatis-containing chromatin Remodeling Complex (TORC), and several additional non-complex associated SNF2-like remodeler proteins (**Table 4.S1**). To summarize the results of the screen we quantified the average intensity of the br^{disc} reporter in RNAi expressing cells (anterior compartment), normalized to WT cells (posterior compartment) within the same wing (KD/WT) (**Fig 4.2D**). 2 genes were identified that decreased reporter activity in pupal wings, including Iswi, which is a component of the ACF, CHRAC, and NURF remodeling complexes (Bouazoune and Brehm, 2006; **Fig 4.S2C**). 8 genes were identified that increased reporter activity (**Fig 4.2D**; **Table 4.S1**). Remarkably, 5 of these 8 genes are subunits of the *Drosophila* SWI/SNF BAP complex. These include, *osa*, *moira* (*mor*), *Snr1*, *Bap111*, and the core ATP-ase Brahma (*brm*). In some cases, we found that RNAi lines targeting the same gene gave divergent results in our screen. For instance, two independent RNAi lines for *Snr1* yielded some of the strongest increases in br^{disc} activity (lines 32372 and 108599) while a third line (67929) produced little change. Similarly, of the two RNAi lines targeting *brm*, only one (31712) had a significant effect on br^{disc} reporter activity. Notably, RNAi lines that significantly impacted reporter activity often caused lethality, with many animals dying as pupae or pharate adults (**Table 4.S1**). By contrast, the *brm* and *Snr1* RNAi lines that did not impact reporter activity had little to no impact on animal survival or wing development. Since both *brm* and *Snr1* are essential genes, we interpret the lack of phenotype caused by these RNAi lines to

be a consequence of poor target knockdown. Due to the enrichment of Brahma complex members among hits, we chose to characterize the role for this nucleosome remodeler in br^{disc} repression. We did not pursue other hits further.

There are two distinct versions of the Brahma complex in *Drosophila*, BAP and PBAP, which are defined by the mutually exclusive association of either Osa (BAP), or Polybromo, SAYP, and Bap170 (PBAP; Cenik and Shilatifard, 2021). We find that multiple RNAi lines targeting *osa* resulted in de-repression of br^{disc} in the pupal wing, whereas three independent RNAi lines for *polybromo* had no effect on the normal dynamics of br^{disc} by either qualitative observation or image quantification (**Fig 4.2E**; **Fig 4.S2D**). We did not observe significant lethality or dramatic changes in wing morphology with any of the tested *polybromo* RNAi lines, suggesting that either these *polybromo* RNAi reagents are ineffective in the context of our screen or Polybromo is not required for wing development at this stage. Although we cannot definitively exclude PBAP, the finding that Osa is required for br^{disc} reporter repression demonstrates a role for the Osa-specific BAP complex in the dynamic regulation of this enhancer. Homozygous *osa* mutant cells generated by mitotic recombination also exhibited increased br^{disc} reporter activity (**Fig 4.S2E**), further supporting a role of Osa and the BAP complex in br^{disc} repression. Accordingly, we focused on the Osa-specific BAP complex in subsequent experiments.

4.2.3 Osa is largely dispensable for pupal patterns of chromatin accessibility

Deactivation of temporally dynamic enhancers is associated with decreased chromatin accessibility over developmental time, and failure to deactivate temporally dynamic enhancers coincides with aberrantly persistent chromatin accessibility (Uyehara *et al.,* 2017). Our observation that Osa depletion causes de-repression of the br^{disc} reporter in pupal wings (**Fig 4.2E**) raised the possibility that the BAP complex may be required for closing of temporally dynamic enhancers. To test the genome-wide role of Osa in developmental control of chromatin accessibility, we performed FAIRE-seq in an *osa* degradation genotype. We employed the GFP deGrad system in conjunction with a genotype, osa^{GFP}, in which both *osa* alleles are tagged with GFP (hereafter: Osa-deGrad; Buszcak *et al.,* 2007; Caussinus *et al.,* 2012; **Fig 4.S3A**). The GFP deGrad system enables target proteins to be rapidly degraded, which is

especially important in pupal wings because they undergo few cell divisions following pupariation (Ma *et al.,* 2019; **Fig 4.3A**). Animals homozygous for osa^{GFP} are viable and do not exhibit any morphological or developmental defects, indicating that Osa-GFP protein is functional. Confocal microscopy of osa^{GFP} heterozygous imaginal wing discs showed nuclear-localized GFP that colocalized with endogenous Osa. Moreover, GFP signal was specifically depleted upon expression of Osa RNAi, validating the identity of this genotype (**Fig 4.S3B**). Osa-GFP degradation was induced in animals homozygous for osa^{GFP} during the late larval stage (3LW). Prepupal animals were staged (0-12h APF) and aged for ~24h before dissection such that total degradation time was ~36h (**Fig 4.3A**). Consistent with our RNAi results, we observed near-complete loss of Osa-GFP protein in the pupal wing blade under these conditions and a corresponding increase in br^{disc} reporter activity, demonstrating the efficacy of Osa-deGrad depletion (**Fig 4.3B**). Immunofluorescence for Osa under these degradation conditions confirmed significantly reduced nuclear Osa signal relative to control (**Fig 4.S3C**). Osa-deGrad flies that were permitted to develop longer exhibited reduced wing size and high rates of lethality, with most animals dying as pharate adults. Despite the strong impact of Osa-deGrad on wing development, br^{disc} reporter activity, and survival, FAIRE-seq revealed minimal changes in chromatin accessibility profiles relative to controls samples, including at br^{disc} (**Fig 4.3C,D**). A union set of 6,826 open chromatin peaks was identified between both control and Osa-deGrad samples (**Fig 4.S3D**). Pearson correlation coefficients of z-normalized FAIRE signal revealed high correlation between both replicates of control and Osa-deGrad pupal wing profiles, indicating that Osa degradation minimally affects open chromatin profiles (**Fig 4.S3E**). We conclude that increased br^{disc} activity observed in osa loss-of-function pupal wings is not due to failure to close the br^{disc} enhancer. These findings also demonstrate that developmentally programmed opening and closing of wing enhancers occurs normally genome wide in the absence of Osa.

Previous studies in mammalian experimental systems have observed a role of Brahma Complex orthologs in promoting chromatin accessibility (Kelso *et al.,* 2017, Hendy *et al.,* 2022). To test for the possibility of subtle changes in accessibility, we compared FAIRE signal between Osa-deGrad and control samples and observed a unidirectional skew toward lower FAIRE signal in Osa-deGrad relative to control (**Fig 4.3E**). We note that while we find 356 regions (5.2%) with reduced accessibility (log_2FoldChange

<= -1, “Osa-dependent”) following Osa-GFP degradation, only 14 (0.2%) were found to be statistically significant (adj p-value <= 0.1) due to variability between replicates, raising the possibility that some of these regions are false positives. Examples of these Osa-dependent sites occurred at genes including *prickle* (*pk*) and the ecdysone response gene *Eip74EF* (**Fig 4.3F**). Both of these Osa-dependent sites exhibit temporally dynamic accessibility, with low accessibility observed in larval wing imaginal discs becoming progressively more open later in pupal stages. To determine if temporally dynamic accessibility is a general feature of Osa-dependent FAIRE peaks, we categorized each peak as either ‘Increased’, ‘Static’, or ‘Decreased’ based on the wild-type FAIRE-seq signal at that site during pupal stages relative to the late larval stage (see Methods). We find that 64% (228/356) of Osa-dependent sites correspond to regions that increase in accessibility between larval and pupal stages (**Fig 4.3G**), whereas only 4.2% of Osa-dependent sites decrease in accessibility over the same time interval. This finding suggests that while the effect of Osa-GFP degradation is minor, the subtle losses in accessibility observed are most often associated with regions that open between early and late wing development. Collectively, we conclude that Osa is not required for large, binary changes in “open” or “closed” chromatin over time during wing development. Instead, it is required for only a small number of sites to achieve full accessibility.

4.2.4 The *br^{disc}* reporter is active in a small number of pupal wing cells upon Osa loss of function

Our FAIRE-seq data indicate that Osa is not required for enhancer closing between early and late stages of wing development. The finding that *br^{disc}* is closed in osa loss-of-function pupal wings raised the possibility that the enhancer is inactive despite the apparent increase in reporter activity. To directly test whether the *br^{disc}* enhancer is active in osa loss-of-function pupal wings, we utilized the dual-fluorophore *br^{disc}-switch* reporter (**Fig 4.1A**). We first depleted Osa using the same RNAi-mediated knockdown conditions employed in the nucleosome remodeler screen, but using the posterior *en-GAL4, tub-GAL80^{ts}* (*en^{ts}*) driver. The switch from tdTomato to myr-GFP reporter output was induced at a timepoint after *br^{disc}* deactivation (>24h APF). Under these conditions, we found that the enhancer remains inactive in the great majority of pupal wing cells, with a few notable exceptions. Whereas control lexA knockdown pupal

wings exhibited nascent GFP along the margin and in the posterior crossvein, similar to the enhancer's pattern of activity in wild-type pupal wings (**Fig 4.1B**), osa knockdown pupal wings also exhibited nascent GFP expression in a subset of cells in the wing blade (**Fig 4.4A**). Notably, the membrane localized myr-GFP of the *br^{disc}-switch* reporter revealed that wing blade cells in which *br^{disc}* was active exhibited a distinct morphology resembling shaft cells of adult sensory organs. These were similar in appearance to the shaft cells located along the wing margin in which the *br^{disc}* reporter normally reactivates during later pupal stages in wild-type animals (**Fig 4.4A**, Inset). Elevated levels of nascent GFP were also observed in the posterior margin of osa knockdown pupal wings (**Fig 4.4A**). The detection of nascent GFP after *br^{disc}* normally closes and deactivates indicates that osa knockdown causes the enhancer to be inappropriately active in a small number of cells. However, *br^{disc}* activity was not detected in most cells that exhibited increased reporter levels in the initial nucleosome remodeler screen. It is possible that the small number of additional cells in which *br^{disc}* is active in osa knockdown pupal wings is too few to impact whole wing open chromatin profiles, thus explaining the closed appearance of the enhancer in our FAIRE-seq data.

Sensory organs do not normally develop within the wing blade. In wild-type tissues, sensory organ precursors (SOPs) are specified with stereotypical spatial and temporal patterns, with the last SOPs in the wing being specified during prepupal stages. Once specified, SOPs undergo two rounds of cell division and fate specification, resulting in development of a single shaft, socket, sheath, and neural cell, which together compose an adult sensory organ (Couso *et al.,* 1994; Furman and Bukharina, 2012). The appearance of *br^{disc}* activity in cells with shaft-like morphology in the wing blade indicated that osa knockdown leads to development of ectopic sensory organs. Consistent with this hypothesis, osa knockdown also resulted in ectopic expression in the wing blade of Elav, a marker of neural cell identity (**Fig 4.S6**). This finding is in agreement with prior studies in which combinations of osa hypomorphic alleles and loss-of-function clones caused ectopic sensory organ development (Heitzler *et al.,* 2003; Terriente-Félix and de Celis, 2009). We speculated that by initiating RNAi expression in larval wing discs, early loss of osa function leads to ectopic sensory organ development accompanied by *br^{disc}* activation. To test this hypothesis, we sought to knockdown osa function later in wing development, reasoning that the delay would reduce the likelihood of disrupting development of sensory organs, which are determined

by the end of prepupal stages (Couso *et al.,* 1994). We returned to the Osa-deGrad system due to its rapid depletion of Osa protein, in combination with the ents driver. Osa degradation was initiated in 0-12h prepupae, ~48h later than initiation of knockdown in the RNAi screen. Examination of br^{disc} reporter activity 30h later revealed two phenotypic classes that correlated with wing age. In younger pupal wings, there was clear de-repression of br^{disc} in Osa-deGrad cells relative to wild-type cells in the same wing. By contrast, older pupal wings exhibited no sign of br^{disc} de-repression in the wing blade (**Fig 4.4B**). We interpret these findings as being a consequence of the developmental stage when Osa degradation was initiated. Since the duration of Osa depletion was the same for both phenotypic classes, the younger pupal wings, which exhibit br^{disc} de-repression, would have been at an earlier developmental stage when Osa depletion initiated than the older pupal wings, which do not exhibit br^{disc} de-repression. We conclude that Osa is not required for br^{disc} deactivation. Instead, any detected increase in reporter activity is likely due to indirect consequences stemming from disruption of osa function early in sensory organ development.

4.2.5 Osa is required to constrain br^{disc} reporter activity in wing imaginal discs

We hypothesized that if Osa and other BAP complex members are required for reduced br^{disc} reporter levels in pupal wings, as indicated by our RNAi screen results, but they are not required for chromatin closing or for br^{disc} reporter deactivation, then Osa may be required to repress br^{disc} reporter activity at an earlier stage of development (**Fig 4.2B**). To test this hypothesis, we assayed br^{disc} reporter activity in wing imaginal discs following Osa knockdown, which corresponds to a developmental stage when br^{disc} is normally active. At this timepoint, wing discs are approximately two days younger than the pupal wings assayed in our RNAi screen. We observed a marked increase in reporter activity in osa knockdown cells relative to control cells. By contrast, a negative control RNAi targeting lexA did not affect br^{disc} reporter activity at this stage (**Fig 4.4C**). Quantification of the ratio of reporter signal in RNAi expressing versus control cells confirmed significant hyperactivation of the reporter in osa knockdown but not in control lexA knockdown cells (p-value=6.84e-14, Two-sample t-test; **Fig 4.4D**). The requirement of the BAP complex to constrain br^{disc} activity in the wing disc was further validated by independent

knockdown of a different BAP complex member brm, as well as an independent *osa* RNAi line (330350), both of which also resulted in increased br^{disc} reporter activity (**Fig 4.S4A,B**). Thus, loss of Osa function results in hyperactivation of the br^{disc} enhancer in cells in which it is already active. Increased br^{disc} reporter levels following knockdown of BAP complex members indicates that BAP is required to constrain activity of the enhancer in wing imaginal discs. Because we find no evidence that Osa is required to close the br^{disc} enhancer in pupal wings, we interpret the increased reporter activity observed in pupal wings to be a consequence of persistent reporter fluorophore following enhancer hyperactivation in wing imaginal discs (**Fig 4.2B**, magenta line).

4.2.6 Osa directly binds br^{disc} in larval wing imaginal discs as well as thousands of putative enhancers genome wide

Hyperactivation of the br^{disc} reporter in wing imaginal discs following degradation of BAP complex members could be due to a direct loss of BAP function at the enhancer, or an indirect consequence of dysregulation of other br^{disc} inputs. To determine if the BAP complex directly binds br^{disc}, we performed CUT&RUN for Osa using the osa^{GFP} allele. We performed anti-GFP CUT&RUN in homozygous osa^{GFP} and WT control female wing imaginal discs. We identified 2,150 Osa-GFP peaks (see Methods), the great majority of which (1,953) did not overlap control peaks (**Fig 4.5A,B**). We focused on this set of Osa-GFP-specific peaks (“Osa peaks”) for all subsequent analysis.

Genomic feature annotation revealed that a majority of Osa peaks were enriched in distal intergenic regions and introns relative to a shuffled Osa peak control annotation (**Fig 4.5C**). We found that Osa peaks were significantly more abundant in “Introns” (48.6%, p-value=6.4e-58), and “5’ UTRs” (6.3%, p-value=7e-5). Osa peaks were significantly less abundant in “Exons” (2.4%, p-value=5.7e-46) and “3’ UTRs” (0.8%, p-value=5e-35, two-proportion z-test). Collectively, these findings indicate that Osa is predominantly bound to non-coding regions of the genome (86.6% Promoter | Distal Intergenic | Intron), consistent with an expected role in gene regulation. In order to focus our analysis on *cis*-regulatory elements with potential roles as developmentally dynamic enhancers, we selected Osa peaks that lie distal to promoters for use in subsequent analysis (1,358 peaks, “distal Osa peaks”).

To evaluate the relationship between Osa binding and potential enhancer activity, we next examined the overlap between distal Osa peaks and open chromatin sites in wing imaginal discs (Uyehara *et al.,* 2017). We found that most distal Osa peaks (65%, 889) were associated with a high-degree of chromatin accessibility, whereas 35% (469) of distal Osa peaks did not overlap a FAIRE peak in wing imaginal discs (**Fig 4.5D**). Notably, 25% (119) of these Osa-bound "closed" sites were identified as a FAIRE peak in at least one later stage of wing development (**Fig 4.S5F**). Thus, 74.2% (1008) of distal Osa peaks are bound at regions that are either open in wing imaginal discs or will open subsequently during a later stage of wing development. To further examine the regulatory potential of distal Osa peaks, we performed CUT&RUN for histone H3 lysine 27 acetylation (H3K27ac), an epigenetic mark associated with active enhancers, in wing imaginal discs. We found an enrichment of H3K27ac signal at highly accessible distal Osa peaks (**Fig 4.5D**). Interestingly, we also found H3K27ac signal at distal Osa peaks that do not overlap a FAIRE peak, suggesting that some of these sites possess enhancer activity despite exhibiting low chromatin accessibility (**Fig 4.5D**). Together, the correlation between chromatin accessibility and H3K27ac enrichment at distal Osa peaks indicates these sites are likely to function as enhancers in developing wings.

To further define the relationship between Osa occupancy and regulatory DNA, we examined binding at previously characterized enhancers. Firstly, we found that Osa is bound at the endogenous br^{disc} enhancer with broad signal observed across the entire enhancer in both replicates. By contrast, CUT&RUN signal apparent at the br^{disc} enhancer in control experiments was non-reproducible and restricted to narrow regions, which we interpret as being due to opportunistic MNase digestion of this highly accessible DNA (**Fig 4.5E**). The presence of Osa at the endogenous br^{disc} enhancer strongly suggests that direct binding of the BAP complex to br^{disc} is required to constrain its activity.

In addition to br^{disc}, we observed Osa bound at multiple genes known to be regulated by the Brahma Complex during wing development, such as at components of the *Drosophila* Notch signaling pathway. There is a well-established connection between Brahma complexes and Notch signaling. Mutants of Notch pathway genes enhance brm dominant negative allele phenotypes, Osa loss of function increases expression of the proneural Notch targets *achaete* and *scute* (*ac/sc*), and both Brm and Mor

are required for full induction of the Notch target genes in the Enhancer of Split complex (*E(spl)-C*) locus (Elfring *et al.,* 1998; Heitzler *et al.,* 2003; Armstrong *et al.,* 2005; Pillidge and Bray, 2019). Consistent with this relationship, we observed high-amplitude Osa binding sites at the genes encoding the Notch ligands Delta (Dl) and Serrate (ser), the Notch receptor Notch (N), and Notch target E(spl)-C genes (**Fig 4.5F, 4.S5A-C**). At least two of the Osa peaks in the Dl locus corresponded to previously characterized enhancers, including the Dl^{SOP} enhancer, which is active within sensory organ precursor cells in wing imaginal discs, and the Dl^{teg} enhancer, which is active in the tegula, hinge, and anterior notum (Uyehara and McKay, 2019). Osa binding in the *E(spl)-C* locus overlaps the m^{α}, m^{β}, m^{2}, and m^{3} enhancers, which contribute to proneural cluster development in wing imaginal discs. Like many signaling pathways, Notch signaling relies on the action of co-repressors to limit expression of Notch targets in the absence of signal. In *Drosophila*, the co-repressor Hairless binds the Notch signaling effector Suppressor of Hairless (Su(H)) and has been found to bind hundreds of sites across the genome in the wing disc, including known regulatory sites that require Hairless for negative regulation (Chan *et al.,* 2017). Using previously published Hairless ChIP data from wing imaginal discs, we examined the correlation between Osa and Hairless binding (Chan *et al.,* 2017). We found that the majority (64.2%) of Hairless peaks intersect an Osa binding site, indicating a significant overlap between these gene regulatory proteins (adj p-value=9.99e-4, Fisher's exact test; **Fig 4.5G**). Notably, we also observed that Hairless was bound at the endogenous br^{disc} enhancer, as well as at known and putative enhancers of the *Dl* and *E(spl)-C* loci (**Fig 4.5E,F**). These findings further support the strong association between the BAP complex and Notch signaling. More generally, the concerted presence of Osa binding at *bona fide* enhancers indicates that the BAP complex is a direct regulator of transcriptional programs with major roles in wing development.

In addition to binding known regulatory elements, we found that Osa binding is also correlated with genomic loci that exhibit temporal changes in chromatin accessibility. A previous FAIRE-seq time course of wild-type wings identified distinct patterns of temporal accessibility changes (Uyehara *et al.,* 2017; Nystrom *et al.,* 2020; **Fig 4.5H, 4.S5E**). By clustering FAIRE signal in Osa-bound regulatory sites, we found that 84.5% of Osa-bound distal regulatory sites were associated with FAIRE-seq peaks that exhibited temporal changes during wing development, whereas only 15.5% of peaks exhibited

static accessibility (**Fig 4.5H**). The correlation between distal Osa peaks and dynamic rather than static accessibility, indicates that Osa is associated with regulatory regions that are likely stage-specific and are either being actively used at larval stages or possibly constrained from being used until a later stage.

Like most nucleosome remodeling complexes, the BAP Complex does not exhibit sequence-specific DNA binding but is instead thought to be recruited to target loci by transcription factors. Osa contains an AT-Rich Interacting Domain (ARID) that facilitates interaction with DNA, but this domain has been shown to confer little to no sequence preference on BAP complex DNA binding (Collins *et al.,* 1999; Patsialou *et al.,* 2005). To identify candidate factors that contribute to the recruitment of Osa to its binding sites, we performed motif enrichment analysis of sequences around distal Osa peaks. Of the highest significance motifs, several were associated with major signaling pathways and wing patterning programs. Notably, we found motifs for the homeodomain factors Extradenticle (Exd) and Araucan (Ara), the Wingless-signaling effector Pangolin (Pan), and the zinc-finger transcription factors Squeeze (Sqz) and Rotund (Rn) (**Fig 4.5I**). Enrichment of Pan motifs in Osa binding sites is notable because Osa has been proposed to repress Wingless target genes (Collins and Treisman, 2000). Our findings indicate that this repression could be direct. For instance, the Wingless target gene, nubbin, which is ectopically expressed in *osa* mutants, has several Osa binding sites in wing imaginal discs (Collins and Treisman, 2000; **Fig 4.S5D**). The enrichment of Pan motifs and others in Osa binding sites suggests that the BAP complex is broadly utilized by the major signaling pathways and patterning factors that shape wing development. To extend this observation further, we examined recently published Rn ChIP-seq data from wing imaginal discs and found that 23% (312) of distal Osa peaks overlap with a Rn peak, which is greater than expected by chance as tested by overlap with shuffled Osa peak controls (adj p-value=9.99e-4, Two-sample t-test) (Loker *et al.,* 2022; **Fig 4.5J**). This correlation between Rn and Osa binding at regulatory sites in the wing disc further supports the connection between Osa and active wing developmental programs.

4.2.7 Osa is required to constrain Delta activation in wing imaginal discs

Notch signaling performs multiple critical roles in wing imaginal discs. Notch-mediated lateral

inhibition is necessary for selecting the sensory organ precursor cells that form the chemosensory and mechanosensory organs of the adult wing. Notch signaling also initiates specification of wing vein cell fates. Both of these processes depend on patterned expression of the Notch ligand, Dl, which has an extensive *cis*-regulatory domain. It has been previously observed that Osa is involved in the regulation of Dl expression in parts of the wing disc pouch (Terriente-Félix and de Celis, 2009). Due to the discovery of multiple Osa binding sites at known and putative enhancers within the Dl locus, we hypothesized that Osa regulates Dl expression directly. Dl is expressed in larval wing discs in two rows of cells flanking the dorsal/ventral (DV) boundary of the developing wing margin, and in perpendicular stripes marking the developing veins (Doherty *et al.,* 1996). We found that depletion of Osa from the anterior compartment of the wing disc resulted in increased Dl levels and subtle expansion of the Dl pattern most notably around the L2 provein stripe (**Fig 4.6A**). To support this observation, we quantified Dl levels around the margin in both Osa and lexA control knockdown experiments. For each wing disc, measurements around the RNAi expressing anterior margin were normalized to non-RNAi expressing cells in the posterior margin (see Methods). We find that Dl levels were significantly higher in Osa knockdown relative to control (p-value=9.67e-11, Two-sample t-test; **Fig 4.6B**). Notably, our observation that Osa negatively regulates Dl expression is in disagreement with previous work that found Osa depletion leads to reduced Dl in the L3 and L4 proveins (Terriente-Félix and de Celis, 2009; see Discussion). Together, these findings demonstrate that enhancer hyperactivation in the absence of the BAP complex is correlated with increased expression of the Notch ligand.

4.3 Discussion

We set out to investigate possible roles of nucleosome remodeling complexes in developmentally programmed enhancer regulation, with a particular focus on enhancer closing and deactivation. Using reporters of the previously characterized and developmentally dynamic wing enhancer, br^{disc}, we performed an *in vivo* RNAi screen that identified members of the *Drosophila* SWI/SNF (BAP) complex as repressors of enhancer reporter activity. Surprisingly, we find that the BAP-specific subunit Osa is not required to close br^{disc} and is globally dispensable for binary changes in accessibility, closing or opening,

between early and late stages of wing development (**Fig 4.3**). Rather than being required for enhancer deactivation, we instead find that Osa is required to constrain activity of the br^{disc} enhancer when it is in the ON state in wing discs (**Fig 4.4**). Genome-wide profiling of Osa binding revealed that Osa bound extensively to sites with signatures of active regulatory DNA (open and H3K27ac enriched), including at multiple known and putative enhancers of Notch pathway component genes (**Fig 4.5**). Analysis of binding sites of Osa and the Notch co-repressor Hairless revealed significant co-enrichment of these proteins genome wide, suggesting a direct coregulatory relationship between Notch signaling responses and the BAP complex. Finally, we find that Osa depletion in wing discs leads to upregulation of the Notch ligand, Delta, further supporting a central role of Osa and the BAP complex in regulating Notch pathway activity (**Fig 4.6**).

4.3.1 Is the BAP complex required for control of chromatin accessibility in developing *Drosophila* wings?

Thousands of *cis*-regulatory elements exhibit chromatin accessibility changes during the first two days of pupal wing development in *Drosophila*, which drive the dynamic gene expression changes that underlie progressive determination of cell fates (Uyehara *et al.,* 2017; Ma *et al.,* 2019). We hypothesized that nucleosome remodeling complexes work with sequence-specific transcription factors to bring about these kilobase-sized transitions in chromatin state. However, we observed no requirement for Osa in either opening or closing enhancers genome-wide (**Fig 4.3**). This is a surprising finding because SWI/SNF complex function has been found to be required for proper control of chromatin accessibility in mammalian cells. For example, genetic removal or chemical inhibition of the SWI/SNF ATPase Brg1 in mouse embryonic stem cells results in loss of accessibility genome wide (Lurlaro *et al.,* 2020). Similarly, loss of the Osa ortholog ARID1A, which is commonly mutated in cancers (Kadoch *et al.,* 2013), results in both loss and gain of open chromatin sites in human cells (Kelso *et al.,* 2017). Whereas we observed subtle decreases in accessibility at a subset of open chromatin sites upon Osa knockdown, we did not find evidence for a global role of Osa in binary chromatin state transitions from closed to open or open to closed, leading us to conclude that Osa is not required for these developmentally programmed

epigenetic changes. An alternative explanation is that our methods did not sufficiently deplete Osa below a minimal threshold. We disfavor this possibility because no Osa-GFP signal remains after nanobody-mediated degradation, and immunostaining with Osa antibodies likewise revealed little nuclear signal above background (Fig S3). Moreover, we observed developmental phenotypes consistent with Osa loss of function. Another possible explanation is that the role of the BAP complex in regulating chromatin accessibility is compensated for by the PBAP complex. Synthetic lethal phenotypes caused by perturbation of subunits from distinct SWI/SNF complex subtypes have been reported, supporting the potential of functional redundancy (Michel *et al.,* 2017; Helming *et al.,* 2014; Wilson *et al.,* 2015). Lastly, multiple nucleosome remodelers can be found at the same genomic targets (Morris *et al.,* 2014), raising the possibility of compensation by other complexes.

4.3.2 What is enhancer constraint?

SWI/SNF nucleosome remodeling complexes were first identified for their role in counteracting Polycomb-mediated repression and establishing regions of nucleosome depletion in order to facilitate transcription (Kassis *et al.,* 2017; Cenik and Shilatifard 2021). Subsequent work has demonstrated that SWI/SNF complexes are required to maintain nucleosome depleted regions, high levels of H3K27ac, and enrichment of the histone variant H3.3 at enhancers and promoters (Alver *et al.,* 2017; Schick *et al.,* 2021; Blumli *et al.,* 2021; Weber *et al.,* 2021; Hendy *et al.,* 2022; Reske *et al.,* 2022). In addition to their role in gene activation, SWI/SNF complexes have also been implicated in gene repression (Treisman *et al.,* 1997; Moshkin *et al.,* 2007; Zraly *et al.,* 2012; Kelso *et al.,* 2017; Weber *et al.,* 2021), including repression of Wingless target genes during wing development (Collins *et al.,* 2000). Here, we find that the BAP complex constrains activity of the developmentally dynamic br^{disc} enhancer, but it is not required for closing or deactivation. DNA binding profiles reveal that Osa binds the br^{disc} enhancer while it is active in developing imaginal wing discs, suggesting its role in enhancer constraint is direct. How might SWI/SNF function to achieve constraint? SWI/SNF complexes are generally understood to slide and/or eject nucleosomes by translocating DNA around the histone octamer (Clapier *et al.,* 2017). Nucleosome mobilization could result in repression if DNA translocation blocked a binding site for an

activator. Conversely, increased accessibility mediated by SWI/SNF could uncover a repressor binding site. Differential accessibility of repressor binding sites in a wing spot enhancer was recently proposed as a mechanism involved in morphological diversification between *Drosophila* species (Ling *et al.,* 2023). Another possible direct mechanism is through changes in histone acetylation via collaboration with the NuRD complex. A recent study in human endometriotic epithelial cells demonstrated that the Osa ortholog ARID1A is required to maintain levels of the histone variant H3.3 at active enhancers, which in turn is required to recruit NuRD complex components and limit the accumulation of active H3K27ac levels (Reske *et al.,* 2022). Lastly, iterative cycles of nucleosome remodeling activity driven by ATP hydrolysis could impact the dynamics of transcription factor occupancy at target enhancers, which in turn could impact their potency as transcriptional regulators (Morris *et al.,* 2014; Brahma and Henikoff, 2023). In addition to these direct mechanisms, it is also possible, though not mutually exclusive, that SWI/SNF-dependent enhancer constraint is an indirect consequence of SWI/SNF-dependent repressor activation. For example, failure to activate the transcriptional repressors encoded by the Enhancer of split complex locus could contribute to hyperactivation of Notch pathway target genes in Osa loss of function wings (see below).

4.3.3 The BAP complex as a direct regulator of Notch signaling

Our findings point to an important role of Osa in Notch pathway function. This is supported by prior studies that have discovered strong regulatory connections between the Notch pathway and the BAP complex. Genetic screens found that alleles of Dl dominantly enhance phenotypes of an ATP-ase dead *brm* allele (brm^{K804R}; Armstrong *et al.,* 2005). BAP complex members have also been found to regulate the expression of Notch signaling targets, such as genes encoded by the Enhancer of split complex and achaete/scute loci (Armstrong *et al.,* 2005; Pillidge *et al.,* 2019). Our genomic profiling of Osa in wing imaginal discs revealed clusters of Osa binding at putative regulatory sites at loci encoding the Notch ligands Dl and Ser, at the gene encoding the Notch receptor itself, and at enhancers of the Enhancer of split complex (**Fig 4.5**, **4.S5**). Interestingly, it has been previously reported that Osa negatively regulates expression of the proneural genes achaete and scute, but we observed little binding of Osa around

these genes sparing a single potential binding site that also has a relatively high degree of signal in negative controls (Armstrong *et al.,* 2005). This suggests the regulation of achaete and scute by the BAP complex may be indirect. In addition to extensive binding of Osa at genes encoding Notch pathway components, we also find significant co-enrichment of Osa binding and the Notch pathway co-repressor Hairless, including at the br^{disc} enhancer (**Fig 4.5G**). Thus, the BAP complex may directly regulate Notch target genes genome wide. Together, our binding data strengthen the previously observed regulatory relationship between the BAP complex and Notch signaling.

Several observations made through the course of our study suggest a regulatory connection between the br^{disc} enhancer, the BAP complex, and the Notch signaling pathway. The br^{disc} enhancer may itself be a Notch pathway target gene. In addition to being bound Hairless, the pattern of br^{disc} activity in wing imaginal discs suggests positive input from Notch signaling. The highest levels of enhancer activity in the pouch of wing imaginal discs are typically observed along the presumptive wing margin and in two dorsal-ventral stripes that extend away from the margin that resemble the wing proveins (**Fig 4.4C**). Each of these regions overlap high levels of Dl expression. The activity of br^{disc} in pupal wings is also suggestive of Notch pathway input. Br^{disc} is reactivated in the sensory organs located along the wing margin approximately 40hAPF. Notch signaling is required for determining the fates of these sensory organ cells. Moreover, sensory organ development is particularly sensitive to the levels of Notch pathway signaling, with too much or too little Notch signaling leading to sensory organ developmental defects. Hyperactivation of the Notch pathway may also explain development of ectopic sensory organs and activation of the br^{disc} enhancer in shaft cells of the developing pupal wing blade upon Osa loss of function. Collectively, these observations suggest that the br^{disc} enhancer is responsive to Notch signaling, and that the BAP complex may be required to directly constrain Notch target gene activity, possibly in collaboration with Hairless. A lack of proper constraint by the BAP complex at enhancers of Notch signaling component genes and of Notch target genes may result in the observed development of ectopic of bristles and neurons (**Fig 4.S6**). This possibility is further supported by our observation that Osa negatively regulates Dl (**Fig 4.6**). We note that prior studies describe a role of Osa in activation of Dl in wing imaginal discs, which contrasts with our observations (Terriente-Félix *et al.,* 2009). We attribute this

discrepancy as being due to the different spatial patterns and timing of the GAL4 drivers used. Altogether, our data support a direct role for the BAP nucleosome remodeling complex in mediating the proper levels of Notch pathway signaling during wing development.

4.4 Methods

4.4.1 Plasmid construction

The *br^{disc}-tdTomato-PEST* vector was made by cloning a PEST degradation tag from *w ; 20xUAS-FLPG5.PEST^{attP40} ;* (Bloomington 55806), using previously published primers (Nern *et al.,* 2011). The PEST sequence was inserted into the previously described pDEST-attR1/2-tdTomato by HiFi assembly (Uyehara *et al.,* 2017). The *br^{disc}* enhancer was moved into the destination vector by Gateway cloning (Invitrogen). The reporter was integrated into the *^{attP2}*, VK33, and 86FB landing sites. The *br^{disc}-FRT-tdTomato-2xSTOP-FRT-myrGFP* (*br^{disc}-switch*) reporter was generated from pJFRC177 *10xUAS-FRT-2xSTOP-FRT-myrGFP* (Addgene 32149). The *br^{disc}* enhancer was restriction cloned into the HindIII and AatII sites, replacing the upstream UAS elements. TdTomato cDNA sequence was subsequently restriction cloned into the NheI site. The reporter was integrated into the *attP2* landing site. Genomic insertions were made via PhiC31 integration. Injections were performed by BestGene.

Primers used:

tdTomato_NheI_Fwd	gaccatacgctagctttcgtttagccaagactcg
tdTomato_NheI_Rev	attctagggctagcagtgttgcatgtttcgaagg
BrA_hindIII_Fwd	ggccgcaagcttgagtgtgtgcgagtgaatga
BrA_AatII_Rev	gcgctcgacgtcccgaggaaagagcagaagatg
PEST_fwd	tgaagttgccctcgctagcCATGGCTTCCCTCCAGAG
PEST_rev	tgccgactggcttagttaattaattctagaTTACACGTTGATGCGAGC

4.4.2 *Drosophila* culture and genetics

For *br^{disc}-switch* experiments RNAi expression was driven by *en-GAL4, tub-GAL80$^{ts.10}$* driver.

Crosses were raised at 23°C until being shifted to 29°C to induce RNAi. Animals were heat shocked at 37°C for 1 hour to induce Flippase (FLP) expression under the control of the heat-inducible *hsFLP* promoter, and then recovered at 29°C for several hours to allow expression of myr-GFP before dissection. For imaginal discs, crosses were moved to 29°C 72-96h after egg laying (AEL), third larval wandering (3LW) animals were heat shocked 48h later, and then recovered for 4 hours before dissection. For pupal wings, crosses were moved to 29°C 96-120h AEL, prepupae (0-12h APF) were staged using the absence of head-eversion as a developmental marker, heat shocked 24 hours later (24-36h APF), and then recovered for either 4 hours (28-40h APF) or 6 hours (30-42h APF).

For RNAi screening using the *br^{disc}-tdTomato-PEST^{86Fb}* reporter, RNAi expression was driven by *ci-GAL4, UAS-GFP, tub-GAL80^{ts,10}* driver. Crosses were raised at 23°C until being shifted to 29°C to induce RNAi at 72-96h or 96-120h AEL, depending on the severity of phenotypes with individual RNAi lines. Prepupae were staged as described above and then dissected 24h later (24-36h APF). The same protocol was followed to evaluate enhancer hyperactivation except imaginal discs were dissected at 3LW.

For Osa-deGrad experiments, females of the genotype *UAS-Nslmb-vhhGFP ; osa^{GFP} / (TM6B, Tb)* were crossed to males with either *nub-GAL4, tub-GAL80^{ts,10} / CyO, Tb-RFP ; osa^{GFP} / (TM6B, Tb)* or *osa^{GFP} / (TM6B, Tb)* for the negative control lacking GAL4. Crosses were raised at 23°C until 3LW stage. Larvae were moved to 29°C, prepupae were staged 12h later, and non-Tubby female pupal wings were dissected 24h later (24-36h APF). For late Osa-deGrad immunofluorescence experiments, females with *en-GAL4, tub-GAL80$^{ts.10}$; osa^{GFP} / TM6B, Tb* were crossed to males with *UAS-Nslmb-vhhGFP4 ; br^{disc}-tdTomato-PEST^{VK33}, osa^{GFP} / TM6B, Tb*. Crosses were kept at 23°C until prepupal stage (0-12h APF) and then moved to 29°C to induce degradation. Non-tubby pupae (*osa^{GFP}* homozygous) were dissected 30h later (30-42h APF). Tubby pupae were (*osa^{GFP}* heterozygous) were used as a negative control. Younger wings (~28-38h APF) were identified within the staged range of 28-40h APF and by morphology (small size, absence of folding, absence of elongated bristle shafts along the margin). Older wings (>40h APF) were identified within the staged range of 30-42h APF and by morphology (presence of folds, flattened/ expanded cells in wing blade, presence of elongated bristle shafts along the margin) (Sobala and Adler, 2016; Diaz and Thompson, 2017; Guild *et al.,* 2005; Choo *et al.,* 2020).

For *osa*^{308} mitotic clone experiments, males with the genotype *yw122 ; ; br*^{disc}*-tdTomato-PEST* ^{attP2}*, FRT82B, ubi-GFP / TM6B, Tb* were crossed to females with the genotype *yw ; ; FRT82B, osa*^{308} */ TM6B, Tb* at 23^{o}C (day 0). On day 5, vials with larvae were heat shocked in a 37^{o}C water bath for 20 minutes, and then recovered at 25^{o}C for 48h. 0-12h APF prepupae were staged (pre head-eversion) and aged for ~28h before dissection. Wings were stained with mouse anti-Osa (1:200) and goat anti-mouse Alexa 633 (1:1000).

For CUT&RUN, cultures were raised at 25^{o}C.

Lines used:

yw ; en-GAL4, tub-GAL80$^{ts.10}$ *; br*^{disc}*-FRT-tdTomato-2xSTOP-FRT-myr-GFP* ^{attP2} */ (TM6B, Tb)*

yw ; ci-GAL4, UAS-GFP, tub-GAL80$^{ts.10}$ */ (CyO) ; br*^{disc}*-tdTomato-PEST*^{86Fb} */ (TM6B, Tb)*

yw ; ci-GAL4, UAS-GFP, tub-GAL80$^{ts.10}$ */ (CyO) ; br*^{disc}*-tdTomato-PEST*^{VK33} */ (TM6B, Tb)*

yw ; en-GAL4, tub-GAL80$^{ts.10}$ *; osa*^{GFP} */ (TM6B, Tb)*

yw ; UAS-Nslmb-vhhGFP4 ; osa^{GFP} */ (TM6B, Tb)*

w ; nub-GAL4^{AC-62}*, tub-GAL80*$^{ts.10}$ */ CyO, Tb-RFP ; osa*^{GFP} */ (TM6B, Tb)*

yw122 ; ; UAS-osa-RNAi ^{attP2} */ (TM6B)* – (Derived Bloomington 31266)

yw122 ; ; UAS-lexA-RNAi ^{attP2} */ (TM6B)* – (Derived Bloomington 67945)

yw ; ; osa^{GFP} */ (TM6B, Tb)*

yw122 ; ; br^{disc}*-tdTomato-PEST* ^{attP2}*, FRT82B, ubi-GFP / TM6B, Tb*

yw ; ; FRT82B, osa^{308} */ TM6B, Tb*

y, sc, v ; UAS-Eip93F-RNAi^{attP40} – (Bloomington 57868; TRiP.HMC04773)

yw ; ;

See Table S1 for complete list of RNAi lines.

4.4.3 Immunofluorescence and image analysis

Larvae and pupae were dissected as previously described (Uyehara *et al.*, 2017). Primary antibodies: 1:100 mouse anti-Osa (DSHB), 1:100 rat anti-Elav (DSHB), and 1:10 mouse anti-Delta

(DSHB). Secondary antibodies: goat anti-mouse Alexa-633 and goat anti-rat Cy5 were used at 1:1000 (Invitrogen). Tissue was mounted in VECTASHIELD (Vector Labs) with 1.5 coverslips.

For image quantification of RNAi screen microscopy, a custom python script was used to compare reporter signal in RNAi expressing versus WT cells in each wing. Briefly, 10-20 slice z-stacks were converted to maximum intensity projections (MIP). Masks were generated of DAPI, GFP-positive RNAi expressing, and DAPI – GFP (GFP-negative) non-RNAi expressing regions. A ratio of mean grey value in GFP-positive and GFP-negative regions was calculated for each wing.

For image quantification of br^{disc} hyperactivation and Delta immunofluorescence experiments, MIP were made for each wing, and then regions were selected in RNAi-expressing and WT control cells of the imaginal disc pouch for each wing. For br^{disc} hyperactivation, square regions were selected that straddled the margin. For Delta quantification, regions were manually drawn around the margin from the anterior-posterior boundary (A/P) to the approximate edge of the most distal provein, L2 in anterior and L5 in the posterior. For both experiments mean grey values were measured using ImageJ (Schindelin *et al.,* 2012), and a ratio of mean grey value in RNAi versus WT control was calculated. Student's two-sample t-tests were performed in R to calculate significance.

4.4.4 High throughput sequencing & data analysis

For FAIRE-seq, wings of female pupae were prepared as previously described (Uyehara *et al.,*, 2017; Uyehara *et al.,*, 2019). 40 wings were used per biological replicate. Libraries were prepared using the Takara ThruPLEX DNA-seq kit with unique dual-indexes following manufacturer's specifications and sequenced on an Illumina NextSeq 2000. Adapters were trimmed from paired-end reads using BBmap BBDuk (v38.71), and then aligned to the dm6 *Drosophila* genome assembly with Bowtie2 (v2.3.4.1; Langmead and Salzberg 2012) with the following parameters: --very-sensitive --no-unal --no-mixed --no-discordant --phred33 -I 10 -X 700. Aligned reads were filtered using an exclusion list for dm6 from ENCODE (Amemiya *et al.,* 2019), and quality filtered (q > 5) with Samtools (v1.9; Danecek *et al.,* 2021), and duplicate reads were removed with Picard (v2.2.4). Coverage files were generated with deepTools (v2.4.1; Ramirez *et al.,* 2016) and normalized to 1x genomic coverage (RPGC). Peaks were

called with MACS2 (v2.1.2; Zhang *et al.,* 2008) using standard parameters. z-normalized coverage files were generated with a custom R script (4.1.3) from RPGC normalized files. For visualization, biological replicates were pooled using Samtools (v1.9). Differential peak analysis was performed in R using DiffBind (v3.8.4; Stark and Brown, 2011) and DEseq2 (v1.38.3; Love *et al.,* 2014). For assignment of "Osa-dependent" peaks into "Increasing," "Decreasing," or "Static" categories, each peak was annotated with z-normalized WT FAIRE-seq data from 3LW, 6h, 18h, 24h, 36h, and 44h APF wings (Uyehara *et al.,* 2017). A $\log_2$ ratio was calculated at each timepoint relative to 3LW. "Increasing" peaks were those that had a $\log_2$FoldChange >= 1 at 24h, 36h, or 44h APF. "Static" peaks were those that had a $\log_2$FoldChange between -1 and 1 at 24h, 36h, and 44h APF. "Decreasing" peaks were all remaining peaks. Later pupal stages (24h, 36h, 44h) were used for categorization because they corresponded with approximate stage of wings used for Osa-deGrad FAIRE-seq. Pearson correlation heatmaps of z-normalized coverage files were generated using deepTools (3.5.1).

For WT FAIRE-seq timecourse previously published raw data was accessed from GEO GSE131981 (Ma *et al.,* 2019). Data was aligned and processed as described above except alignment was run using Bowtie2 with the --very-sensitive parameter and no additional changes.

For Osa-GFP CUT&RUN female wing imaginal discs from either yw;;osa^{GFP} or yw negative control animals were dissected and processed as previously described (Uyehara *et al.,* 2019). 20-22 wing discs were used for each replicate, with a rabbit anti-GFP (1:100, Rockland 600-401-2156), a pAG-MNase (1:100; UNC core; Salzler *et al.,* 2023), and 0.5ng of yeast genomic DNA spike-in (gift of Steve Henikoff). Libraries were prepared from the "supernatant" fraction using the Takara ThruPLEX DNA-seq kit with unique dual-indexes and following the manufacturer's specifications but with a modified amplification step as previously described (Uyehara *et al.,* 2019). Libraries were pooled and sequenced on an Illumina NextSeq 2000 with a 75bp read length. Adapters were trimmed from paired-end reads using BBmap BBDuk (v38.71), and then aligned to the dm6 *Drosophila* genome assembly with Bowtie2 (v2.3.4.1) with the following parameters: --local --very-sensitive-local --no-unal --no-mixed --no-discordant --phred33 -I 10 -X 700. Aligned reads were filtered using a custom exclusion list generated from the "supernatant" of IgG negative controls, as well as anti-Flag and anti-GFP experiments in genotypes that lacked either the

Flag or GFP epitopes. Peaks shared among all these negative controls were used to make a conservative list of reproducible high-signal regions. This exclusion list included ~80 regions. Reads were then quality filtered (q > 5) with Samtools (v1.10), and duplicate reads were removed with Picard (v2.2.4). Coverage files were generated with deepTools (v2.4.1) and normalized to 1x genomic coverage (RPGC). Peaks were called with MACS2 (v2.1.2) without a control and using the –nomodel and –nolamda parameters. Z-normalized coverage files were generated with a custom R script (v4.1.3) from RPGC normalized files.

For H3K27ac CUT&RUN, 20 male imaginal wing discs were used per replicate, with a rabbit anti-H3K27ac (1:100, Active Motif #39135). Libraries were prepared from the “pellet” fractions using the Takara ThruPLEX DNA-seq kit as described above. Libraries were pooled and sequenced on an Illumina Novaseq SP with a 75bp read length. Reads were aligned and processed as described above, except peaks were called with standard MACS2 settings and a sheared genomic DNA control.

For CUT&RUN analysis, only Osa-GFP peak calls greater than or equal to the 50th percentile of MACS2 quality scores (qval) and that were identified in both replicates were kept. Osa-peaks were identified as those that passed screens for quality and reproducibility but did not intersect a reproducible control peak. Peak annotation was performed in R using the ChIPseeker package (v1.34.1; Yu *et al.,* 2015), and a negative control bootstrapped shuffle of Osa-peaks was generated using the nullranges package (v1.4.0; Mu *et al.,* 2023). Peak overlap enrichment analysis for Hairless ChIP and Rotund ChIP-seq (Fig 5G,J) was performed in R using ChIPseeker. Osa-peaks were clustered by dynamic accessibility patterns (Fig 5H) by annotating peaks with replicate pooled and z-normalized WT FAIRE-seq data at 3LW, 6h, 18h, 24h, 36h, and 44h APF. For each peak, the fraction of max FAIRE signal was calculated for each timepoint. K-means clustering was performed in R with a k of 8, based on previously described 8 distinct clusters of FAIRE patterns using this data (Nystrom *et al.,* 2020). Motif enrichment analysis was performed in R using the memes package (v1.6.0; Nystrom and McKay 2021) and the AME software (McLeay *et al.,* 2010; Nystrom *et al.,* 2021).

For Rotund ChIP-seq, raw sequencing data was downloaded from the Gene Expression Omnibus (GEO) database (GSE203208, Loker *et al.,* 2022). Rotund ChIP-seq data was processed using snakePipes (v2.7.3, Bhardwaj *et al.,* 2019). Reads were aligned to dm6 with Bowtie2 (v2.4.5), and peaks

were called with MACS2 (v2.2.7.1).

For Hairless ChIP-chip analysis, peak calls were downloaded from GEO (GSE97603, Chan 2017).

All plots were generated in R using the ggplot2 package (v3.4.2), and genome browser plots were generated with the Gviz package (v1.42.1)

4.4.5 Data Availability Statement

Strains and plasmids are available upon request. High-throughput sequencing data is publicly available online at GEO. Code used to process sequencing data and generate plots can be found at https://github.com/mniederhuber/Niederhuber_2023.

4.5 Figures

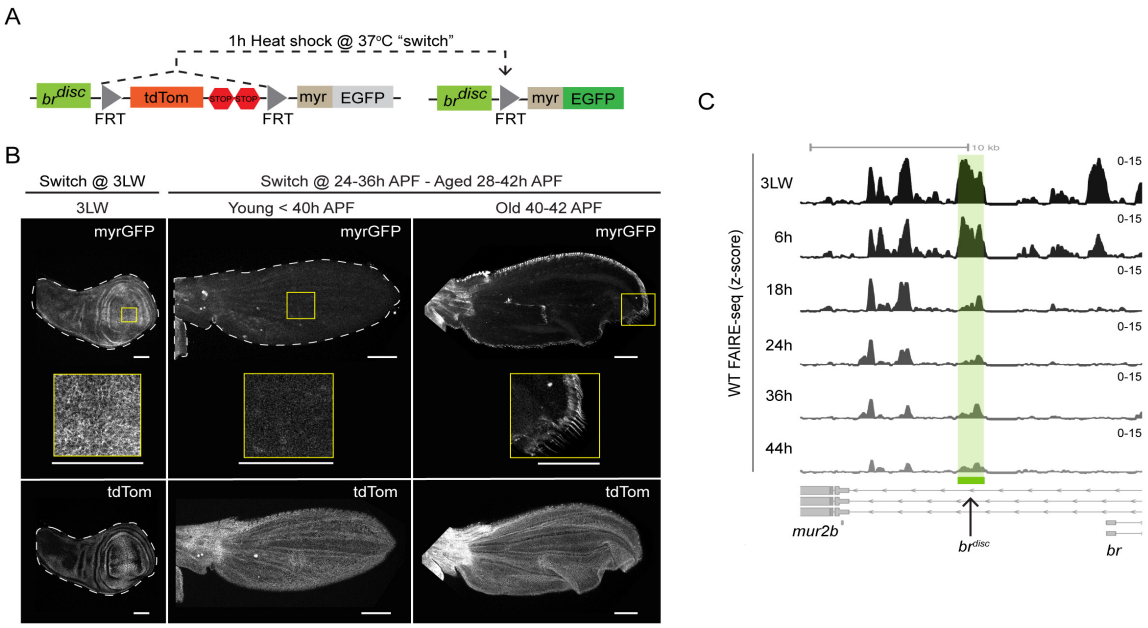

Figure 4.1: The *br*^{disc} enhancer is a model of a developmentally dynamic regulatory element. (A) Illustration of the *br*^{disc}*-switch* reporter. Heat shock-induced FLP expression excises the FRT-flanked "*tdTomato, 2xSTOP*" cassette to allow expression of myr-GFP. (B) Confocal images of *br*^{disc}*-switch* activity in 3rd Larval Wandering (3LW) imaginal wing discs and pupal wings aged 28-42h APF. "Young" and "Old" denote pupal wings categorized by morphology (see Methods). "Switch @" denotes ages of animals at time of heat shock. Images pupal wings are maximum intensity projections. Image of imaginal wing disc is single slice. Scale bars are 100μm. Wings are shown with anterior up. (C) Genome browser shot of z-normalized FAIRE-seq signal at the *br*^{disc} enhancer (green highlight) from time course of WT wing development.

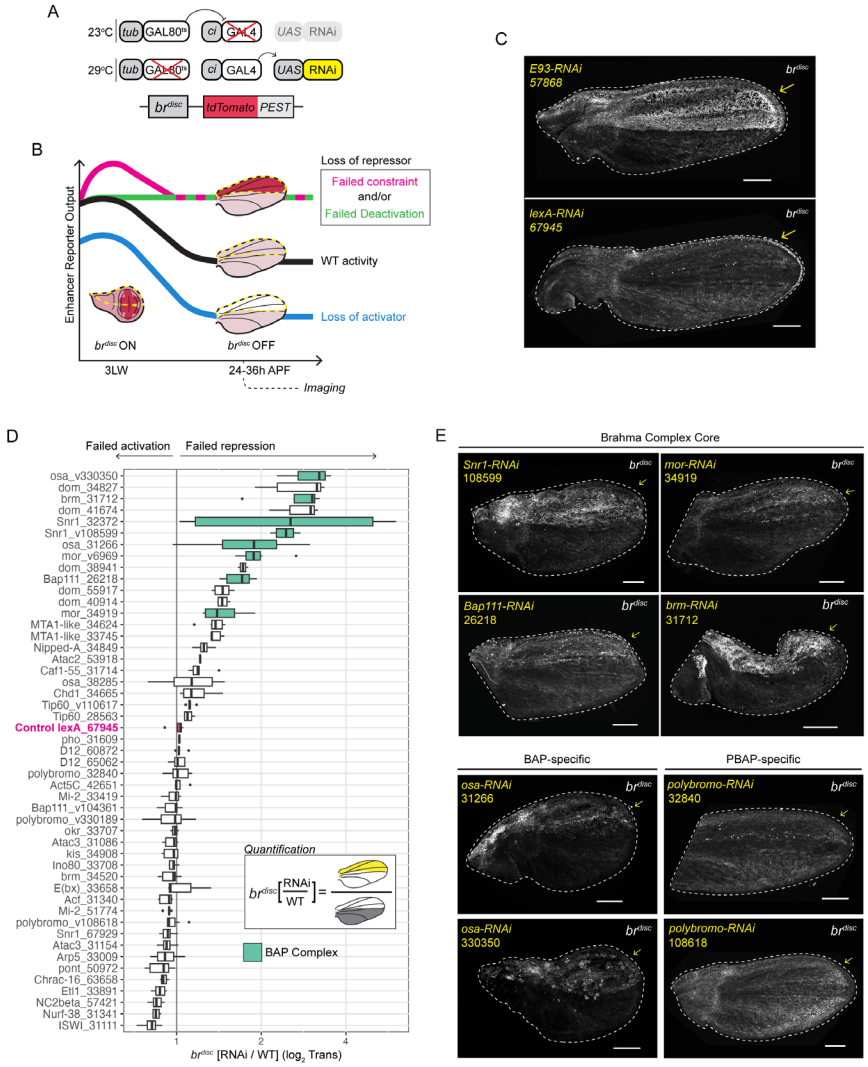

Figure 4.2: The BAP Complex is required to repress the *br*^{disc} enhancer. (A) Illustration of the *br*^{disc}*-tdTomato-PEST* reporter and inducible RNAi system used to screen for genes required for *br*^{disc} regulation. (B) Schematic of types of enhancer dysregulation detectable in the RNAi screen. RNAi-expressing cells are located within the yellow dashed outline. Temporal activity of reporter in WT cells is indicated by black line. Loss of an activator in 3LW imaginal wing discs (*br*^{disc} ON) would cause reduced reporter levels in RNAi cells (Blue line). Failed deactivation (*br*^{disc} OFF) would cause increased levels of reporter activity in RNAi cells (Green line). Failed constraint in wing discs (*br*^{disc} ON) would also cause increased levels in RNAi cells (Magenta line). (C) Confocal images of positive (*E93-RNAi*) and negative (*lexA-RNAi*) controls. Yellow arrows indicate regions of RNAi expression. Stock identification numbers are indicated (see Table S1). (D) Quantification of changes in *br*^{disc} reporter activity induced by RNAi. Boxplots summarize ratios of *br*^{disc} signal in RNAi cells to WT cells. Each datapoint is a different wing. Each RNAi line tested is plotted on the y-axis, with gene symbol followed by RNAi line ID. "v" preceding line number indicates VDRC. A negative control *lexA* RNAi (magenta) has a ratio of ~1. Subunits of the BAP complex are indicated in teal. Inset illustration depicts method of quantification. X-axis is $\log_2$ transformed. (E) Confocal images of *br*^{disc} activity after RNAi of select core components of the BAP complex. Images are maximum projections. Scale bars are 100μm.

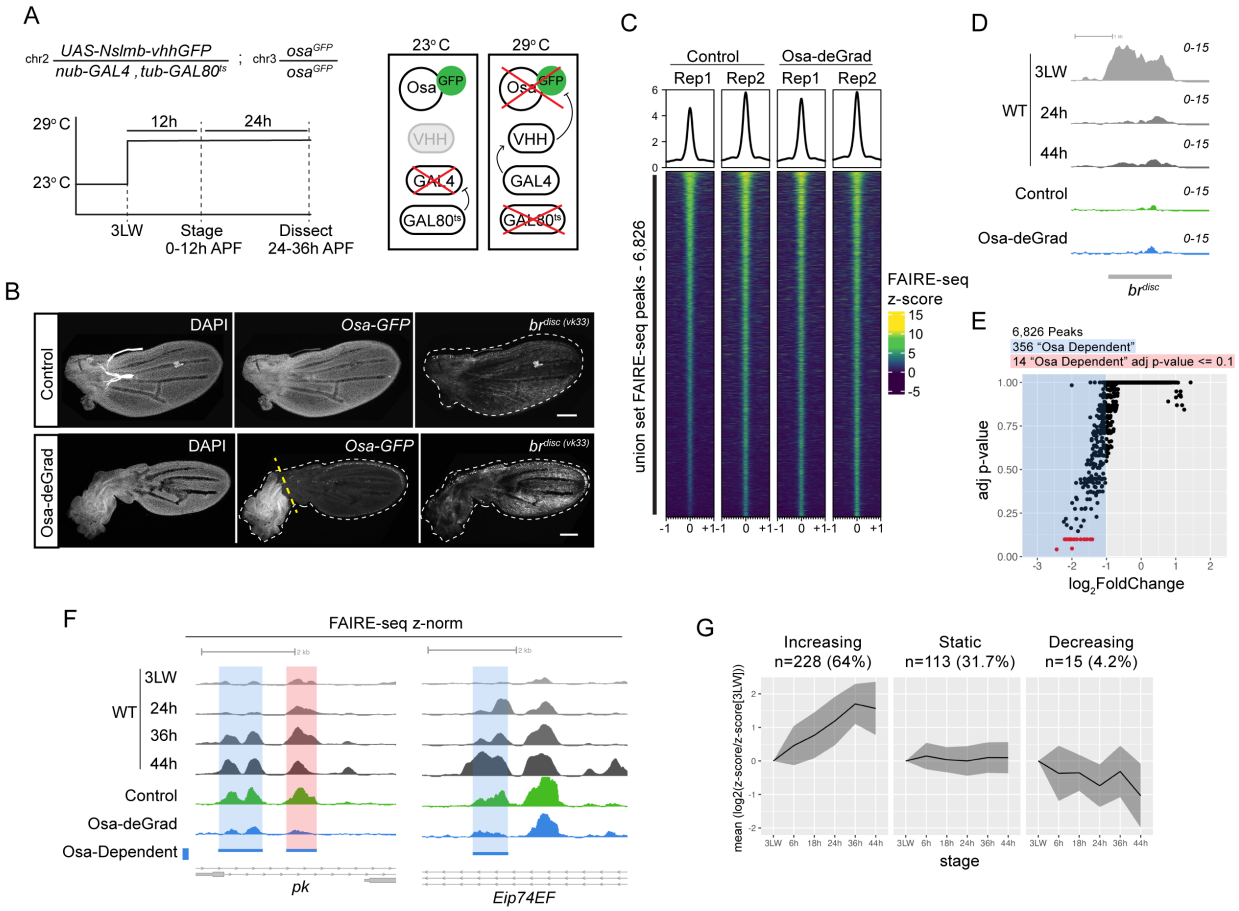

Figure 4.3: Osa is not required to close *br*^{disc} and is dispensable for pupal chromatin accessibility patterns. (A) Illustrations of Osa-GFP degradation (Osa-deGrad) genotypes and experimental design. (B) Confocal images of Osa-deGrad experimental genotypes. Yellow dashed line indicates where wings were cut during sample collection. Scale bars are 100μm. Images are maximum intensity projections. (C) Heatmaps and average signal plots of z-normalized FAIRE signal within the union set of FAIRE peaks from Control and Osa-deGrad pupal wings. Plotted range is +/- 1kb from peak center. Peaks are ranked by signal in Control Rep1. (D) Browser shot of z-normalized FAIRE signal from Osa-deGrad (blue), Osa-deGrad Control (green), and WT (grey) imaginal wing discs at the endogenous *br*^{disc} enhancer. (E) Scatterplot of log_2FoldChange of Osa-deGrad/Control FAIRE-seq signal (x axis) relative to adjusted p-value (y axis). Peaks with log_2FoldChange <= –1 (Osa-dependent) are highlighted in blue. Peaks with an adjusted p-value <= 0.1 are colored red. (F) Browser shot of FAIRE signal at representative "Osa-dependent" sites (blue bars and highlights, red highlight indicates adjusted p-value < 0.1) near the *prickle* (*pk*) and *Eip74EF* loci. (G) Line plots of the average WT FAIRE log_2FoldChange relative to 3LW, with standard deviation as grey ribbon, within 356 "Osa-dependent" sites. Sites are split by whether they increase in accessibility relative to the 3LW stage ("Increasing"), have little change ("Static"), or lose accessibility ("Decreasing") (see Methods). The x-axis denotes stages of wing development from 3LW to 44h APF. All z-normalized FAIRE signal in browser shots are pooled replicates.

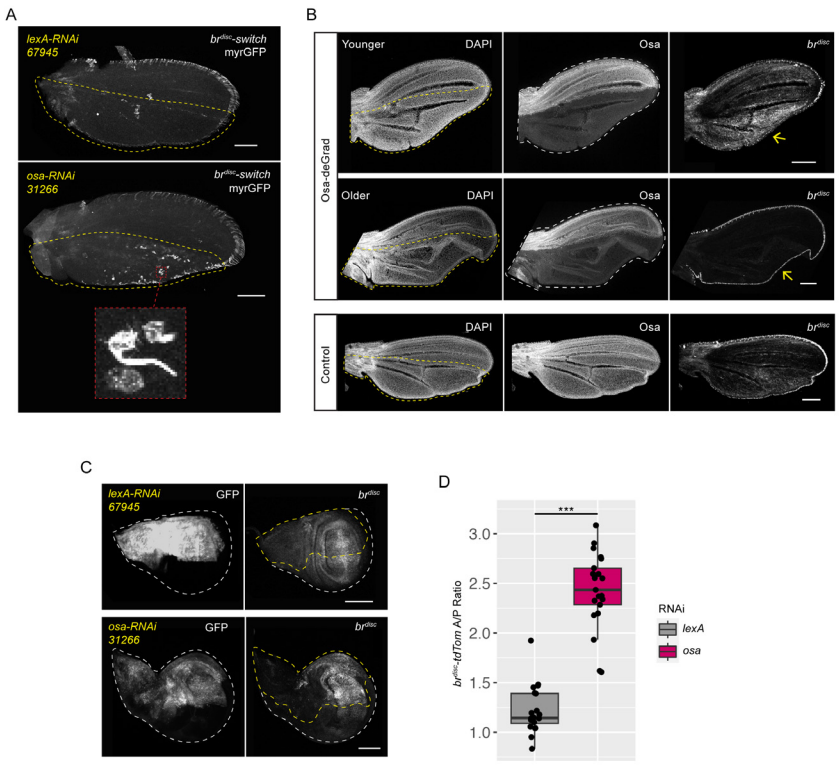

Figure 4.4: Osa is required to constrain *br*^{disc} activity in wing imaginal discs. (A) Confocal images of *br*^{disc}*-switch* nascent myr-GFP signal in the pupal wing in negative control *lexA*-RNAi or *osa*-RNAi. (B) Confocal images of *br*^{disc}*-tdTomato-PEST* activity in 30-42h APF wings following late induction of Osa-deGrad. Approximate regions of Osa degradation are outlined with yellow dashed line in the DAPI channel. "Younger" indicates a wing closer to 30h APF of age. "Older" indicates a wing closer to 42h APF (see Methods). A negative control in which Osa-deGrad was induced in an *osa*^{GFP} heterozygote (*osa*^{GFP}/*osa*) is shown for comparison (Control). Yellow arrows denote regions of differential reporter activity for comparison. (C) Confocal images of *br*^{disc} activity in *osa-RNAi* and control *lexA-RNAi* wing imaginal discs. GFP marks domain of RNAi expression (outlined by dashed yellow line). (D) Quantification of *br*^{disc} reporter increase in response to *osa-RNAi* in wing imaginal discs, compared to control *lexA-RNAi*. The y-axis is a ratio of *br*^{disc} signal in the anterior (RNAi-expressing) versus the posterior (WT) cells. Asterisks indicate significance (*** = p-value < 1e-13, Two-sample t-test). Images are maximum intensity projections. Scale bars are 100μm.

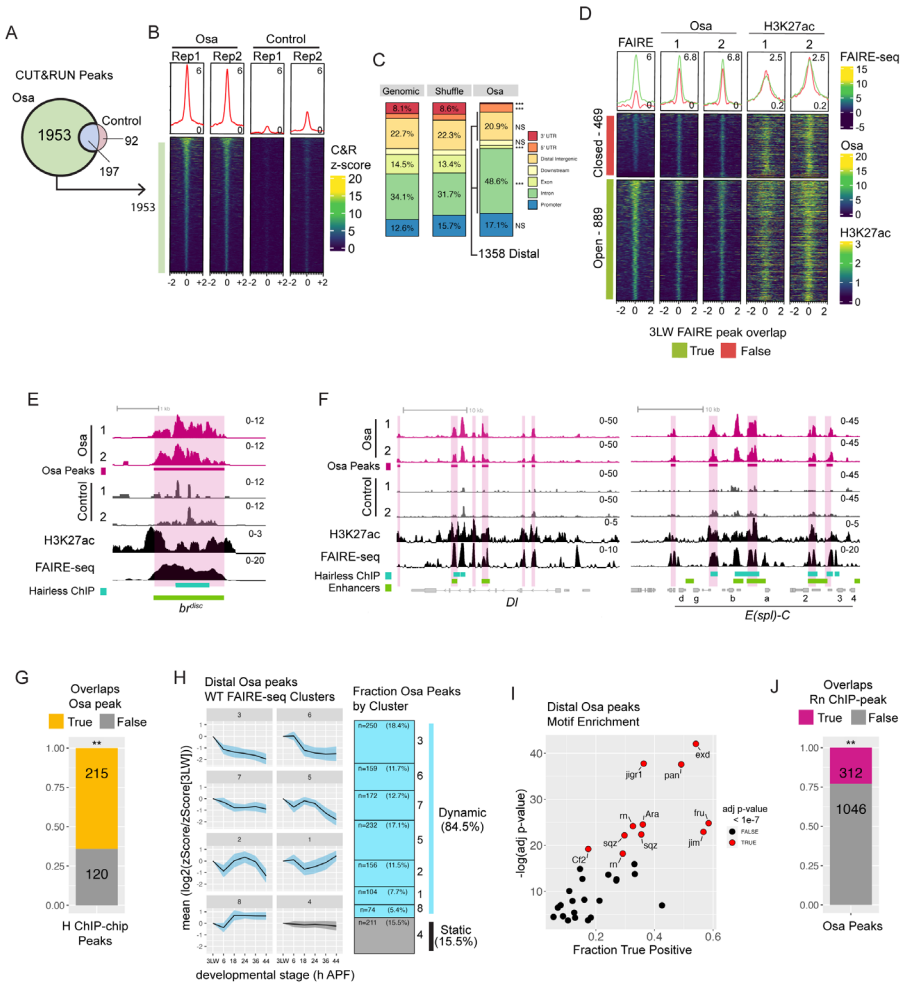

Figure 4.5: **Osa directly binds *br*^{disc} and thousands of putative enhancers in wing imaginal discs.** (A) Venn diagram of peaks called in Osa-GFP (Osa) versus Control wing imaginal disc CUT&RUN experiments. (B) Heatmap and average signal plots of z-normalized CUT&RUN signal between experimental replicates within Osa-specific peaks. (C) Stacked barplots of the distribution of Osa peak genomic annotations relative to a 500bp-tiled genome-wide annotation (Genome), and a bootstrapped shuffle of Osa peaks (Shuffle). Asterisks indicate significance (*** = p-value < 0.0001, two-proportion z-test). (D) Heatmap and average signal plots of wing imaginal disc z-normalized FAIRE-seq, Osa CUT&RUN, and H3K27ac CUT&RUN signal within distal Osa peaks. Heatmaps are grouped by whether Osa peaks overlap a FAIRE peak in 3LW wing discs. (E,F) Browser shots of Osa CUT&RUN signal (magenta) versus control (grey), H3K27ac z-normalized signal (black), and WT FAIRE-seq (black). Coordinates for Osa peaks (magenta), Hairless ChIP peaks (teal), and annotated enhancers (green) are indicated. Browsers depict the *br*^{disc} enhancer (E), and the *Dl* and *E(spl)-C* loci (F). (G) Bar plot showing fraction of Hairless ChIP peaks that overlap Osa peaks (not restricted to distal only). Asterisks indicate significance (** = adj p-value < 0.001, Fisher's exact test). (H) Line plots of the ratio of wild-type wing FAIRE-seq signal in distal Osa peaks for each of six developmental stages relative to 3LW (log2). Osa peaks were placed into eight categories by k-means clustering of the wild-type FAIRE time course data. Standard deviation shown by blue ribbon. Stacked barplot depicts fraction of distal Osa peaks associated with each cluster. Dynamic clusters (1,2,3,5,6,7,8) are colored blue. Static cluster (4) is colored grey. (I) Scatterplot of motifs enriched in distal Osa peaks, plotted by -log(adj p-value) and fraction of true positive. Motifs with an adjusted p-value < 1e-7 are colored in red. (J) Bar plot of the fraction of distal Osa peaks that overlap Rotund (Rn) ChIP-seq peaks. Asterisks indicate significance (** = adj p-value < 0.001, Fisher's exact test).

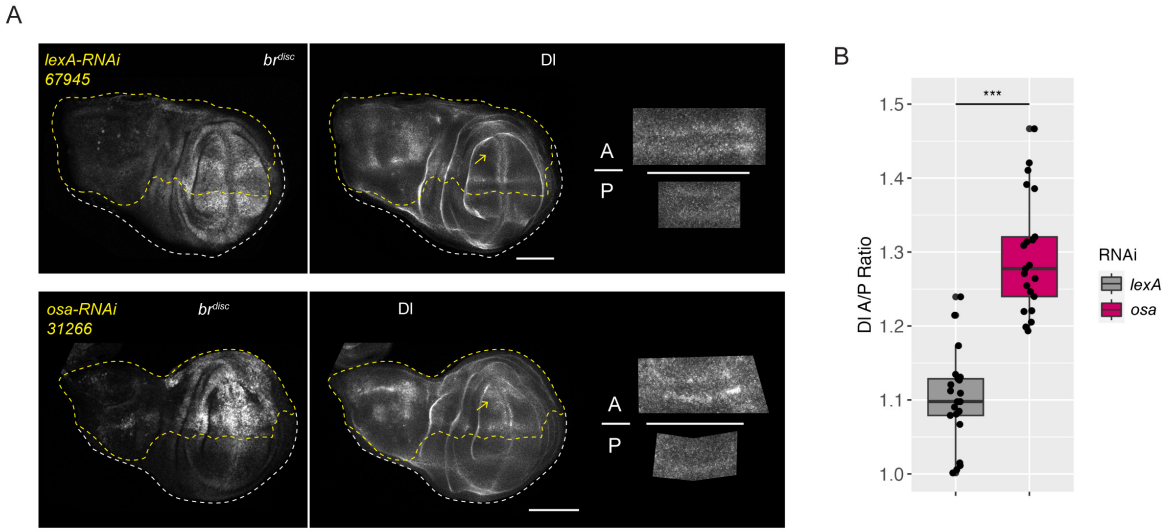

Figure 4.6: **Osa negatively regulates Delta expression.**
(A) Confocal images of *br*^{disc} reporter activity and immunofluorescence of Delta protein in wing imaginal discs from negative control *lexA* or *osa-RNAi*. RNAi expressing cells are outlined with yellow dashed line. Insets show representative ROI selections in the anterior ("A") and posterior ("P") used for quantification (see Methods). Yellow arrows highlight expansion of Dl pattern around L2 provein relative to control.
(B) Image quantification of Delta levels in *lexA* control and *osa-RNAi* experiments. Asterisks indicate significance (*** = p-value < 1e-10, Two-sample t-test). Maximum intensity projections are shown. Scale bars are 100μm.

Symbol	Complex	Line	Library	RNAi	Vector	Insertion Site	Isoforms	OTE	Lethality	Wing Phenotype	mean KD/WT	SD KD/WT	n
Acf	ACF	31340	TRiP	JF01298	VALIUM1	attP2	1/1	0	Low	WT	0.92	0.05	5
Act5c	Brahma/INO80	42651	TRiP	HMS02487	VALIUM20	attP2	5/5	0	High	NA	1.02	0.06	4
Arp5	INO80	33009	TRiP	HMS00809	VALIUM1	attP2	2/2	0	None	Small ectopic vein spots along L2	0.92	0.11	4
Atac2	ATAC	53918	TRiP	HMS00678	VALIUM20	attP2	1/1	0	Low	Shrunken anterior, incomplete L2	1.21	0.01	2
Atac3	ATAC	31086	TRiP	JF01631	VALIUM1	attP2	4/4	0	None	WT	0.96	0.05	7
Atac3	ATAC	31154	TRiP	JF01538	VALIUM1	attP2	4/4	0	None	WT	0.93	0.07	4
Bap111	Brahma	26218	VDRC	107909	KK	chr2	1/1	0	None	WT	1.68	0.17	12
Bap111	Brahma	104361	TRiP	JF02116	VALIUM10	attP2	1/1	1	High	NA	0.96	0.07	7
Brm	Brahma	31712	TRiP	HM04019	VALIUM1	attP2	6/6	0	High	Heldout wings, shrunken anterior, subtle vein defects, ectopic bristles thoracic	2.75	0.70	4
Brm	Brahma	34520	TRiP	HMS00050	VALIUM20	attP2	6/6	0	None	WT	0.95	0.08	5
Caf1-55	NURF/NURD	31714	TRiP	HM04021	VALIUM1	attP2	2/2	0	High	NA	1.20	0.09	8
Chd1	SNF_2-like	34665	TRiP	HMS01142	VALIUM20	attP2	3/3	0	Low	Small ectopic veins along L2	1.19	0.20	4
Chrac-16	ACF	63658	TRiP	HMJ30225	VALIUM20	attP40	2/2	0	Low	WT	0.90	0.04	3
D12	ATAC	60872	TRiP	HMJ22553	VALIUM20	attP40	2/2	0	Low	Small ectopic veins along L2	1.03	0.04	5
D12	ATAC	65062	TRiP	HMC06021	VALIUM20	attP40	1/1	0	Low	Defects in L2	1.01	0.06	5
Dom	Domino	34827	TRiP	HMS00142	VALIUM20	attP2	4/4	0	High	Subtle ectopic veins and defects in vein formation	2.82	0.66	6
Dom	Domino	38941	TRiP	HMS01855	VALIUM20	attP2	4/4	0	High	NA	1.72	0.10	2
Dom	Domino	40914	TRiP	HMS02162	VALIUM20	attP2	4/4	0	High	NA	1.46	0.07	4
Dom	Domino	41674	TRiP	HMS02208	VALIUM20	attP2	4/4	0	None	Ectopic vein between L2-L3	2.77	0.56	3
Dom	Domino	55917	TRiP	HMC04203	VALIUM20	attP2	1/4	0	NA	NA	1.46	0.10	11
E(Bx)	NURF	33658	TRiP	HMS00065	VALIUM20	attP2	9/9	0	Low	WT	1.07	0.22	3
Eft1	SNF_2-like	33891	TRiP	HMS00829	VALIUM20	attP2	1/1	0	None	WT	0.87	0.04	6
Ino80	INO80	33708	TRiP	HMS00586	VALIUM20	attP2	1/1	0	Low	WT	0.97	0.03	5
Iswi	NURF	31111	TRiP	JF01582	VALIUM1	attP2	3/3	0	Low	Ectopic vein spots L1-L2	0.81	0.07	4
Kis	SNF_2-like	34908	TRiP	HMS01254	VALIUM20	attP2	6/6	0	None	WT	0.96	0.06	5
LexA	CONTROL	67945	TRiP	HMS05773	VALIUM20	attP2	-	-	None	WT	1.01	0.05	6
Mi-2	NURD	33419	TRiP	HMS00301	VALIUM20	attP2	4/4	0	High	WT	0.98	0.05	9
Mi-2	NURD	51774	TRiP	HMC03329	VALIUM20	attP40	4/4	0	Low	WT	0.93	0.02	5
Mor	Brahma	34919	TRiP	HMS01267	VALIUM20	attP2	2/2	0	High	NA	1.47	0.26	12
Mor	Brahma	6969	VDRC	1257	GD	chr3	2/2	0	High	NA	1.96	0.37	6
Mta1-Like	NURD	33745	TRiP	HMS01084	VALIUM20	attP2	4/4	0	Low	Ectopic vein along L3	1.38	0.07	5
Mta1-Like	NURD	34624	TRiP	HMS01299	VALIUM20	attP2	4/4	0	None	Ectopic vein along L3	1.37	0.12	6
Nc2beta	ATAC	57421	TRiP	HMC04728	VALIUM20	attP40	1/1	0	None	WT	0.85	0.04	8
Nipped-A	Domino	34849	TRiP	HMS00167	VALIUM20	attP2	2/2	0	High	NA	1.25	0.10	4
Nurf-38	NURF	31341	TRiP	JF01299	VALIUM1	attP2	3/3	0	High	NA	0.85	0.03	4
Okr	SNF_2-like	33707	TRiP	HMS00585	VALIUM20	attP2	1/1	0	None	WT	0.99	0.03	3
Osa	Brahma BAP	31266	TRiP	JF01207	VALIUM1	attP2	6/6	0	High	NA	1.83	0.55	27
Osa	Brahma BAP	38285	TRiP	HMS01738	VALIUM20	attP40	6/6	0	None	-	1.14	0.20	13
Osa	Brahma BAP	330350	VDRC	330350	shRNA	attP40	-	-	High	NA	3.01	0.66	3
Pho	INO80	31609	TRiP	JF01393	VALIUM1	attP2	2/2	0	Low	Small ectopic veins along L2	1.02	0.00	3
Polybromo	Brahma PBAP	32840	TRiP	HMS00531	VALIUM20	attP2	1/1	0	-	-	1.03	0.09	7
Polybromo	Brahma PBAP	108618	VDRC	101808	KK	chr2	1/1	0	Low	WT	0.97	0.07	7
Polybromo	Brahma PBAP	330189	VDRC	330189	shRNA	attP40	-	-	Low	Mostly WT, some small ectopic veins along L2	0.97	0.14	8
Pont	Domino	50972	TRiP	HMJ21078	VALIUM20	attP40	1/1	0	Mid	Ectopic veins between L3-L4	0.88	0.08	7
Snr1	Brahma	32372	TRiP	HMS00363	VALIUM20	attP2	1/1	0	High	NA	3.13	2.17	7
Snr1	Brahma	67929	TRiP	HMS05749	VALIUM20	attP40	1/1	0	Low	Small ectopic veins along L2	0.93	0.04	9
Snr1	Brahma	108599	VDRC	101602	KK	chr2	1/1	0	High	NA	2.44	0.23	6
Tip60	Domino	28563	TRiP	HM05049	VALIUM10	attP2	3/3	0	-	-	1.10	0.05	4
Tip60	Domino	110617	VDRC	107642	KK	chr2	3/3	0	High	NA	1.12	0.04	5

Table 4.S1. Table of lines used in the RNAi screen. “OTE” denotes any predicted non-specific Off Targets. “Lethality” is a qualitative measure of pupal death in each RNAi experiment. “High” lethality denotes most or all animals with RNAi expression die before eclosion. “Low” lethality denotes some animals die before eclosion, but most survive. “None” lethality denotes most or all animals expressing RNAi survive to adulthood. “Wing phenotype” provides descriptions of any observed wing phenotypes. “KD/WT” mean and standard deviation (SD) columns list quantification of changes in enhancer activity following RNAi expression as plotted in Fig 2D. “n” describes the total number of unique wings imaged and quantified for each RNAi line.

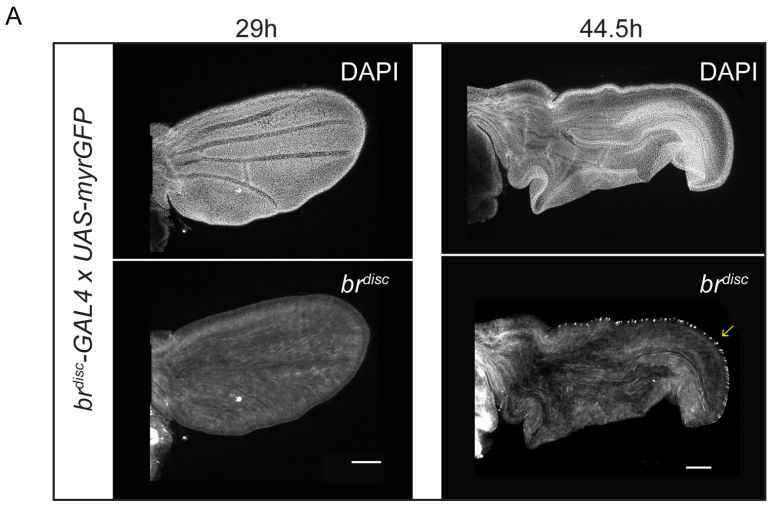

Figure 4.S1. (A) Confocal images of br^{disc}-GAL4 reporter driving nascent expression of *UAS-myrGFP* in younger (29h APF) and older (44.5h APF) pupal wings. Yellow arrow highlights late activation of br^{disc} in the elongating bristles of the anterior margin. Images are maximum intensity projections. Scale bars are 100μm.

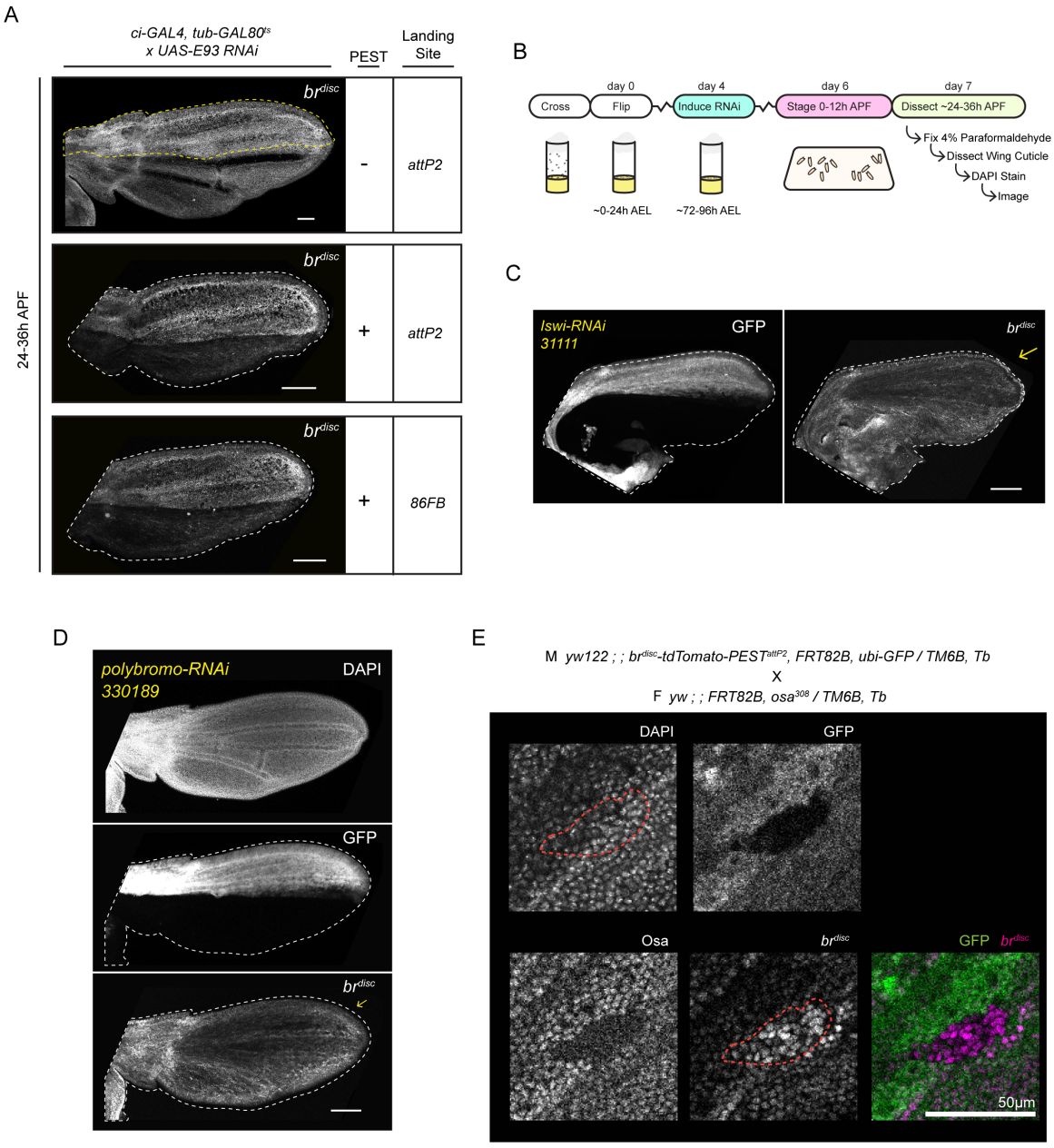

Figure 4.S2. (A) Confocal images of increased *br*^{disc} reporter activity following E93-KD in the anterior (top-half, outlined with yellow dashed line) compartment relative to WT cells of the posterior (bottom-half), with or without the addition of the PEST degradation tag. Reporter activity from two independent attP integration sites (*attP2* and *86Fb*) are shown. (B) Illustration of experimental setup for RNAi screen. (C). Confocal images of reduced *br*^{disc} reporter activity following Iswi knockdown (line 31111) in the RNAi screen. GFP marks the region of RNAi expression. Yellow arrow highlights reduced reporter activity in RNAi-expressing cells. (D) Confocal images of *br*^{disc} reporter activity following polybromo knockdown (line 330189). (E) Confocal images of *br*^{disc} reporter activity in loss-of-function *osa*^{308} mitotic clones with anti-Osa immunofluorescence. *Osa*^{308} homozygous clones are GFP-, and wild-type twin spots are strong GFP+. Red dashed line marks area of clone. All images are maximum intensity projections. Scale bars are 100µm unless noted.

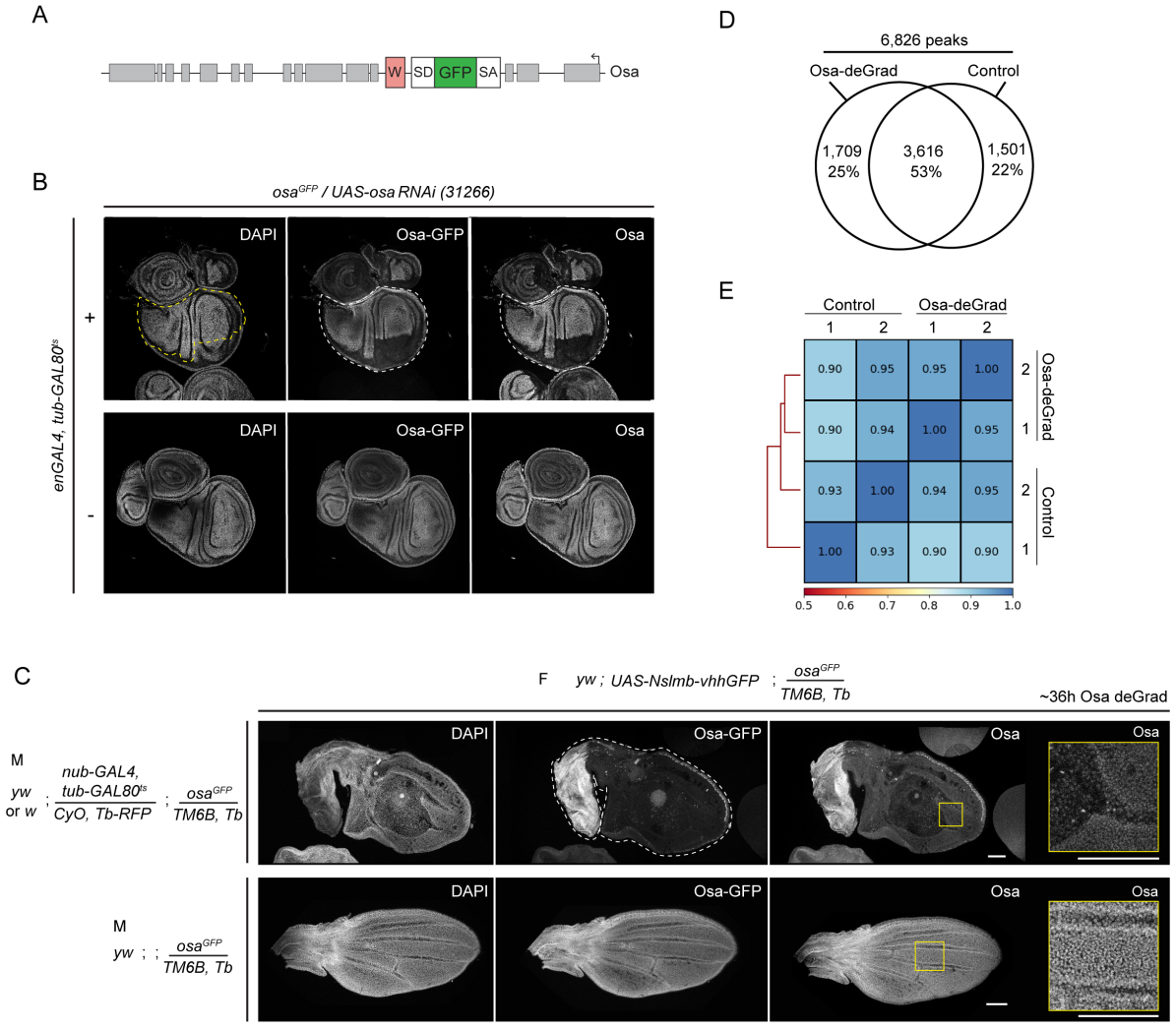

Figure 4.S3. (A) Illustration of GFP insertion in the *osa*^{GFP} allele. (B) Confocal images of Osa-GFP and anti-Osa immunofluorescence in wing imaginal discs following *osa* knockdown (line 31266) with or without the posterior *en-GAL4, tub-GAL80*^{ts} (*en*^{ts}) driver (right-side). (C) Confocal images of Osa-GFP and anti-Osa immunofluorescence in ~24-36h APF pupal wings following Osa-deGrad with conditions used for FAIRE-seq, with or without the *nub-GAL4, Tub-GAL80*^{ts} (*nub*^{ts}) driver. Yellow boxes highlight zoomed regions showing changes in nuclear anti-Osa immunofluorescence signal following Osa-deGrad. (D) Venn diagram of Osa-deGrad and Control FAIRE-seq peak calls. (E) Pearson correlation heatmap of z-normalized Osa-deGrad and Control FAIRE-seq coverage files. Microscopy images are maximum intensity projections. Scale bars are 100μm.

A

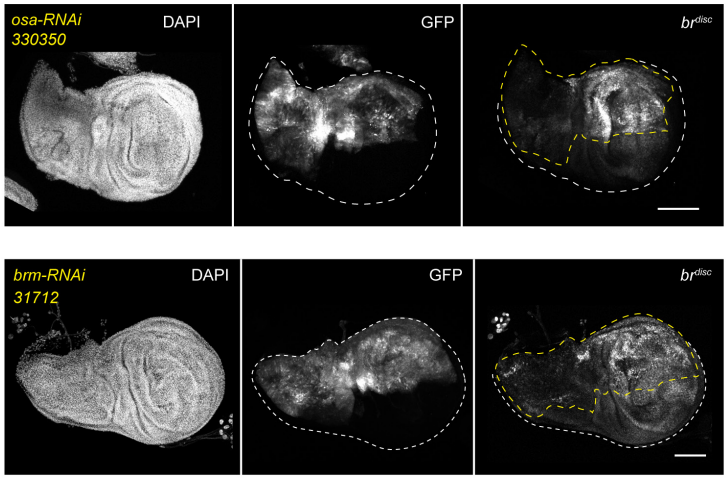

Figure 4.S4. (A) Confocal microscopy of *br*^{disc} reporter hyperactivation in imaginal wing discs following target gene knockdown with an independent *osa-RNAi* line (line 330350) and *brm-RNAi* line (line 31712). GFP marks the region of *ci*^{ts} and RNAi expression (yellow dashed line). (B) Confocal microscopy of *br*^{disc} reporter hyperactivation and anti-Br immunofluorescence following osa knockdown (line 31266) with the *ci*^{ts} driver. Images are all maximum intensity projections. Scale bars are 100μm.

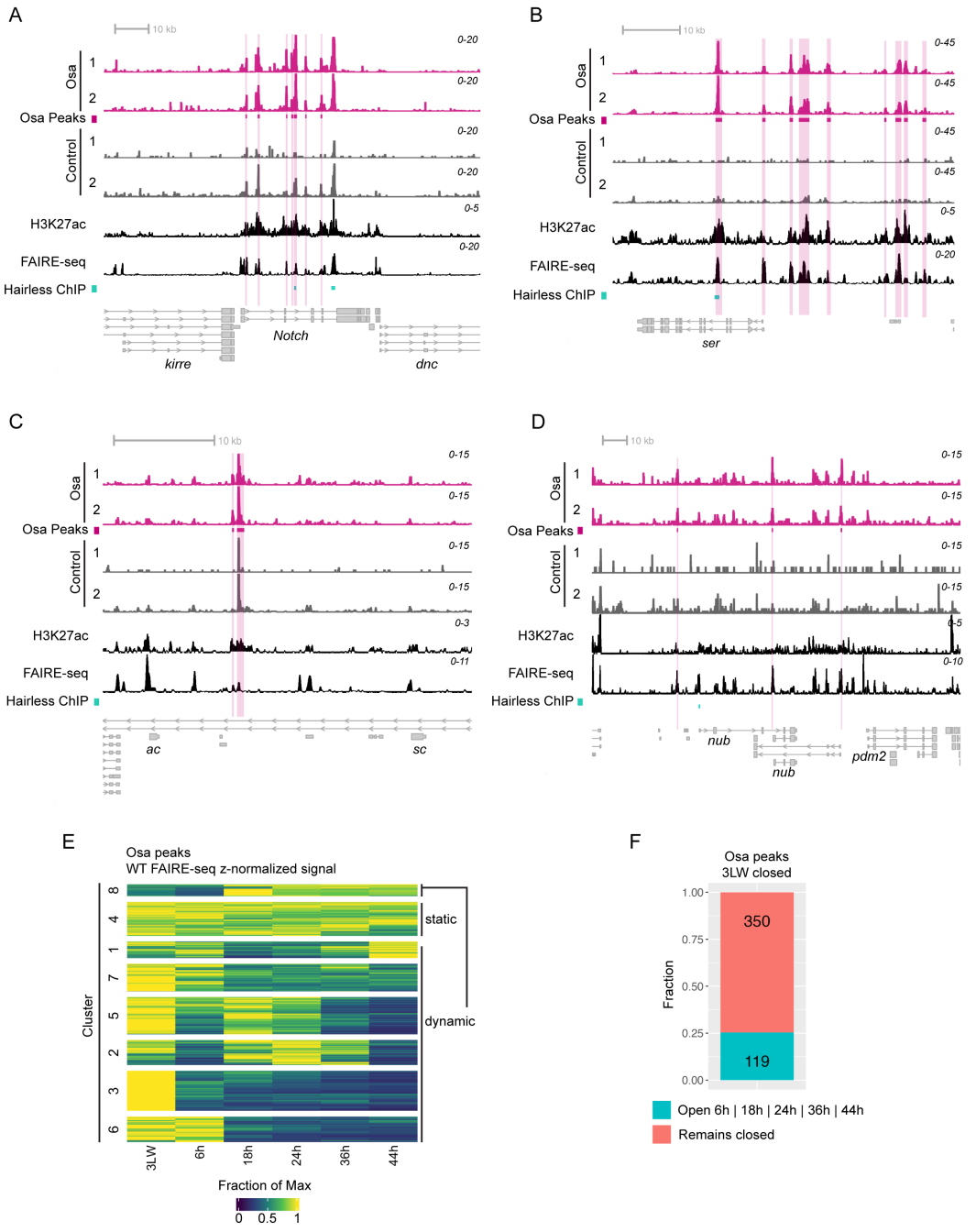

Figure 4.S5. (A-D) Genome browser shots of z-normalized Osa (magenta) CUT&RUN, Control (grey) CUT&RUN, H3K27ac CUT&RUN (black), and WT FAIRE-seq (black) in wing imaginal discs. Tracks are annotated with Osa peaks (magenta bars and highlights), and Hairless ChIP peaks (teal bars). (E) Heatmap of k-means clustered Fraction of Max z-normalized WT FAIRE-seq signal within distal Osa peaks (see Methods). (F) Stacked barplot of Osa peaks that do not overlap a FAIRE peak in imaginal wing discs (3LW) grouped by if those peaks overlap any FAIRE peak at a later stage in the WT FAIRE-seq timecourse.

A

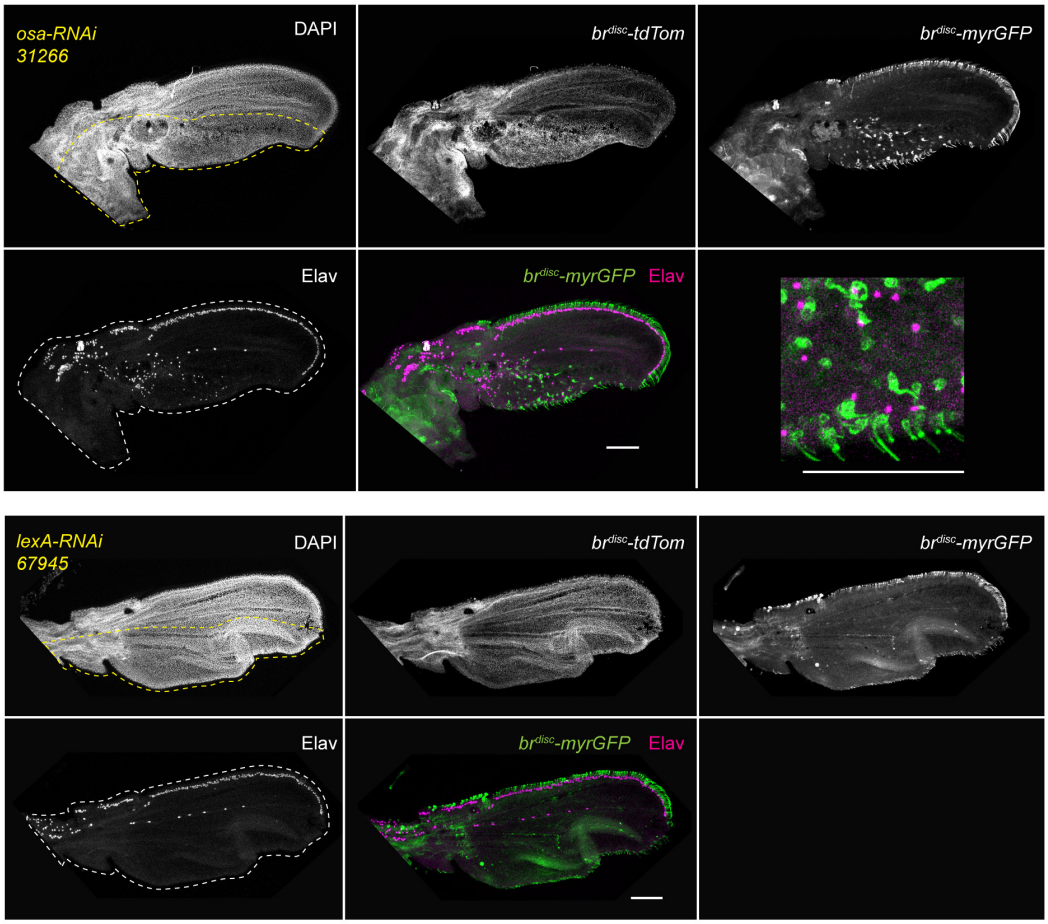

Figure 4.S6. (A) Confocal images of *br^{disc}-switch* reporter activity and anti-Elav immunofluorescence in ~40h APF pupal wings following either *osa* knockdown (line 31266) or control *lexA* knockdown (line 67945) with the posterior (bottom-half) *en^{ts}* driver. Zoom inset shows ectopic bristles with nascent myr-GFP signal near to with Elav+ nuclei. All images are maximum intensity projections. Scale bars are 100μm.

REFERENCES

Alver BH, Kim KH, Lu P, Wang X, Manchester HE, Wang W, Haswell JR, Park PJ, Roberts CWM. 2017. The SWI/SNF chromatin remodelling complex is required for maintenance of lineage specific enhancers. Nature Communications. 8. doi:10.1038/ncomms14648.

Amemiya HM, Kundaje A, Boyle AP. 2019. The ENCODE Blacklist: Identification of Problematic Regions of the Genome. Sci Rep. 9(1):9354. doi:10.1038/s41598-019-45839-z.

Armstrong JA, Sperling AS, Deuring R, Manning L, Moseley SL, Papoulas O, Piatek CI, Doe CQ, Tamkun JW. 2005. Genetic screens for enhancers of brahma reveal functional interactions between the BRM chromatin-remodeling complex and the Delta-Notch signal transduction pathway in *Drosophila*. Genetics. 170(4):1761–1774. doi:10.1534/genetics.105.041327.

Barrio R, de Celis JF. 2004. Regulation of spalt expression in the *Drosophila* wing blade in response to the Decapentaplegic signaling pathway. Proceedings of the National Academy of Sciences. 101(16):6021–6026. doi:10.1073/pnas.0401590101.

Bhardwaj V, Heyne S, Sikora K, Rabbani L, Rauer M, Kilpert F, Richter AS, Ryan DP, Manke T. 2019. snakePipes: facilitating flexible, scalable and integrative epigenomic analysis. Bioinformatics. 35(22):4757–4759. doi:10.1093/bioinformatics/btz436.

Blümli S, Wiechens N, Wu M-Y, Singh V, Gierlinski M, Schweikert G, Gilbert N, Naughton C, Sundaramoorthy R, Varghese J, *et al.,* 2021. Acute depletion of the ARID1A subunit of SWI/SNF complexes reveals distinct pathways for activation and repression of transcription. Cell Reports. 37(5):109943. doi:10.1016/j.celrep.2021.109943.

Bouazoune K, Brehm A. 2006. ATP-dependent chromatin remodeling complexes in *Drosophila*. Chromosome Res. 14(4):433–449. doi:10.1007/s10577-006-1067-0.

Brahma S, Henikoff S. 2020. Epigenome Regulation by Dynamic Nucleosome Unwrapping. Trends in Biochemical Sciences. 45(1):13–26. doi:10.1016/j.tibs.2019.09.003.

Brahma S, Henikoff S. 2023 Jan 22. RNA Polymerase II, the BAF remodeler and transcription factors synergize to evict nucleosomes. bioRxiv.:2023.01.22.525083. doi:10.1101/2023.01.22.525083.

Buszczak M, Paterno S, Lighthouse D, Bachman J, Planck J, Owen S, Skora AD, Nystul TG, Ohlstein B, Allen A, *et al.,* 2007. The carnegie protein trap library: a versatile tool for *Drosophila* developmental studies. Genetics. 175(3):1505–1531. doi:10.1534/genetics.106.065961.

Caussinus E, Kanca O, Affolter M. 2012. Fluorescent fusion protein knockout mediated by anti-GFP nanobody. Nature Structural and Molecular Biology. 19(1):117–122. doi:10.1038/nsmb.2180.

Cenik BK, Shilatifard A. 2021. COMPASS and SWI/SNF complexes in development and disease. Nature Reviews Genetics. 22(1):38–58. doi:10.1038/s41576-020-0278-0.

Chan SKK, Cerda-Moya G, Stojnic R, Millen K, Fischer B, Fexova S, Skalska L, Gomez-Lamarca M, Pillidge Z, Russell S, *et al.,* 2017. Role of co-repressor genomic landscapes in shaping the Notch response. PLOS Genetics. 13(11):e1007096. doi:10.1371/journal.pgen.1007096.

Clapier CR, Iwasa J, Cairns BR, Peterson CL. 2017. Mechanisms of action and regulation of ATP-dependent chromatin-remodelling complexes. Nature Reviews Molecular Cell Biology. 18(7):407–422. doi:10.1038/nrm.2017.26.

Collins RT, Furukawa T, Tanese N, Treisman JE. 1999. Osa associates with the Brahma chromatin remodeling complex and promotes the activation of some target genes. The EMBO Journal. 18(24):7029–7040. doi:10.1093/emboj/18.24.7029.

Collins RT, Treisman JE. 2000. Osa-containing Brahma chromatin remodeling complexes are required for the repression of Wingless target genes. Genes and Development. 14(24):3140–3152. doi:10.1101/gad.854300.

Couso JP, Bishop SA, Martinez Arias A. 1994. The wingless signalling pathway and the patterning of the wing margin in *Drosophila*. Development. 120(3):621–636. doi:10.1242/dev.120.3.621.

Cruz C, Glavic A, Casado M, de Celis JF. 2009. A Gain-of-Function Screen Identifying Genes Required for Growth and Pattern Formation of the *Drosophila melanogaster* Wing. Genetics. 183(3):1005–1026. doi:10.1534/genetics.109.107748.

Danecek P, Bonfield JK, Liddle J, Marshall J, Ohan V, Pollard MO, Whitwham A, Keane T, McCarthy SA, Davies RM, *et al.,* 2021. Twelve years of SAMtools and BCFtools. GigaScience. 10(2):giab008. doi:10.1093/gigascience/giab008.

Diaz de la Loza MC, Thompson BJ. 2017. Forces shaping the *Drosophila* wing. Mechanisms of Development. 144:23–32. doi:10.1016/j.mod.2016.10.003.

Doherty D, Feger G, Younger-Shepherd S, Jan LY, Jan YN. 1996. Delta is a ventral to dorsal signal complementary to Serrate, another Notch ligand, in *Drosophila* wing formation. Genes Dev. 10(4):421–434. doi:10.1101/gad.10.4.421.

Elfring LK, Daniel C, Papoulas O, Deuring R, Sarte M, Moseley S, Beek SJ, Waldrip WR, Daubresse G, DePace A, *et al.,* 1998. Genetic analysis of brahma: the *Drosophila* homolog of the yeast chromatin remodeling factor SWI2/SNF2. Genetics. 148(1):251–265. doi:10.1093/genetics/148.1.251.

Falo-Sanjuan J, Bray SJ. 2020. Decoding the Notch signal. Development, Growth & Differentiation. 62(1):4–14. doi:10.1111/dgd.12644.

Furman DP, Bukharina TA. 2012. Morphogenesis of *Drosophila melanogaster* Macrochaetes: Cell Fate Determination for Bristle Organ. Journal of Stem Cells. 7(1):19–41.

Gaskill MM, Gibson TJ, Larson ED, Harrison MM. 2021. GAF is essential for zygotic genome activation and chromatin accessibility in the early *Drosophila* embryo. Yamashita YM, Struhl K, editors. eLife. 10:e66668. doi:10.7554/eLife.66668.

Gu Z, Eils R, Schlesner M. 2016. Complex heatmaps reveal patterns and correlations in multidimensional genomic data. Bioinformatics. 32(18):2847–2849. doi:10.1093/bioinformatics/btw313.

Guild GM, Connelly PS, Ruggiero L, Vranich KA, Tilney LG. 2005. Actin Filament Bundles in *Drosophila* Wing Hairs: Hairs and Bristles Use Different Strategies for Assembly. Mol Biol Cell. 16(8):3620–3631. doi:10.1091/mbc.E05-03-0185.

Hahne F, Ivanek R (2016). “Statistical Genomics: Methods and Protocols.” In Mathé E, Davis S (eds.), chapter Visualizing Genomic Data Using Gviz and Bioconductor, 335–351. Springer New York, New York, NY. ISBN 978-1-4939-3578-9, doi:10.1007/978-1-4939-3578-9_16,

Hartenstein V, Posakony JW. 1990. A dual function of the Notch gene in *Drosophila* sensillum development. Dev Biol. 142(1):13–30. doi:10.1016/0012-1606(90)90147-b.

Heitzler P, Vanolst L, Biryukova I, Ramain P. 2003. Enhancer-promoter communication mediated by Chip during Pannier-driven proneural patterning is regulated by Osa. Genes Dev. 17(5):591–596. doi:10.1101/gad.255703.

Helming KC, Wang X, Wilson BG, Vazquez F, Haswell JR, Manchester HE, Kim Y, Kryukov GV, Ghandi M, Aguirre AJ, *et al.,* 2014. ARID1B is a specific vulnerability in ARID1A-mutant cancers. Nat Med.
20(3):251–254. doi:10.1038/nm.3480.

Hendy O, Serebreni L, Bergauer K, Muerdter F, Huber L, Nemčko F, Stark A. 2022. Developmental and housekeeping transcriptional programs in *Drosophila* require distinct chromatin remodelers. Mol Cell. 82:3598-3612. doi:10.1016/j.molcel.2022.08.019.

Isbel L, Grand RS, Schübeler D. 2022. Generating specificity in genome regulation through transcription factor sensitivity to chromatin. Nat Rev Genet. 23(12):728–740. doi:10.1038/s41576-022-00512-6.

Iurlaro M, Stadler MB, Masoni F, Jagani Z, Galli GG, Schübeler D. 2021. Mammalian SWI/SNF continuously restores local accessibility to chromatin. Nature Genetics. 53(3):279–287. doi:10.1038/s41588-020-00768-w.

Kadoch C, Hargreaves DC, Hodges C, Elias L, Ho L, Ranish J, Crabtree GR. 2013. Proteomic and bioinformatic analysis of mammalian SWI/SNF complexes identifies extensive roles in human malignancy. Nat Genet. 45(6):592–601. doi:10.1038/ng.2628.

Kassis JA, Kennison JA, Tamkun JW. 2017. Polycomb and Trithorax Group Genes in *Drosophila*. Genetics. 206(4):1699–1725. doi:10.1534/genetics.115.185116.

Kelso TWR, Porter DK, Amaral ML, Shokhirev MN, Benner C, Hargreaves DC. 2017. Chromatin accessibility underlies synthetic lethality of SWI/SNF subunits in ARID1A-mutant cancers. eLife. 6:1–29. doi:10.7554/eLife.30506.001.

Langmead B, Salzberg SL. 2012. Fast gapped-read alignment with Bowtie 2. Nat Methods. 9(4):357–359. doi:10.1038/nmeth.1923.

Li X, Zhao X, Fang Y, Jiang X, Duong T, Fan C, Huang CC, Kain SR. 1998. Generation of destabilized green fluorescent protein as a transcription reporter. Journal of Biological Chemistry. 273(52):34970–34975. doi:10.1074/jbc.273.52.34970.

Ling L, Mühling B, Jaenichen R, Gompel N. 2023. Increased chromatin accessibility promotes the evolution of a transcriptional silencer in *Drosophila*. Science Advances. 9(7):eade6529. doi:10.1126/sciadv.ade6529.

Loker R, Mann RS. 2022. Divergent expression of paralogous genes by modification of shared enhancer activity through a promoter-proximal silencer. Curr Biol. 32(16):3545-3555. doi: 10.1016/j.cub.2022.06.069

Love MI, Huber W, Anders S. 2014. Moderated estimation of fold change and dispersion for RNA-seq data with DESeq2. Genome Biology. 15(12):550. doi:10.1186/s13059-014-0550-8.

Ma Y, McKay DJ, Buttitta L. 2019. Changes in chromatin accessibility ensure robust cell cycle exit in terminally differentiated cells. PLoS Biology. 17(9). doi:10.1371/journal.pbio.3000378.

Mallo M, Alonso CR. 2013. The regulation of Hox gene expression during animal development.

Development. 140(19):3951–3963. doi:10.1242/dev.068346.

McLeay RC, Bailey TL. 2010. Motif Enrichment Analysis: a unified framework and an evaluation on ChIP data. BMC Bioinformatics. 11(1):165. doi:10.1186/1471-2105-11-165.

Michel BC, D'Avino AR, Cassel SH, Mashtalir N, McKenzie ZM, McBride MJ, Valencia AM, Zhou Q, Bocker M, Soares LMM, *et al.,* 2018. A non-canonical SWI/SNF complex is a synthetic lethal target in cancers driven by BAF complex perturbation. Nat Cell Biol. 20(12):1410–1420. doi:10.1038/s41556-018-0221-1.

Millán-Zambrano G, Burton A, Bannister AJ, Schneider R. 2022. Histone post-translational modifications — cause and consequence of genome function. Nat Rev Genet. 23(9):563–580. doi:10.1038/s41576-022-00468-7.

Morris SA, Baek S, Sung M-H, John S, Wiench M, Johnson TA, Schiltz RL, Hager GL. 2014. Overlapping chromatin-remodeling systems collaborate genome wide at dynamic chromatin transitions. Nat Struct Mol Biol. 21(1):73–81. doi:10.1038/nsmb.2718.

Moshkin YM, Mohrmann L, van Ijcken WFJ, Verrijzer CP. 2007. Functional differentiation of SWI/SNF remodelers in transcription and cell cycle control. Mol Cell Biol. 27(2):651–661. doi:10.1128/MCB.01257-06.

Mu W, Davis ES, Lee S, Dozmorov MG, Phanstiel DH, Love MI. 2023. bootRanges: flexible generation of null sets of genomic ranges for hypothesis testing. Bioinformatics. 39(5):btad190. doi:10.1093/bioinformatics/btad190.

Nern A, Pfeiffer BD, Svoboda K, Rubin GM. 2011. Multiple new site-specific recombinases for use in manipulating animal genomes. Proceedings of the National Academy of Sciences of the United States of America. 108(34):14198–14203. doi:10.1073/pnas.1111704108.

Niederhuber MJ, McKay DJ. 2020. Mechanisms underlying the control of dynamic regulatory element activity and chromatin accessibility during metamorphosis. Curr Opin Insect Sci. 43:21–28. doi:10.1016/j.cois.2020.08.007.

Nystrom SL, McKay DJ. 2021. Memes: A motif analysis environment in R using tools from the MEME Suite. PLoS Comput Biol. 17(9):e1008991. doi:10.1371/journal.pcbi.1008991.

Nystrom SL, Niederhuber MJ, McKay DJ. 2020. Expression of E93 provides an instructive cue to control dynamic enhancer activity and chromatin accessibility during development. Development (Cambridge). 147(6). doi:10.1242/dev.181909.

Parks AL, Muskavitch MA. 1993. Delta function is required for bristle organ determination and morphogenesis in *Drosophila*. Dev Biol. 157(2):484–496. doi:10.1006/dbio.1993.1151.

Patsialou A, Wilsker D, Moran E. 2005. DNA-binding properties of ARID family proteins. Nucleic Acids Res. 33(1):66–80. doi:10.1093/nar/gki145.

Pillidge Z, Bray SJ. 2019. SWI / SNF chromatin remodeling controls Notch-responsive enhancer accessibility. EMBO reports. 20(5). doi:10.15252/embr.201846944.

Ramírez F, Ryan DP, Grüning B, Bhardwaj V, Kilpert F, Richter AS, Heyne S, Dündar F, Manke T. 2016. deepTools2: a next generation web server for deep-sequencing data analysis. Nucleic Acids Research. 44(W1):W160–W165. doi:10.1093/nar/gkw257.

Ren N, Zhu C, Lee H, Adler PN. 2005. Gene expression during *Drosophila* wing morphogenesis and differentiation. Genetics. 171(2):625–638. doi:10.1534/genetics.105.043687.

Reske JJ, Wilson MR, Armistead B, Harkins S, Perez C, Hrit J, Adams M, Rothbart SB, Missmer SA, Fazleabas AT, *et al.,* 2022. ARID1A-dependent maintenance of H3.3 is required for repressive CHD4-ZMYND8 chromatin interactions at super-enhancers. BMC Biol. 20(1):209. doi:10.1186/s12915-022-01407-y.

Salzler HR, Vandadi V, McMichael BD, Brown JC, Boerma SA, Leatham-Jensen MP, Adams KM, Meers MP, Simon JM, Duronio RJ, *et al.,* 2023. Distinct roles for canonical and variant histone H3 lysine-36 in Polycomb silencing. Sci Adv. 9(9):eadf2451. doi:10.1126/sciadv.adf2451.

Schick S, Grosche S, Kohl KE, Drpic D, Jaeger MG, Marella NC, Imrichova H, Lin JMG, Hofstätter G, Schuster M, *et al.,* 2021. Acute BAF perturbation causes immediate changes in chromatin accessibility. Nature Genetics. 53(3):269–278. doi:10.1038/s41588-021-00777-3.

Schindelin J, Arganda-Carreras I, Frise E, Kaynig V, Longair M, Pietzsch T, Preibisch S, Rueden C, Saalfeld S, Schmid B, *et al.,* 2012. Fiji: an open-source platform for biological-image analysis. Nat Methods. 9(7):676–682. doi:10.1038/nmeth.2019.

Sobala LF, Adler PN. 2016. The Gene Expression Program for the Formation of Wing Cuticle in *Drosophila*. PLOS Genetics. 12(5):e1006100. doi:10.1371/journal.pgen.1006100.

Spitz F, Furlong EEM. 2012. Transcription factors: From enhancer binding to developmental control. Nature Reviews Genetics. 13(9):613–626. doi:10.1038/nrg3207.

Stark R, Brown G. DiffBind: Differential binding analysis of ChIP-Seq peak data.
Tang Y-C, Amon A. 2013. Gene copy-number alterations: a cost-benefit analysis. Cell. 152(3):394–405. doi:10.1016/j.cell.2012.11.043.

Terriente-Félix A, de Celis JF. 2009. Osa, a subunit of the BAP chromatin-remodelling complex, participates in the regulation of gene expression in response to EGFR signalling in the *Drosophila* wing. Developmental Biology. 329(2):350–361. doi:10.1016/j.ydbio.2009.03.010.

Treisman JE, Luk A, Rubin GM, Heberlein U. 1997. Eyelid antagonizes wingless signaling during *Drosophila* development and has homology to the bright family of DNA-binding proteins. Genes and Development. 11(15):1949–1962. doi:10.1101/gad.11.15.1949.

Uyehara CM, Apostolou E. 2023. 3D enhancer-promoter interactions and multi-connected hubs: Organizational principles and functional roles. Cell Reports. 42(4):112068. doi:10.1016/j.celrep.2023.112068.

Uyehara CM, McKay DJ. 2019. Direct and widespread role for the nuclear receptor EcR in mediating the response to ecdysone in *Drosophila*. Proceedings of the National Academy of Sciences of the United States of America. 116(20):9893–9902. doi:10.1073/pnas.1900343116.

Uyehara CM, Nystrom SL, Niederhuber MJ, Leatham-Jensen M, Ma Y, Buttitta LA, McKay DJ. 2017. Hormone-dependent control of developmental timing through regulation of chromatin accessibility. Genes and Development. 31(9):862–875. doi:10.1101/gad.298182.117.

Weber CM, Hafner A, Kirkland JG, Braun SMG, Stanton BZ, Boettiger AN, Crabtree GR. 2021. mSWI/SNF promotes Polycomb repression both directly and through genome-wide redistribution. Nat Struct Mol Biol. 28(6):501–511. doi:10.1038/s41594-021-00604-7.

Wickham H. 2016. ggplot2: Elegant Graphics for Data Analysis (3e). Springer-Verlag New York. https://ggplot2-book.org/.

Wilson BG, Helming KC, Wang X, Kim Y, Vazquez F, Jagani Z, Hahn WC, Roberts CWM. 2014. Residual complexes containing SMARCA2 (BRM) underlie the oncogenic drive of SMARCA4 (BRG1) mutation. Mol Cell Biol. 34(6):1136–1144. doi:10.1128/MCB.01372-13.

Yamanaka N, Rewitz KF, O'Connor MB. 2013. Ecdysone Control of Developmental Transitions: Lessons from *Drosophila* Research. Annual Review of Entomology. 58(1):497–516. doi:10.1146/annurev-ento-120811-153608.

Yu G, Wang L-G, He Q-Y. 2015. ChIPseeker: an R/Bioconductor package for ChIP peak annotation, comparison and visualization. Bioinformatics. 31(14):2382–2383. doi:10.1093/bioinformatics/btv145.

Zhang Y, Liu T, Meyer CA, Eeckhoute J, Johnson DS, Bernstein BE, Nusbaum C, Myers RM, Brown M, Li W, *et al.,* 2008. Model-based Analysis of ChIP-Seq (MACS). Genome Biology. 9(9):R137. doi:10.1186/gb-2008-9-9-r137.

Zraly CB, Dingwall AK. 2012. The chromatin remodeling and mRNA splicing functions of the Brahma (SWI/SNF) complex are mediated by the SNR1/SNF5 regulatory subunit. Nucleic Acids Research. 40(13):5975–5987. doi:10.1093/nar/gks288.

CHAPTER 5: CHARACTERIZATION OF E93 PROTEIN DOMAIN FUNCTION AND POTENTIAL COREGULATORS

5.1 Introduction

The *Drosophila* ecdysone hormone induced transcription factor (TF) Eip93F (E93) is a developmental stage-coordinating temporal TF expressed in pupal stages around 18-24h After Puparium Formation (APF; Baehrecke and Thummel, 1995). E93 is the major adult-specifying factor during metamorphosis and is found conserved among many holo- and hemimetabolous insects (Lam *et al.,* 2022). E93 controls the proper transition from prepupal to pupal stages by coordinating repression of early gene expression programs and the activation of late adult expression programs. E93 mutants fail to properly complete development and show a variety of defects such as incomplete adult appendage development, incomplete abdominal cuticle, and a lack of pigmentation (Lam *et al.,* 2022). One of the means by which E93 achieves this systemic developmental regulation is through coordination of changes in chromatin accessibility (Mou *et al.,* 2012; Uyehara *et al.,* 2017). Genome-wide chromatin accessibility profiling during *Drosophila* wing metamorphosis has shown that patterns of accessibility are highly dynamic over time. In E93 mutants ~25% of the accessibility changes that normally occur in wings between third larval wandering (3LW) and 24h APF fail to occur, indicating a general requirement for E93 to regulate increases (“opening”) and decreases (“closing”) in chromatin accessibility (Uyehara *et al.,* 2017). Precocious expression of E93 in the wing disc has also demonstrated that E93 is sufficient to instruct many of these accessibility changes at an earlier stage of wing development (Nystrom *et al.,* 2020). *In vivo* transgenic enhancer reporter assays have validated several E93 bound sites as functional enhancers and demonstrated that E93 is necessary and sufficient to cue changes to enhancer activity that correlate with changes in accessibility (Uyehara *et al.,* 2017; Nystrom *et al.,* 2020). Surprisingly, experiments with transgenic enhancer reporters demonstrated that E93 was sufficient to deactivate and activate enhancers that had overlapping patterns of reporter activity, strongly suggesting that E93 is a bifunctional tTF capable of eliciting distinct regulatory effects at different loci within the same cell

(Nystrom *et al.,* 2023). How a stage-specifying tTF like E93 is able to mediate these divergent changes to chromatin accessibility and enhancer activity is not clear.

There are several possible, but not mutually exclusive, explanations for how E93 function is specified. E93 may interact differently with sites that it differentially regulates. For example, E93 may depend on direct DNA interaction when closing and deactivating enhancers, but not when it opens and activates. This possibility is supported by an observed differential enrichment of E93 motifs in E93-dependent closing sites relative to opening sites (Uyehara *et al.,* 2017). However, E93 is observed by ChIP-seq to be present at both closing and opening sites. Another possibility is that E93 interacts with different coregulators at different target sites. This could involve direct modification of E93 function, such as how readily it binds DNA, or differential function of the coregulators themselves.

E93 contains a series of protein domains with predicted function that have been identified by homology to several conserved domains. These include a C-terminal Binding Protein (CtBP) corepressor interaction domain (PXDLS), several nuclear hormone receptor interaction domains (LXXLL), and a Pipsqueak family DNA binding domain (Psq; Siegmund and Lehmann, 2001; Mou *et al.,* 2012; **Figure 5.1A**). We hypothesized that these domains may be functional and that E93 may differentially utilize some of these domains for distinct functions. In order to test this, we generated a series of inducible E93 domain mutant transgenes and tested how they impacted E93-mediated enhancer regulation *in vivo*. In parallel, we directly tested the role of CtBP as a potential coregulator of E93 target enhancers. In order to screen for additional putative E93 coregulators, we built a dual-expression tool, based on a previously described system, to initially deplete target proteins via RNAi and then ectopically express E93 to specifically test for E93 coregulators (Cohen *et al.,* 2018). Preliminary experiments with these approaches find that the putative E93 PXDLS domain is largely dispensable for E93-mediated deactivation of the *Drosophila* wing disc br^{disc} enhancer. However, even minor disruption of the putative E93 Psq DNA-binding domain reduces the ability of E93 to induce either br^{disc} deactivation or premature activation of the late tncwv enhancer. We also find that contrary to the canonical role of CtBP as a corepressor, we find it is required to maximally activate the br^{disc} enhancer in third larval wandering (3LW) imaginal wing discs. Finally, we find that Osa, a member of the *Drosophila* SWI/SNF BAP complex, and a known negative

regulator of *br^{disc}* activity, is not required for E93-mediated precocious *br^{disc}* deactivation (Niederhuber *et al.,* 2023). Together, these preliminary experiments have generated several tools that will be generally useful to the E93 research field and provided exciting initial results for future study.

5.2 Results

5.2.1 The putative E93 CtBP interaction domain is not required for E93-initiated enhancer deactivation.

CtBP is a family of corepressors conserved from insects to mammals (Chinnadurai, 2007). In *Drosophila*, CtBP is essential to properly establish segmental domains during embryogenesis. For example, the repressor Krüppel binds CtBP and requires it to repress expression of the second stripe of the pair-rule gene even-skipped (Mannervik, 2014). CtBP functions like a bridge, linking site-specific repressor TFs to histone modifying machinery like histone demethylases and deacetylases (Chinnadurai, 2007). This interaction depends on a conserved protein domain consisting of Pro-X-Asp-Leu-Ser (PXDLS). The E93 human homolog Ligand-dependent Corepressor (LCOR) has been identified as containing two N-terminal tandem PXDLS domains that are required for interaction with CtBP and CtBP corepression (Palijan *et al.,* 2009). In *Drosophila*, E93 contains a single domain with homology to the extended consensus PXDLS motif consisting of Pro-Leu-Asp-Leu-Ser-Ser-Lys (PLDLSSK). To test the role of this potential CtBP interaction domain, we generated GAL4 inducible E93 transgenes that carried a C-terminal 3x-HA tag and a deletion of the full PLDLSSK sequence (*UAS-E93$^{\Delta PXDLS}$-3XHA*). This E93 transgene was made from the *UAS-E93-3xHA* transgene generated by the FlyORF project (Bischof *et al.,* 2020). We have previously demonstrated that the *UAS-E93-3xHA* transgene can successfully express E93 in 3LW imaginal wing discs, and that ectopic E93 expression prior to its normal period of expression ~6-24h APF is sufficient to precociously deactivate the E93-regulated enhancer *br^{disc}* enhancer (Nystrom *et al.,* 2020). When we ectopically expressed E93$^{\Delta PXDLS}$ in wing discs, using a temperature sensitive *ci-GAL4, UAS-GFP, tub-GAL80^{ts,10}* anterior compartment driver (*ci^{ts}*), we observed a significant reduction in *br^{disc}-tdTomato* (*br^{disc}*) reporter activity relative to WT cells of the posterior compartment (**Figure 5.1B**). In comparison, induction of WT E93 showed a similar reduction of *br^{disc}* reporter activity

(yellow arrows, **Figure 5.1B**). In some discs we observed that *br^{disc}* reporter activity was slightly stronger in cells immediately along the developing margin in E93$^{\Delta PXDLS}$ vs E93 induction experiments (red arrows). However, these differences also appeared to correlate with apparent gaps in the cits expression domain, as marked by *UAS-GFP*, and thus could be due to incomplete E93 expression and not solely to a disruption in E93 function caused by the PXDLS deletion. Together, these data indicate that this putative E93 PXDLS domain is not required for E93-mediated deactivation of *br^{disc}*.

5.2.2 CtBP is required to activate the *br^{disc}* enhancer

The apparent lack of requirement for the consensus PXDLS domain in E93 to repress the *br^{disc}* enhancer reporter does not exclude CtBP as a possible E93 coregulator. In order to test if CtBP was required to regulate *br^{disc}* deactivation during wing metamorphosis, we depleted CtBP with RNAi in pupal wings and assayed changes in *br^{disc}* activity using a previously described reporter optimized for increased fluorophore turnover (*br^{disc}-tdTomato-PEST^{VK33}*; Niederhuber *et al.,* 2023). When CtBP was knocked-down in the anterior compartment with the cits driver, we observed marked reduction of *br^{disc}* reporter activity relative to WT cells of the posterior compartment, and compared to a *lexA-RNAi* negative control (**Figure 5.1C**). This result was surprising because reduced reporter activity suggests that CtBP is required to fully activate the *br^{disc}* enhancer, contrary to its normal role as a corepressor. While CtBP is canonically described as a corepressor it has been observed that CtBP is necessary for gene activation at certain genes. For example, *Drosophila* CtBP has been found to be necessary both for repression and activation of wingless signaling targets in a gene-specific manner, and that this switch between repressor and activator is a consequence of different states of CtBP oligomerization (Fang *et al.,* 2006; Bhambhani *et al.,* 2011).

To further examine the observation that CtBP is required for *br^{disc}* reporter activity we used a strong CtBP loss of function allele *CtBP$^{87de-10}$*, which is a nonsense mutation of Q299 to STOP (*CtBP^{Q229*}*), to generate mitotic clones in both imaginal wing discs and pupal wings (Poortinga *et al.,* 1998; Bhambhani 2007 flybase correspondence). When *CtBP^{Q229*}* clones were generated 48-72 AEL and assayed in 3LW wing discs aged ~120-144h AEL, we observed a strong reduction in activity of the *br^{disc}-*

tdTomato-PEST reporter within clones (**Figure 5.1D**). Similarly, when *CtBP*^{Q229*} clones were generated a day later (~72-96h AEL) and then assayed in pupal wings aged approximately ~24-36h APF, there was strong reduction in reporter activity within clones (**Figure 5.1E**). Notably, the *br*^{disc} enhancer deactivates between mid-prepupal stages (6h APF) and pupal stages (18h APF). Using a more temporally sensitive *br*^{disc} reporter, we have previously shown that *br*^{disc} reporter activity detected at these pupal stages is likely due to the perdurance of previously translated reporter fluorophore (Niederhuber *et al.,* 2023). Thus, we interpret the loss of *br*^{disc} reporter activity within *CtBP*^{Q229*} pupal wing clones as a consequence of reduced reporter activity when the enhancer is on earlier in wing discs. Together, these experiments indicate that CtBP is not a corepressor, but instead it functions as a coactivator of the *br*^{disc} enhancer in developing wings, and that the consensus PXDLS CtBP interaction domain within E93 is not required for E93 to deactivate the enhancer. Since the requirement of CtBP to activate *br*^{disc} precedes the normal expression window of E93 (~6h-24h APF), CtBP likely regulates *br*^{disc} independently of E93 and is likely cooperating with additional factors at this stage.

5.2.2 The E93 Psq DNA-binding domain is required for E93 enhancer regulation

E93 is a sequence specific DNA-binding TF of the Pipsqueak family that binds thousands of sites genome-wide (Uyehara *et al.,* 2017). Pipsqueak family TFs are found in insects and mammals and share a conserved three alpha-helix Psq DNA-binding domain (Siegmund and Lehmann, 2002). Within *Drosophila*, Psq domain proteins include E93, the Broad-complex, Tramtrack, and Bric-a-brac, among others. In humans, Psq domains are found in the Centromere Binding Protein (CENP-B) and the E93 homolog LCOR, and it has been recently demonstrated by ChIP-seq in human mammary cells that the putative LCOR Psq DNA-binding is necessary for normal levels of LCOR binding genome-wide as well as normal LCOR transcriptional regulation (Pérez-Núñez *et al.,* 2022).

We hypothesized that similarly to LCOR, E93 required the putative Psq DNA-binding domain for its ability to correctly regulate enhancer activity. We tested this by again generating a series of domain mutations within the *UAS-E93-3xHA* transgene. We made three mutations of varying severity to the E93 Psq domain. A full deletion of all three helices from T784 to R839 (*E93*$^{\Delta Psq}$), a deletion of the second and

third helix from S811 to R833 (*E93$^{\Delta HTH}$*), and mutation of three highly-conserved residues of the third helix to Alanines (S824A, T824A, L826A; *E93$^{H3.AAA}$*; **Figure 5.2A**). Based on published structure of human CENB-P, the second and third helices of the Psq domain are predicted to form the DNA-interacting Helix-turn-Helix motif, with the third helix interfacing with the DNA major groove (Tanaka *et al.,* 2001; **Figure 5.2A**). We expressed these E93 mutant transgenes using the cits in wing imaginal discs that also had the *br^{disc}-tdTomato-PEST* reporter. Compared to ectopic expression of WT E93, which normally leads to significant reduction of *br^{disc}* reporter activity (**Figure 5.1B**), expression of these Psq domain mutations led to little change in *br^{disc}* activity relative to WT cells of the posterior compartment (**Figure 5.2B**). Another enhancer, the *tnc^{wv}* enhancer, is inactive in WT 3LW wing discs but activates in pupal wings along the developing veins in an E93-dependent manner (Uyehara *et al.,* 2017). The *tnc^{wv}* enhancer will precociously activate in the wing disc in the presence of ectopic E93 expression (Nystrom *et al.,* 2020; **Figure 5.2C**). When we expressed E93$^{H3.AAA}$ in the wing discs with a *tnc^{wv}-tdTomato* reporter we observed no induction of the reporter (**Figure 5.2C**). Importantly, anti-HA immunofluorescence staining showed strong nuclear signal following cits induction of all E93 Psq mutant transgenes, indicating that mutations were not leading to incomplete protein translation, significant protein degradation, or incorrect localization. Notably, despite the apparent lack of effect on enhancer activity, we observed near total lethality of animals expressing any of the E93 Psq mutants, with most dying as pupae or pharate adults, suggesting that expression of these mutants still impact developmental programs. Together, these results suggest that the putative Psq domain of E93 is required for E93-mediated regulation of both deactivated (*br^{disc}*) and activated (*tnc^{wv}*) enhancers, implicating E93 DNA binding as a critical mechanism for E93 function.

5.2.3 E93 does not require Osa to sufficiently deactivate *br^{disc}* in the wing disc

E93 does not contain any domains with documented enzymatic function or homology to known catalytic domains, suggesting that E93 likely partners with additional coregulators to modify its target sites. This is supported by the observation that E93 contains several LXXLL nuclear hormone interaction domains, indicating that E93 likely has some capacity for protein-protein interaction. We hypothesized that E93 may not only require coregulators to alter enhancer activity and accessibility, but that it may

achieve differential enhancer regulation by interacting with distinct partners at specific sites. To first identify potential E93 coregulators we decided to employ an RNAi based screen. While RNAi forward-genetic screens can be successful approaches they will capture both direct and indirect effects of target knockdown. To identify coregulators that were more likely to be specifically required for E93-mediated enhancer regulation we chose to express RNAi in the context of ectopic E93 expression in the imaginal wing disc. Based on a previously developed genetic method for dual-expression with GAL4, we built an E93 induction tool that would allow *UAS-RNAi* expression but prevent *UAS-E93-3xHA* transcription with an FRT-flanked transcriptional stop cassette (*UAS-FRT-STOP-FRT-E93-3xHA*; Cohen *et al.,* 2018). The STOP could be inducibly removed via expression of Flippase (FLP) under the control of a heat-shock sensitive promoter to subsequently allow E93 expression (*hsFLP*; **Figure 5.3A**). We termed this tool the E93 Flip-Out System (*E93^{FlOS}*). With the addition of a *ci^{ts}* GAL4 driver that limited GAL4 induction below 29^{O}C, this tool allowed for expression of RNAi to first effectively establish target knockdown, prior to induction of ectopic E93.

We recently identified the *Drosophila* SWI/SNF nucleosome remodeling complex BAP as a negative regulator of *br^{disc}* enhancer activity in imaginal wing discs (Niederhuber *et al.,* 2023). The BAP-specific complex member Osa, which is a non-specific DNA binding subunit of the complex, directly binds the *br^{disc}* enhancer in 3LW wing discs and is required to constrain the enhancer's activity when it is normally on (Niederhuber *et al.,* 2023). Because Osa and the BAP complex lack the ability to recognize regions of the genome with sequence specificity, they are thought to depend on sequence-specific TFs to recruit them to target loci. Using the E93^{FlOS} tool, in combination with the *br^{disc}-tdTomato-PEST* reporter, we first depleted Osa with *osa-RNAi* in the anterior wing disc compartment and then removed the block on E93 expression with a 37^{o}C heatshock ~40h later. E93 was then allowed to be expressed for 24h prior to the dissection of 3LW imaginal wing discs (**Figure 5.3B**). Under these conditions we observed strong reduction of *br^{disc}* reporter activity in cells expressing both *osa-RNAi* and E93 (**Figure 5.3C**). This was true for most of the anterior wing disc, except in a number of small clones that showed increased *br^{disc}* reporter activity. Close inspection of E93 positive regions following flip-out, determined by anti-HA immunofluorescence, revealed that strong *br^{disc}* activity occurred within regions that were E93 negative

(red outlines inset **Figure 5.3C**), indicating the heat shock failed to remove the STOP cassette in these cells. While E93 is not ectopically expressed in these cells, *osa-RNAi* is, and the increased br^{disc} activity relative to control cells of the posterior demonstrates hyperactivation of the enhancer in the absence of Osa. A negative control experiment performed with similar conditions but without heatshock induced FLP expression showed strong upregulation of the br^{disc} reporter, but no E93 expression (**Figure 5.3C**). These preliminary experiments demonstrate the successful application of the $E93^{FIOS}$ dual-expression tool to screen for E93 coregulators in the context of an E93-sufficiency experiment. They also show that while Osa directly constrains the br^{disc} enhancer, it is not required for E93-mediated enhancer deactivation.

5.3 Discussion

5.3.1 CtBP may function with E93 through a non-consensus domain

In these preliminary experiments we find that a domain within E93 with homology to the consensus CtBP interacting PXDLS domain is not necessary for E93 to deactivate the E93-sensitive br^{disc} enhancer. However, this observation is not sufficient to determine whether or not E93 either directly or indirectly collaborates with CtBP to regulate target enhancers. We have also not yet determined if E93 and CtBP directly interact. In order to understand the impact of the ΔPXDLS mutation it will be necessary to first determine interaction and subsequently determine if this domain deletion abrogates that interaction. Importantly though, while many CtBP-interacting proteins rely on PXDLS domains for CtBP interaction and repressor function, some CtBP partners have been observed to either interact with more degenerate PXDLS domains or in a PXDLS-independent manner (Wen *et al.,* 2000). Thus, further study on the potential cooperation between CtBP and E93 will need to appropriately test these possibilities.

5.3.2 Is the putative Pipsqueak domain required for E93 DNA-binding?

We have made multiple mutations to the putative Psq DNA-binding domain within E93 and described preliminary evidence that this domain is necessary for E93 to regulate target enhancers, both those it activates and deactivates. It remains to be determined if disruption of this domain effects E93's ability to bind DNA. We have previously utilized CUT&RUN in wing discs to profile TF binding and histone

post-translational modifications with a great deal of success (Skene *et al.,* 2018; Uyehara and McKay 2019; Niederhuber *et al.,* 2023). Ectopic expression of WT and Psq domain mutant *UAS-E93-3xHA* in the wing disc, followed by CUT&RUN for E93 would provide a robust test of the importance of this domain and may offer new insights into E93 site-specific function.

5.4 Methods

5.4.1 Plasmid construction

E93 domain mutations were generated as follows: E93 isoform B (UniProt Q7YU18) cDNA was cloned by PCR from the *UAS-E93-3xHA* FlyORF line (F000587; Bischof *et al.,* 2013) into the gateway cloning donor vector pDONR221 (Invitrogen). Mutations were made to pDONR221-E93 using Q5 mutagenesis. Mutated E93 cDNA was subsequently moved into the FlyORF vector pGW-HA by gateway cloning, and genomic insertions were made at the 86FB landing site by PhiC31-mediated integration (BestGene).

The dual-expression E93 flip-out tool (E93-FIOS) was based on the dual-expression system developed by Cohen *et al.,* and was constructed by cloning E93 isoform B cDNA by PCR from the *UAS-E93-3xHA* FlyORF line into vector pUAST (*UAS-FRT-STOP-FRT-insert_site*; gift of Don Fox lab) by HiFi assembly. The resulting vector pUAST-E93 was sent for P-element transformation (BestGene). Integrations were validated genetically and by positive GAL4 induction of E93 following Stop cassette removal.

Primers:

ID	Name	Sequence
MJN074	uas-FlipOut E93 fwd	gtaccgcggccgcggctcgagctagATGGCCGATTGTTCATATGTGAGAT
MJN075	uas-FlipOut E93 rev	ccttcacaaagatcctctagaccggTCAAGCGTAATCTGGAACGTCATAT
MJN079	E93_mid_rev	GGCCATCATCTTCTGTATGC
MJN080	E93_mid_fwd	GCAACAGTTTGCTGACCTCA
EL3	PxDLS_del_fwd	CCATCGCCGAACTCATCG
EL4	PxDLS_deletion_rev	TGCATCCACACTGGGACT
MJN083	Psq_Del_Q5_F	CGCAAGCGAGAGCCCAAG
MJN084	Psq_Del_Q5_R	CGTTCCCTTGCCCAATGC
MJN085	HTH_Del_Q5_F and H3_Del_Q5_F	CGTCACCTGATGCGACCG

MJN086	HTH_Del_Q5_R	CGACATTTCACCTCTCTGCAC
MJN087	H3_Del_Q5_R	TACGCCATAGTAGCTACCC
MJN088	Psq_AAA_Q5_F	cgcaGAGTACAAGGTCAAGGAAC
MJN089	Psq_AAA_Q5_R	gccgcATGCGGTACGCCATAGTA

Plasmids:

Vector	**Content**	**Source**
pUAST	*UAS-FRT-STOP-FRT-cDNA_insert_site*	Gift of Don Fox; Cohen *et al.,* 2018
pGW-HA	*5xUAS-attR1-ccdB-attR2-3xHA*	FlyORF; Bischof *et al.,* 2013

5.4.2 *Drosophila* culture and genetics

For CtBP knockdown experiments, *UAS-ctbp_RNAi TRiP.HMS00677^{attP2}* flies were crossed to *ci-GAL4, UAS-GFP, tub-GAL80^{ts,10}* (*ci^{ts}*) driver flies with the *br^{disc}-tdTomato-PEST^{VK33}* reporter. Crosses were kept at 23^{O}C to limit GAL4 induction, and then moved to 29^{O}C XX days after egg laying (AEL) to destabilize GAL80^{ts} and permit GAL4 induction. Prepupae (0-12h APF) were staged by morphology (cuticle but with no head eversion) and aged for ~24h at 29^{O}C. Wings were then dissected and fixed as previously described (Uyehara *et al.,* 2017).

For CtBP mitotic clone experiments, flies with the genotype *br^{disc}-tdTomato-PEST^{attP2}, FRT82B, ubi-GFP* were crossed to flies with a heat shock inducible Flippase (*hsFLP*) and the EMS strong loss-of-function *ctbp$^{87de-10}$* allele (identified as *ctbp^{Q229*}* in this chapter), *hsFLP ; ; FRT82B, osa$^{87de-10}$* (Portinga *et al.,* 1998). For 3LW wing disc clones, vials with larvae were heat shocked in a 37^{O}C water bath for 20m ~3d AEL to induce FLP expression. For pupal wing clones, vials with larvae were similarly heat shocked ~4d AEL. Pupae were not staged for this experiment but were collected ~9d AEL, and the wing used in **Figure 5.1** is ~24-36h APF based on the lack of bristles or folds that occur ~38-40h APF. All clone experiments were raised at 25^{O}C expect during heat shock.

For all E93 domain mutant experiments, *UAS-E93-3xHA* WT or mutant flies were crossed to *ci^{ts}* driver flies with the *br^{disc}-tdTomato-PEST^{86FB}* reporter and raised at 23^{O}C. E93 expression was induced by moving vials with larvae to 29^{O}C 5d AEL for ~24h prior to dissection 3LW wing discs.

For E93 FlOS experiments, flies with the genotype *hsFLP ; ci-GAL4, UAS-GFP, tub-GAL80^{ts,10} ; br^{disc}-tdTomato-PEST^{86FB}, UAS-E93^{FlOS}* were crossed to flies with the *UAS-osa-RNAi* at 23^{O}C. Vials with

larvae were moved to 29^{O}C to induce RNAi expression ~4d AEL, 24h later vials were heat shocked in a 37^{O}C water bath for 30m and then returned to 29^{O}C. 3LW wing discs were dissected ~24h after heat shock (~6h AEL).

Fly lines:

Genotype	**Source**
yw ; ci-GAL4, UAS-GFP, tub-GAL80^{ts,10} ; br^{disc}-tdTomato_PESTVK33	Niederhuber *et al.,* 2023
yw ; ci-GAL4, UAS-GFP, tub-GAL80^{ts,10} ; br^{disc}-tdTomato^{attP2}	Uyehara *et al.,* 2017
yw122 hsFLP ; IF / Sp ; FRT82B, ctbp$^{87de-10}$ / TM6B, Tb	Gift of Iswar Hariharan
yw ; ; br^{disc}-tdTomato^{attP2}, FRT82B, ubi-GFP	This work
yw ; ; UAS-E93_3xHA	FlyORF; Bischof *et al.,* 2013
yw ; ; UAS-E93$^{\Delta PXDLS}$_3xHA	This work
yw ; ; UAS-E93$^{\Delta Psq}$_3xHA	This work
yw ; ; UAS-E93$^{\Delta HTH}$_3xHA	This work
yw ; ; UAS-E93$^{H3.AAA}$_3xHA	This work
yw ; ; 5xUAS-FRT-Stop-FRT-E93_3xHA	This work
yw122 hsFLP ; ci-GAL4, UAS-GFP, tub-GAL80^{ts,10} ; br^{disc}-tdTomato_PEST86FB , 5xUAS-FRT-Stop-FRT-E93_3xHA	This work
y,sc,v,sev ; ; UAS-ctbp_RNAi TRiP.HMS00677^{attP2}	Bloomington 32889
y,v ; ; UAS-osa_RNAi TRiP.JF01207^{attP2}	Bloomington 31266

5.4.3 Immunofluorescence and microscopy

Dissection and Immunofluorescence was performed as previously described (Uyehara *et al.,* 2017). The following antibodies were used: rabbit anti-HA 1:500 (Abcam ab9110), rabbit anti-CtBP 1:1000 (Gift of David Arnosti), goat anti-rabbit Alexa633 1:1000 (Invitrogen).

5.5 Figures

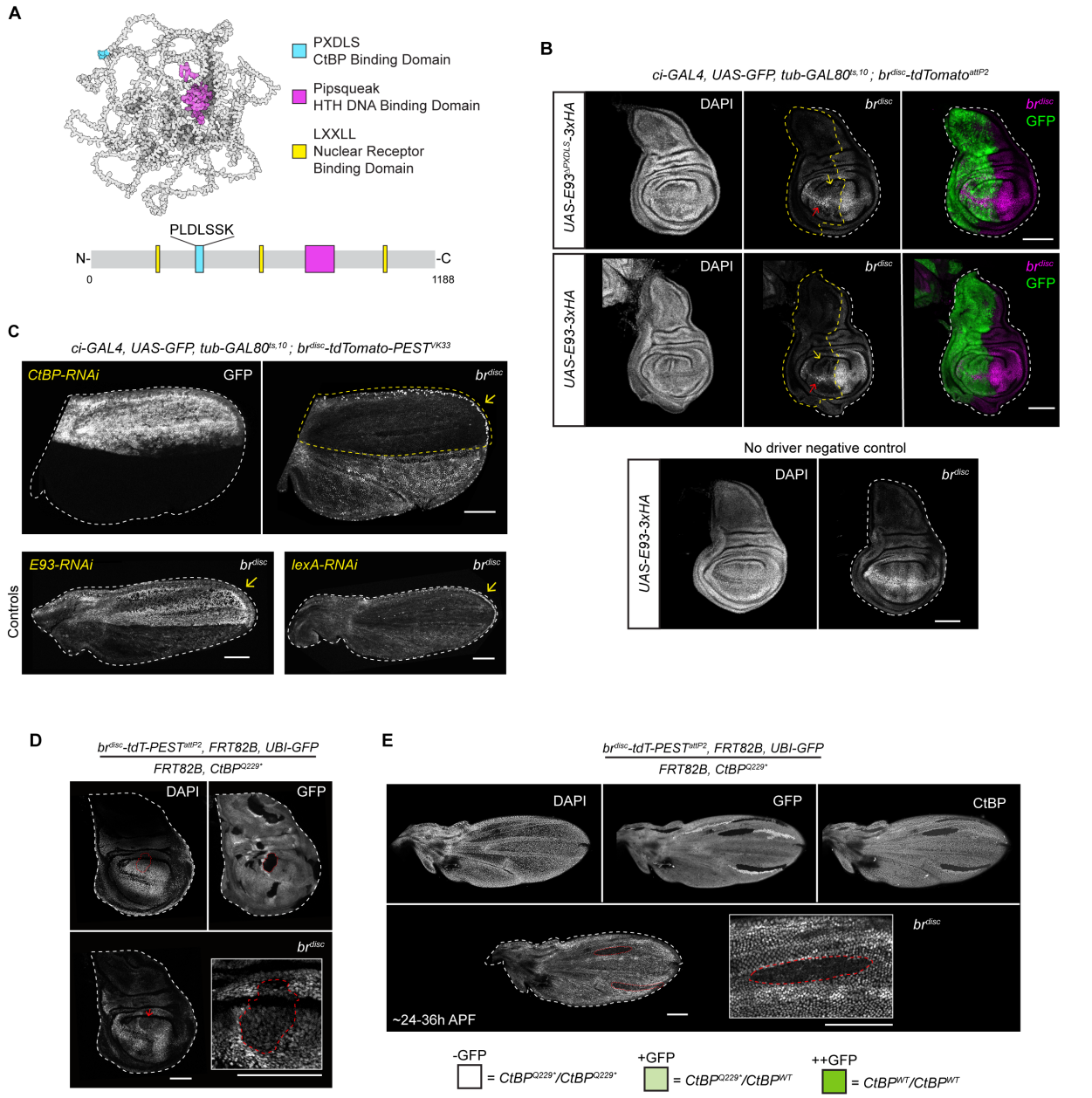

Figure 5.1: (A) Model of *Drosophila* Eip93F (E93) generated by AlphaFold, with corresponding linear map (Jumper *et al.,* 2021). Putative functional domains are highlighted. (B) Confocal microscopy of br^{disc} reporter activity in third larval wandering (3LW) wing discs. Discs are expressing either $E93^{\Delta PXDLS}$*-3xHA* or control WT *E93-3xHA* in the anterior compartment (left) using the ci^{ts} driver (marked by GFP expression and yellow-hash). Yellow arrows indicate cells with strong br^{disc} reduction, and red arrows indicate some subtle difference in br^{disc} activity at the margin between experiments. A no driver control is included for comparison to show WT br^{disc} pattern. (C) Confocal images of br^{disc} reporter activity in pupal wings aged ~24-36h APF with RNAi expression (yellow-hash, GFP positive) in the anterior compartment with ci^{ts} (top). (D,E) Confocal images of $ctbp^{Q229*}$ mitotic clones in (D) 3LW wing discs and (E) pupal wings aged ~24-36h APF with a br^{disc} reporter. Homozygous $ctbp^{Q229*}$ clones are GFP negative (red-hash) and homozygous WT twin-spots are strong GFP positive. All scalle bars are 100µm.

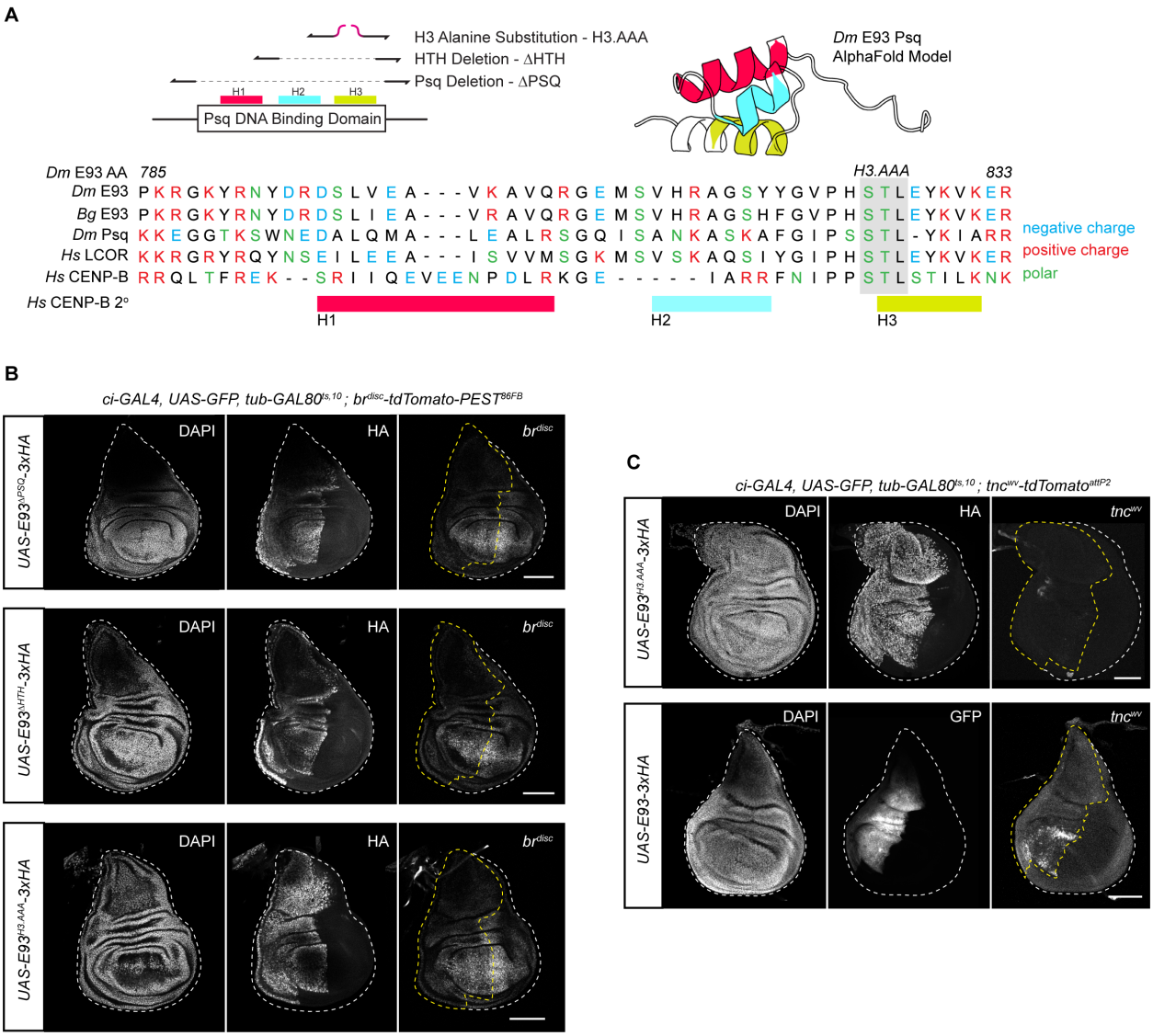

Figure 5.2: (A) Illustration of three mutants generated at the E93 Psq domain, along with a model of the Helix-turn-Helix Psq structure (AlphaFold; Jumper *et a.,* 2021). Multiple sequence aligment of Psq domain containing proteins in *Drosophila melanogaster* (*Dm*), *Blattella germanica* (*Bg*), and *Homo sapiens* (*Hs*). *Hs* CENP-B secondary structure indicated by colored bars (Tanaka *et al.,* 2001). (B,C) Confocal images of 3LW wing discs expressing the three E93 Psq domain mutations in the pressence of either the br^{disc} reporter (B) or tnc^{wv} reporter (C). Expression is driven by the ci^{ts} driver in the anterior compartment (left, yellow-hash). E93 expression is marked by anti-HA immunofluorescence or driver induced GFP. Expression of WT E93 with tnc^{wv} is included for comparison. All scale bars are 100μm.

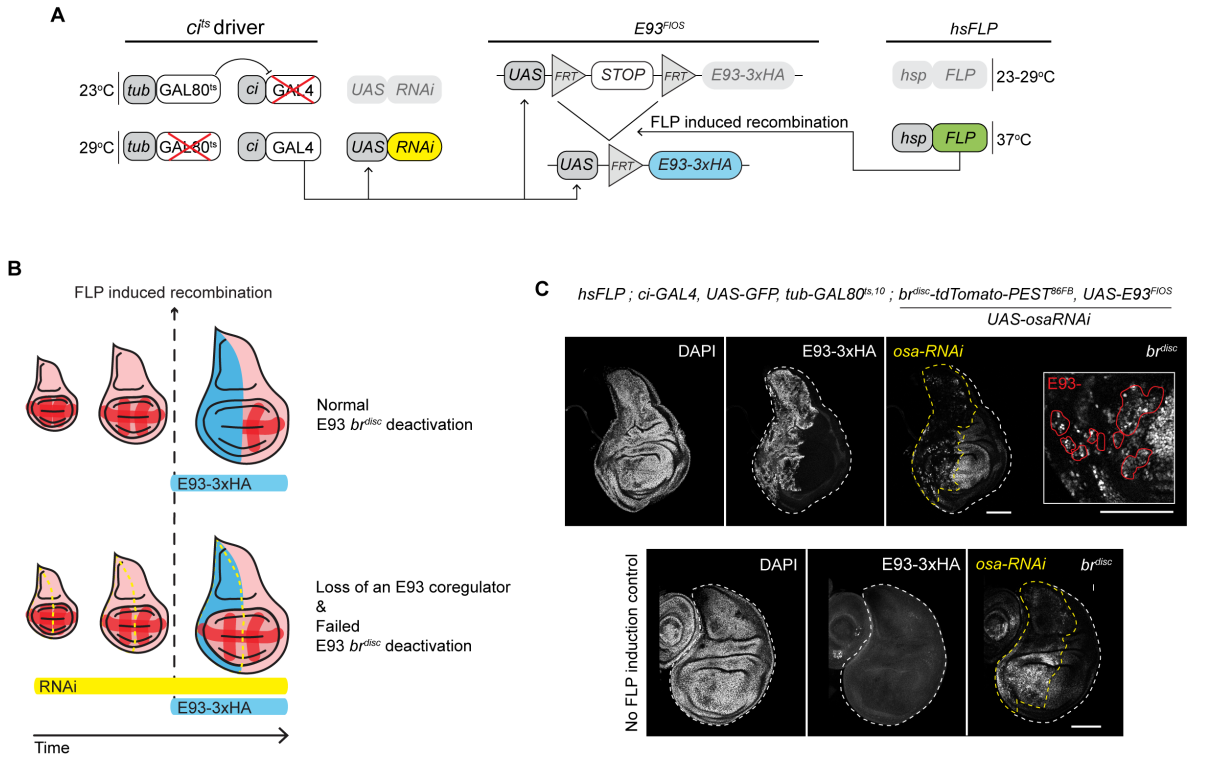

Figure 5.3: (A) Illustration of the genetic components and GAL4 control of the E93 Flip-Out System (*E93^{FIOS}*) with the *ci^{ts}* driver and heat-induced Flippase (*hsFLP*). (B) Illustration of the experimental conditions used to first induce RNAi expression (yellow bar and hash), and then induce E93 expression by FLP mediated Stop cassette removal (blue bar). Two possible effects on *br^{disc}* activity are illustrated. Normal enhancer deactivation, where reporter signal is lost in E93 expressing cells (blue), or alternatively RNAi-depletion of an E93 coregulator in which deactivation fails even in the pressence of precocious E93. (C) Confocal images of E93-FIOS in 3LW wing discs in an Osa knockdown background (*osa-RNAi*). RNAi expressing cells are marked by yellow-hash. Regions without precocious E93 expression following heat-shock induced FLP expression and Stop removal are marked by red outline. A control with no FLP induction and *br^{disc}* hyperactivation following Osa knockdown is included for comparison. Scale bars are 100μm.

REFERENCES

Baehrecke EH, Thummel CS. 1995. The *Drosophila* E93 Gene from the 93F Early Puff Displays Stage- and Tissue-Specific Regulation by 20-Hydroxyecdysone. Developmental Biology. 171(1):85–97. doi:10.1006/dbio.1995.1262.

Bhambhani C, Chang JL, Akey DL, Cadigan KM. 2011. The oligomeric state of CtBP determines its role as a transcriptional co-activator and co-repressor of Wingless targets. The EMBO Journal. 30(10):2031–2043. doi:10.1038/emboj.2011.100.

Bischof J, Björklund M, Furger E, Schertel C, Taipale J, Basler K. 2012. A versatile platform for creating a comprehensive UAS-ORFeome library in *Drosophila*. Development (Cambridge). 140(11):2434–2442. doi:10.1242/dev.088757.

Chinnadurai G. 2008. CtBP Family Proteins. New York (NY): Landes Bioscience and Springer Science+Business Media.

Cohen E, Allen SR, Sawyer JK, Fox DT. 2018. Fizzy-related dictates a cell cycle switch during organ repair and tissue growth responses in the *drosophila* hindgut. eLife. 7:1–22. doi:10.7554/eLife.38327.

Fang M, Li J, Blauwkamp T, Bhambhani C, Campbell N, Cadigan KM. 2006. C-terminal-binding protein directly activates and represses Wnt transcriptional targets in *Drosophila*. EMBO Journal. 25(12):2735–2745. doi:10.1038/sj.emboj.7601153.

Lam G, Nam H-J, Velentzas PD, Baehrecke EH, Thummel CS. 2022. *Drosophila* E93 promotes adult development and suppresses larval responses to ecdysone during metamorphosis. Developmental Biology. 481:104–115. doi:10.1016/j.ydbio.2021.10.001.

Mannervik M. 2014. Control of *Drosophila* embryo patterning by transcriptional co-regulators. Experimental Cell Research. 321(1):47–57. doi:10.1016/j.yexcr.2013.10.010.

Mou X, Duncan DM, Baehrecke EH, Duncan I. 2012. Control of target gene specificity during metamorphosis by the steroid response gene E93. Proceedings of the National Academy of Sciences of the United States of America. 109(8):2949–2954. doi:10.1073/pnas.1117559109.

Niederhuber MJ, Leatham-Jensen M, McKay DJ. 2023. The SWI/SNF nucleosome remodeler constrains enhancer activity during *Drosophila* wing development. bioRxiv. doi:10.1101/2023.07.17.549384.

Nystrom SL, Niederhuber MJ, McKay DJ. 2020. Expression of E93 provides an instructive cue to control dynamic enhancer activity and chromatin accessibility during development. Development (Cambridge). 147(6). doi:10.1242/dev.181909.

Palijan A, Fernandes I, Verway M, Kourelis M, Bastien Y, Tavera-Mendoza LE, Sacheli A, Bourdeau V, Mader S, White JH. 2009. Ligand-dependent corepressor LCoR is an attenuator of progesterone-regulated gene expression. Journal of Biological Chemistry. 284(44):30275–30287. doi:10.1074/jbc.M109.051201.

Pérez-Núñez I, Rozalén C, Palomeque JÁ, Sangrador I, Dalmau M, Comerma L, Hernández-Prat A, Casadevall D, Menendez S, Liu DD, *et al*. 2022. LCOR mediates interferon-independent tumor immunogenicity and responsiveness to immune-checkpoint blockade in triple-negative breast cancer. Nat Cancer. 3(3):355–370. doi:10.1038/s43018-022-00339-4.

Poortinga G, Watanabe M, Parkhurst SM. 1998. *Drosophila* CtBP: a Hairy-interacting protein required

for embryonic segmentation and hairy-mediated transcriptional repression. EMBO J. 17(7):2067–2078. doi:10.1093/emboj/17.7.2067.

Siegmund T, Lehmann M. 2002. The *Drosophila* Pipsqueak protein defines a new family of helix-turn-helix DNA-binding proteins. Development Genes and Evolution. 212(3):152–157. doi:10.1007/s00427-002-0219-2.

Skene PJ, Henikoff JG, Henikoff S. 2018. Targeted in situ genome-wide profiling with high efficiency for low cell numbers. Nature Protocols. 13(5):1006–1019. doi:10.1038/nprot.2018.015.

Tanaka Y, Nureki O, Kurumizaka H, Fukai S, Kawaguchi S, Ikuta M, Iwahara J, Okazaki T, Yokoyama S. 2001. Crystal structure of the CENP-B protein–DNA complex: the DNA-binding domains of CENP-B induce kinks in the CENP-B box DNA. EMBO J. 20(23):6612–6618. doi:10.1093/emboj/20.23.6612.

Uyehara CM, Nystrom SL, Niederhuber MJ, Leatham-Jensen M, Ma Y, Buttitta LA, McKay DJ. 2017. Hormone-dependent control of developmental timing through regulation of chromatin accessibility. Genes and Development. 31(9):862–875. doi:10.1101/gad.298182.117.

Wen Y, Nguyen D, Li Y, Lai ZC. 2000. The N-terminal BTB/POZ domain and C-terminal sequences are essential for Tramtrack69 to specify cell fate in the developing *Drosophila* eye. Genetics. 156(1):195–203.

CHAPTER 6: CONCLUSIONS AND FUTURE DIRECTIONS

The work presented in this dissertation has addressed several open questions in the area of developmental enhancer regulation. In particular we have explored how enhancer activity is regulated over time between developmental stages of *Drosophila* wing development, what roles sequence-specific DNA binding transcription factors (TFs) play in cuing changes in enhancer activity, and how nucleosome remodeling complexes participate in fine-tuning stage-specific enhancers. By employing "ground-level" methods such as traditional genetic perturbations of TF and nucleosome remodeler function in combination with *in vivo* transgenic reporters of developmentally regulated enhancers, in combination with "bird's eye view" genomics methods to assay chromatin accessibility and TF binding profiles, we provide a unique perspective on enhancer regulation in the context of an *in vivo* developmental model system. We find that precocious expression of the *Drosophila* ecdysone-responsive temporal TF (tTF) Eip93F (E93) is sufficient to directly instruct changes in enhancer chromatin accessibility and activity ("E93-sensitive") in such a way as to "advance" the enhancer activity program (Nystrom *et al.,* 2020). Next, we uncover a role of the *Drosophila* SWI/SNF ATP-dependent nucleosome remodeling complex BAP in directly constraining the activity of the E93-sensitive and dependent wing disc enhancer br^{disc}, as well as binding hundreds of temporally regulated putative enhancers genome-wide (Niederhuber *et al.,* 2023). Beyond these specific findings, we uncover a number of aspects of E93 and SWI/SNF biology that raise intriguing questions about the general function of these types of proteins in developmental enhancer regulation.

6.1 Temporal transcription factors and enhancer activity

Like other tTFs, E93 is expressed during a particular period of development, specifically in the wing starting during the prepupal-pupal transition and peaking ~18-24h After Puparium Formation (APF). In addition, E93 is known to be the key adult-specifying factor in holo- and hemimetabolous insects (Lam *et al.,* 2021). Previous work has demonstrated that E93 is necessary for chromatin accessibility

and enhancer activity changes to normally occur during this stage of wing development (Uyehara *et al.,* 2017). These observations suggests that E93 functions as a tTF by establishing particular stage-specific patterns of enhancer accessibility and activity, but it has been unclear to what extent E93 is sufficient to establish these patterns or how temporally constitutive spatial TFs influence E93 enhancer regulation.

We find that when E93 is precociously expressed in wing discs it binds a majority (82%) of its endogenous bindings sites that are normally observed later in pupal wings (Nystrom *et al*., 2020). However, only a small fraction (~25%) of sites that exhibit dependency on E93 for normal temporal changes in chromatin accessibility, change their accessibility in response to precocious E93 ("E93-sensitive"). This suggests that E93 is not sufficient to effect changes at all of its target sites, and likely depends on, or is restrained by, additional factors or local epigenetic information. This conclusion is also supported by the observation that the late pupal active nub^{vein} enhancer does not respond to precocious E93 in the wing disc, but does prematurely activate later during prepupal stages. This suggests that E93 is sensitive to developmental context and may be restricted from binding and effecting late target sites by other tTFs that precede E93. Similarly, some E93-sensitive enhancers are effected only in a subset of all ectopic E93 expressing cells. The tnc^{wv} enhancer for example, activates in the pupal wing in cells along the veins in an E93-dependent manner. This pattern along the veins overlaps with active Decapentaplegic (Dpp) signaling, as marked by high phosphorylated Mothers Against Decapentaplegic (pMad). In precocious E93 experiments, tnc^{wv} does prematurely activate but only in a fraction of E93 expressing cells, specifically in cells of the wing disc pouch that are also pMad positive. These data suggest that while E93 is sufficient at some target enhancers to both instruct accessibility and activity changes, activity may still depend on specific spatial information. Importantly, these observations indicate that tTFs may function by regulating enhancer accessibility such that they become more or less sensitive to spatial inputs at different stages.

In order to further explore E93 tTF function it would be valuable to determine how gene expression changes in response to precocious E93 in the wing disc. This would help elucidate whether the advanced changes to chromatin accessibility and enhancer activity are also correlated with a developmentally advanced gene expression program. In addition, all chromatin accessibility profiling was

done with bulk tissue samples, thus making it difficult to conclude if E93-sensitive changes in chromatin accessibility are present in all E93 expressing cells or just those with particular TF environments that also show E93-sensitive changes in enhancer activity. Single-cell Assay for Transposase-Accessible Chromatin (scATAC-sq) in combination with scRNA-seq, in WT and precocious E93 wing discs, would not only provide greater resolution of accessibility changes, but also allow for correlation of similar groups of cells with accessibility changes, making it possible to determine if E93-sensitivity is more or less associated with particular spatial TF combinations. Notably, similar approaches have already been successfully deployed in the *Drosophila* eye-antennal disc, leg disc, embryos, and scRNA-seq has been successful in the wing disc (González-Blas *et al*., 2020; Everetts *et al*., 2021; Calderon *et al*., 2022; Tse *et al*., 2022).

6.2 Is E93 a pioneer transcription factor?

Pioneer transcription factors (PFs) are defined as factors able to bind their target sites even in the presence of nucleosomes. PFs bind their targets and initiate local DNA-histone destabilization, followed by a larger-scale opening likely by recruiting additional nucleosome remodeling machinery. We do observe instances in which E93 appears to function as a classic PF, binding normally closed sites and triggering opening, but also others in which it doesn't fit the classic PF definition. For one, when E93 is precociously expressed in wing discs it is only sufficient to change accessibility at a relatively small fraction of all it's binding sites, demonstrating limited sufficiency. In addition, precocious E93 directly cues both enhancer opening and closing, apparently in a loci-specific manner within the same cells, indicating bifunctionality. Because the classical PF hypothesis proposes that PFs are sufficient to open closed target sites, and does not include a role for bifunctionality, these observations disfavor classifying E93 as a PF. However, it has been recently shown that several canonical PFs also break the strict PF definition. For example, the archetypal PF FoxA1 appears to be not significantly better at binding and opening closed target sites than a non-PF TF, arguing that "pioneering" is not unique to a particular class of factors but a behavior that can be exhibited by TFs in different contexts (Hansen *et al*., 2022). There have also been documented instances of PFs that can switch between activating and repressing functions, indicating

that “pioneering” does not actually exclude a repressive effect at certain target sites (Lukoseviciute *et al*., 2018). Thus, a rigid definition of which TFs can be anointed the special title of Pioneer appears to be breaking down with more rigorous testing of the PF hypothesis. Further studies of E93, particularly on its DNA binding capacity, identification of interacting partners, and higher resolution genomics may provide a better understanding of if and under what conditions this tTF exhibits pioneer behavior.

6.3 E93 differentially affects chromatin accessibility with site-specificity

E93 demonstrates many interesting regulatory characteristics, including the apparent ability to instruct distinctly different affects at target sites in the same cells. E93 has been previously observed to be necessary during pupal stages for many putative regulatory sites to open and for others to close (Uyehara *et al*., 2017). We find that precocious expression of E93 also leads to distinct changes in chromatin accessibility, with many precociously bound sites opening, but also many closing (Nystrom *et al*., 2020). Notably, we observed that E93-sensitive enhancer reporters with overlapping patterns of activity also exhibit differential response to precocious E93. Specifically, the br^{disc} and tnc^{wv} enhancers are respectively deactivated and activated in the same cells following precocious E93. This raises the question of how a single tTF like E93 can directly cue distinct effects on chromatin accessibility and enhancer activity.

Many TFs have been observed to have context-specific effects, and the model frequently proposed to explain this functional specification is the cooperation of different coregulators at target sites. In the context of E93 function, this model is supported by the observation that the majority of E93-precocious accessibility changes conserve the directionality of change normally observed in WT development. That is, 95% of sites that precociously open in response to E93 normally open, and 75% of sites that precociously close normally close between WT larval and pupal stages. This indicates that the E93 effect is not determined by E93 alone but is encoded within the target site by either the local epigenetic landscape or by the DNA sequence. We attempted to test this model by analyzing histone post-translational modifications (PTMs) and by performing motif analysis at E93-sensitive opening and closing sites (see **Chapter 3** for detailed discussion). While we find no strong correlations between histone PTMs and E93-precocious site behavior, we do find intriguing differences in DNA motif content.

Primarily, the abundance and quality of E93 motifs were greater in E93-sensitive closing sites relative to sensitive opening sites, suggesting that closing may be a result of more direct or stronger E93 interaction. Additionally, E93-sensitive opening sites were found to be more enriched for the earlier larval stage-specifying tTF Br-Z2, suggesting that these sites may be marked for opening after Br levels drop in prepupal stages. Preliminary experiments that precociously expressed an E93 transgene with mutations in the putative Pipsqueak (Psq) DNA-binding domain and assayed the effect on E93-sensitive enhancer reporters (see **Chapter 5**), suggest that E93 requires DNA-binding to both deactivate and activate target enhancers. While these data appear to disfavor an explanation of E93 differential function as the result of direct versus indirect DNA interaction, it does not exclude the possibility that differences in site affinity might influence E93 function. Notably, it has not been determined how Psq domain mutations affect E93-DNA interaction, and additional experiments are necessary to adequately analyze the observed lack of effect on these E93-sensitive enhancer reporters.

How E93 differentially regulates its targets sites remains an open question, and while we favor a model in which function is determined by different coregulators and/or interacting partners, additional work is needed to identify these factors. Approaches such as E93 immunoprecipitation followed my mass-spectrometry (IP-MS), and forward genetic screening will be useful methods to find E93 coregulators. To support these future efforts we have developed an E93 dual-expression tool (E93-FIOS; see **Chapter 5**) to allow for GAL4 based RNAi screening in the context of precocious E93 expression. This tool will allow for screening of factors necessary for regulating E93-sensitive enhancers, providing a more direct test for a relationship with E93 function.

6.4 Enhancer “sensitivity” and constraint

How readily an enhancer responds to inputs, or its “competency,” is often described in terms of binary changes in chromatin accessibility. An enhancer is either in a closed state in which it is not competent to respond to inputs, or an open state in which it is competent. These definitions, however, are overly strict and do not adequately capture the full range of enhancer behavior. Our work on the *Drosophila* SWI/SNF ATP-dependent nucleosome remodeling complex BAP in its role regulating the

E93-sensitive deactivated *br*^{disc} enhancer, supports a more nuanced description of enhancer activity control. We find that the BAP complex is a negative regulator of *br*^{disc} activity (Niederhuber *et al.,* 2023). Surprisingly though, we find that Osa, the defining subunit of the BAP complex, is required to constrain *br*^{disc} activity in the wing disc during the enhancer's normal on-state, but is not required for normal *br*^{disc} deactivation or closing during the prepupal-pupal transition. We also find that Osa directly binds to the endogenous *br*^{disc} enhancer in wing discs, indicating that the requirement for constraint is likely a direct effect. We have suggested several possible mechanisms that might explain enhancer constraint, such as modifying access for activating or repressing TFs, and the recruitment of additional remodeling complexes (see **Chapter 4 Discussion**; Niederhuber *et al*., 2023).

The fact that *br*^{disc} reporter activity can increase beyond its WT levels in the absence of BAP components suggests that it is normally tuned to a particular level of output. This suggests a hypothetical model of enhancer-sensitivity, where a balance of nucleosome density is continually maintained to allow just the right amount of activating and repressing TF interaction. The finding that BAP constrains enhancer activity is not entirely novel, as mutations in the Osa human homolog ARID1A have been associated with histone H3K27 hyperacetylation at super-enhancers (Anglesio *et al*., 2020). In addition, this model is also supported by temporal genomics profiling following nucleosome remodeling complex degradation, which has shown that chromatin accessibility is rapidly lost at some sites (Blümli *et al.,* 2021). This implies that these complexes are continually required to maintain accessibility. Furthermore, this type of active vs repressive balance at *cis*-regulatory elements has been well established in the context of bivalent-promoters and polycomb repression, where a balance of active and repressive histone PTMs poises a site to be subsequently repressed or activated as development proceeds (Schuettengruber *et al*., 2017). Together, these observations demonstrate the nuanced ways that enhancer sensitivity can be regulated and support a continuous "sensitivity balance" model of enhancer activity regulation.

While our data on the BAP complex and *br*^{disc} regulation provide some support for this type of enhancer-sensitivity regulation, there are several missing pieces of the picture. A major problem with our current measurements of enhancer activity is the use of transgenic reporters. While these tools provide a

good readout of spatial enhancer activity patterns they do a poor job of capturing temporal dynamics. This is because imaging of fluorescent protein (FP) is an indirect assessment of transcriptional activity of the enhancer-adjacent promoter. We have made attempts to improve the temporal resolution of our reporters by adding degradation sequences to increase FP turnover, and have built a novel two-fluorophore reporter (Switch), but these systems still have significant temporal limitations. As a result, it is difficult to determine what reduced constraint of enhancer activity means directly at the level of transcription. Methods to visualize transcription in live cells using MS2 reporter systems have been successfully applied in *Drosophila* embryos for several years, but have not been transferred to models of appendage development (Lim *et al.,* 2018). In order to test how BAP mechanistically constrains the br^{disc}, and potentially other developmental enhancers, it will be necessary to develop new reporter methods to more directly assay enhancer activity.

Another critical open question is how enhancer constraint relates to gene expression. RNA-seq in the context of BAP loss-of-function in the wing disc would help determine what the global transcriptional consequences of failed enhancer constraint are. Additionally, we have not determined the impact on chromatin accessibility in wing discs with BAP complex loss-of-function. FAIRE-seq with Osa degradation in pupal wings revealed only subtle changes to accessibility, suggesting that a similar effect may be observed in wing discs. Application of ATAC-seq, which can provide resolution of nucleosome position, may be a strong approach to identify non-binary changes in chromatin accessibility associated with changes in enhancer-sensitivity in BAP-depleted wing discs.

6.5 The relationship of E93 and SWI/SNF

The two research manuscripts presented in this dissertation address developmental enhancer regulation from different perspectives; TF-mediated regulation, and nucleosome remodeler regulation. TFs and nucleosome remodelers are functionally co-dependent as most TFs lack the capacity to catalyze large-scale changes to the nucleosome occupancy, and nucleosome remodeling complexes generally lack the ability to bind DNA with sequence-specificity. Thus, TFs must recruit additional machinery in order to effect the genome, whether those are histone PTMs or chromatin accessibility changes, and

remodelers typically rely on interaction with sequence-specific DNA binding TFs to recruit them to the right sites at the right time. A good example is the *Drosophila* Ecdysone hormone Receptor (EcR), which represses ecdysone response genes during periods of low ecdysone titer, but switches to an ecdysone target activator when the ecdysone titer is high (Dobens *et al*., 1991). EcR has been shown to interact with and recruit the Nucleosome Remodeling Deacetylase (NuRD) complex ATPase Mi-2 to ecdysone response targets in *Drosophila* cells, and that in the absence of Mi-2 some EcR/Mi-2 target genes prematurely activate with a correlated gain of accessibility at nearby Mi-2 binding sites (Kreher *et al*., 2017). These data demonstrate how nucleosome remodeling complexes and site-specific TFs cooperate to regulate *cis*-regulatory element sensitivity and gene expression.

The finding that the BAP complex is involved in direct constraint of the E93-sensitive and dependent wing disc enhancer br^{disc}, raises the question of to what extent E93 and BAP cooperate for enhancer regulation. Are components of the BAP complex necessary to facilitate E93 effects? While our data indicate the proteins regulate some of the same sites, our findings argue against any strong codependence. For one, the BAP-specific component Osa directly binds to the endogenous br^{disc} enhancer in wing discs of late larvae, several hours before E93 expression is detectable, which means that the BAP complex must be recruited to this and other enhancers independently of E93. In addition, we find that Osa is not required for the normal deactivation of br^{disc} that occurs in pupal wings, indicating that E93 likely relies on other machinery to facilitate enhancer closing. We directly tested the necessity of Osa for E93-mediated enhancer deactivation by using the dual-expression E93-FlOS tool described above to first deplete Osa and then precociously express E93. We find that even in the absence of Osa, E93 is still sufficient to trigger br^{disc} deactivation (see **Chapter 5**). Together, these data demonstrate that E93 does not rely on the BAP complex for chromatin accessibility changes, and that the BAP complex does not require E93 for recruitment.

Our screen of nucleosome remodeling complexes involved in br^{disc} regulation did identify other potentially interesting proteins for investigation. Most notably, we find that the ATPase Domino (Dom), which is part of the Tip60 complex, and the NuRD complex component MTA1-like are strongly required to negatively regulate br^{disc} during its normal period of deactivation. While we identify other components

associated with Dom in our screen, we do not find a requirement for the NuRD ATPase Mi-2 suggesting MTA1-like might regulate br^{disc} with other partners. These screen hits offer other possible candidates for the study of E93-mediated enhancer regulation, and developmental enhancer regulation in general.

REFERENCES

Blümli S, Wiechens N, Wu M-Y, Singh V, Gierlinski M, Schweikert G, Gilbert N, Naughton C, Sundaramoorthy R, Varghese J, et al. 2021. Acute depletion of the ARID1A subunit of SWI/SNF complexes reveals distinct pathways for activation and repression of transcription. Cell Reports. 37(5):109943. doi:10.1016/j.celrep.2021.109943.

Bravo González-Blas C, Quan X-J, Duran-Romaña R, Taskiran II, Koldere D, Davie K, Christiaens V, Makhzami S, Hulselmans G, de Waegeneer M, et al. 2020. Identification of genomic enhancers through spatial integration of single-cell transcriptomics and epigenomics. Molecular Systems Biology. 16(5):e9438. doi:10.15252/msb.20209438.

Calderon D, Blecher-Gonen R, Huang X, Secchia S, Kentro J, Daza RM, Martin B, Dulja A, Schaub C, Trapnell C, et al. 2022. The continuum of *Drosophila* embryonic development at single-cell resolution. Science. 377(6606):eabn5800. doi:10.1126/science.abn5800.

Dobens L, Rudolph K, Berger EM. 1991. Ecdysterone regulatory elements function as both transcriptional activators and repressors. Mol Cell Biol. 11(4):1846–1853. doi:10.1128/mcb.11.4.1846-1853.1991.

Everetts NJ, Worley MI, Yasutomi R, Yosef N, Hariharan IK. 2021. Single-cell transcriptomics of the *Drosophila* wing disc reveals instructive epithelium-to-myoblast interactions. Elife. 10:e61276. doi:10.7554/eLife.61276.

Hansen JL, Loell KJ, Cohen BA. 2022. A test of the pioneer factor hypothesis using ectopic liver gene activation. Churchman LS, Tyler JK, editors. eLife. 11:e73358. doi:10.7554/eLife.73358.

Kreher J, Kovač K, Bouazoune K, Mačlnković I, Ernst AL, Engelen E, Pahl R, Finkernagel F, Murawska M, Ullah I, et al. 2017. EcR recruits dMi-2 and increases efficiency of dMi-2-mediated remodelling to constrain transcription of hormone-regulated genes. Nature Communications. 8(May 2016). doi:10.1038/ncomms14806.

Lam G, Nam H-J, Velentzas PD, Baehrecke EH, Thummel CS. 2022. *Drosophila* E93 promotes adult development and suppresses larval responses to ecdysone during metamorphosis. Developmental Biology. 481:104–115. doi:10.1016/j.ydbio.2021.10.001.

Lim B, Fukaya T, Heist T, Levine M. 2018. Temporal dynamics of pair-rule stripes in living *Drosophila* embryos. Proceedings of the National Academy of Sciences of the United States of America. 115(33):8376–8381. doi:10.1073/pnas.1810430115.

Lukoseviciute M, Gavriouchkina D, Williams RM, Hochgreb-Hagele T, Senanayake U, Chong-Morrison V, Thongjuea S, Repapi E, Mead A, Sauka-Spengler T. 2018. From Pioneer to Repressor: Bimodal foxd3 Activity Dynamically Remodels Neural Crest Regulatory Landscape In Vivo. Developmental Cell. 47(5):608-628.e6. doi:10.1016/j.devcel.2018.11.009.

Niederhuber MJ, Leatham-Jensen M, McKay DJ. 2023. The SWI/SNF nucleosome remodeler constrains enhancer activity during *Drosophila* wing development. :2023.07.17.549384. doi:10.1101/2023.07.17.549384.

Nystrom SL, Niederhuber MJ, McKay DJ. 2020. Expression of E93 provides an instructive cue to control dynamic enhancer activity and chromatin accessibility during development. Development (Cambridge). 147(6). doi:10.1242/dev.181909.

Schuettengruber B, Bourbon H-M, Di Croce L, Cavalli G. 2017. Genome Regulation by Polycomb and

Trithorax: 70 Years and Counting. Cell. 171(1):34–57. doi:10.1016/j.cell.2017.08.002.

Tse J, Li TH, Zhang J, Lee ACK, Lee I, Qu Z, Lin X, Hui J, Chan T-F. 2022. Single-Cell Atlas of the *Drosophila* Leg Disc Identifies a Long Non-Coding RNA in Late Development. Int J Mol Sci. 23(12):6796. doi:10.3390/ijms23126796.

Uyehara CM, Nystrom SL, Niederhuber MJ, Leatham-Jensen M, Ma Y, Buttitta LA, McKay DJ. 2017. Hormone-dependent control of developmental timing through regulation of chromatin accessibility. Genes and Development. 31(9):862–875. doi:10.1101/gad.298182.117.